NTNU

Norwegian University of
Science and Technology

Seawater as Magnesium Source for Struvite Crystallization in Wastewater

An assessment of seawater as an alternative magnesium source of struvite production in wastewater treatment plants

Tonje Grini

Civil and Environmental Engineering
Submission date: June 2018
Supervisor: Stein Wold Østerhus, IBM

Norwegian University of Science and Technology
Department of Civil and Environmental Engineering

Abstract

Phosphorus (P) from wastewater and agricultural fertilizers are discharged to water bodies and contribute to eutrophication. At the same time, phosphate rock used for fertilizer production is a non-renewable resource that will be depleted during the next century. It is therefore crucial to remove and recycle phosphorus from discharge sources.

One method for recycling P from wastewater is to crystallize magnesium-ammonium-phosphate (MAP), also known as struvite. Struvite is a suitable slow-release fertilizer that can replace phosphate from mining. For efficient production in wastewater treatment plants we need to add a magnesium (Mg) source. Today, mainly pure Mg salts (e.g. magnesium chloride, $MgCl_2$) are used for this purpose, but cheaper and more sustainable alternatives have been proposed. One of them is seawater, which can be used by wastewater utilities located near the coast. Possible side-effects of using seawater are the interference of seawater constituents on struvite precipitation, and that the dilution from seawater addition will impact P removal efficiency compared to pure Mg sources.

In this study, laboratory-scale experiments, thermodynamic equilibrium calculations and cost estimations were conducted in order to assess the performance of seawater for struvite crystallization. The main objectives were:

- To study the effect of seawater constituents and dilution on P recovery and product characteristics when using seawater as Mg source for struvite precipitation.
- To estimate how much operating costs of struvite production can be reduced by using seawater instead of a pure Mg salt.

The results show that the impact of seawater constituents on P recovery is more apparent at lower supersaturation values of struvite (low pH). Although dilution of the wastewater stream from seawater addition is lowering the supersaturation compared to the pure Mg source, a P recovery of >90% was achieved at pH 8.0 and Mg:P molar ratio ≥1.67. P recovery and solids analysis showed that co-precipitation might have occurred, although to a very little extent. Laboratory experiments and thermodynamic equilibrium calculations showed that seawater can be considered as a good alternative to magnesium chemicals in struvite production, and cost estimations showed a potential cost reduction of ~20%.

Sammendrag

Fosfor (P) fra blant annet avløpsvann og gjødselspredning bidrar til eutrofiering av vassdrag og innsjøer. I tillegg er fosfatstein som brukes i framstilling av kunstgjødsel en begrenset ressurs som er i fare for å bli uttømt det neste århundret. Derfor er det viktig å fjerne og resirkulere fosforen fra avrenningskilder og avløp.

En metode for å resirkulere fosfor fra avløpsvann er ved krystallisasjon av magnesium-ammonium-fosfat (MAP), også kalt struvitt. Struvitt har gode gjødselegenskaper og kan erstatte fosfat fra utvinning av fosfatstein. For effektiv produksjon i avløpsrenseanlegg trenger man imidlertid en ekstern magnesiumkilde. I dag brukes stort sett magnesiumsalter (f.eks. magnesiumklorid, $MgCl_2$) til dette formålet, men billigere og mer bærekraftige kilder har potensiale til å erstatte dette. For renseanlegg nær kysten kan sjøvann være et alternativ, selv om det er ulemper knyttet til det. For det første inneholder sjøvann flere typer ioner og partikler enn bare magnesium (Mg), og disse kan påvirke krystallisasjon og kvaliteten på sluttproduktet. For det andre vil sjøvann fortynne avløpsstrømmen og senke metningsgraden av struvitt.

I denne studien ble det gjennomført eksperimenter i laboratorium, termodynamiske likevektsberegninger og kostnadsestimeringer for å vurdere sjøvannets egenskaper som magnesiumkilde for struvittproduksjon. Hovedmålene var:

- Å studere effekten av andre ioner og fortynning på fosforgjenvinning og struvittfelling når sjøvann brukes som magnesiumkilde.
- Å estimere hvor mye kostnader kan reduseres dersom man går over fra å bruke magnesiumkjemikalier til å bruke sjøvann.

Resultatene viste at fosforgjenvinningen ble mest påvirket av sjøvannsioner ved lav grad av overmetning (lav pH). Fortynning av løsningen som følge av sjøvannstilsetning senket overmetningsgraden av struvitt, men over 90% fosforgjenvinning var mulig å oppnå ved pH 8.0 og et Mg:P molforhold på over 1.67. Gjenvinning og analyse av utfelt produkt viste at utfelling av andre stoffer kan ha forekommet, men bare i svært liten grad. Kostnadsestimeringer anslo at ca. 20% av kostnadene ved struvittproduksjon kan spares ved å bytte fra $MgCl_2$ til sjøvann. Resultatene viser at sjøvann kan anses som en god erstatter for magnesiumkjemikalier.

Preface

This is a Master's thesis written during the spring of 2018 in the Master Program *Civil and Environmental Engineering* at *NTNU* (Norwegian University of Science and Technology). The subject is in the field of *Water Supply and Wastewater Systems* and the thesis equals 30 ECTS credits. A preliminary literature study on the topic was conducted as a project work during autumn 2017. The introduction and theoretical background chapters are mainly a result of that work.

The scope of this study is to assess the applicability and properties of seawater as a magnesium source for struvite precipitation, when this is used as a method to recover phosphorus from wastewater. This is of interest because seawater is a renewable, low-cost resource in near-coastal areas that can lower struvite production costs compared to pure magnesium sources.

The laboratory work of this project was performed at the *NTNU* Wastewater lab and Water analysis lab in Trondheim in the period of january-april 2018.

I would like to thank my supervisor Stein Wold Østerhus for guiding me through this project and for showing a great engagement in discussions about the content and work related to it. I would also like to thank Trine Margrete Hårberg Ness for helping me with analysis and for making a great effort in providing me with results during a hectic period in the laboratory. To all the other lab workers at the wastewater lab – you have made this a very enjoyable part of my study! I also want to thank Arne Kjøsnes at *NTNU SeaLab* for helping me with collecting and characterizing the seawater, as well as the people at *IVAR SNJ* for providing me with reject water from their treatment plant.

Last, but definitely not least, to Sina Shaddel; it would not have been possible to do this without you. I am very thankful for all the effort and time you have put into my master project, and for all the help and encouragement you have given. I also want to thank you for the contribution you have made to this thesis by letting me use some of your earlier work. I hope that my effort also can benefit your future work. I wish you the best of luck towards a doctoral degree, and that no (unintentional) calcium phosphate comes in your way!

Tonje Grini
Trondheim, 14.06.2018

Table of contents

List of tables

List of figures

List of terms and abbreviations

P	Phosphorus
Mg	Magnesium
N	Nitrogen
Ca	Calcium
X:Y	Molar ratio of component X to component Y
MAP	Magnesium ammonium phosphate
Ca-P	Calcium phosphates (Family of materials of calcium and phosphate)
WWTP	Wastewater treatment plant
Bio-P	Biological phosphorus removal
PAO	Polyphosphate accumulating organism
SPP	Struvite precipitation potential
SI	Saturation index
S_a	Saturation
IAP	Ion activity product
Pure Mg source	A source of Mg that does not dilute the liquid it is added to.
XRD	X-ray diffraction
SEM	Scanning electron microscopy
IC	Ion chromatography
M	Molar (Mol/L)
TSS	Total suspended solids
TDS	Total dissolved solids
VSS	Volatile suspended solids
COD	Chemical oxygen demand
sCOD	Soluble chemical oxygen demand
Tot-P	Total orthophosphate

1. Introduction

1.1 Challenges of phosphorus

Phosphorus (P) is an irreplaceable element in the growth of all living organisms and the critical nutrient in freshwater ecosystems [1]. It is introduced to receiving waters mainly through runoff from agricultural areas, wastewater effluent and surface runoff, mainly due to the use of P in fertilizers [2]. This may cause lack of water quality, and in the worst case, eutrophication and fish death. The fertilizers used in agriculture are mainly based on P mined from phosphate rock (P rock). Over-fertilisation of agricultural soils using P fertilizer has been common practice, especially in the northern hemisphere, where it is estimated that close to 25% of the P mined since 1950 has ended up in water bodies or landfills [3]. Besides damaging the nutrient balance in the receiving environment, it is a waste of a limited resource. The pressure on this resource is expected to increase as the world's population keeps growing and the consumption patterns change to products that demand more intensive fertilising [2, 4]. *Cordell* [5] estimate a peak production of P fertilizer around year 2030 (Figure 1-1), while depletion of the world's P rock reserves is expected during the next century. The price of remaining P rock will also increase as the remaining reserves get lower quality, making the availability of P for fertiliser production skewed to countries with high purchasing power[6].

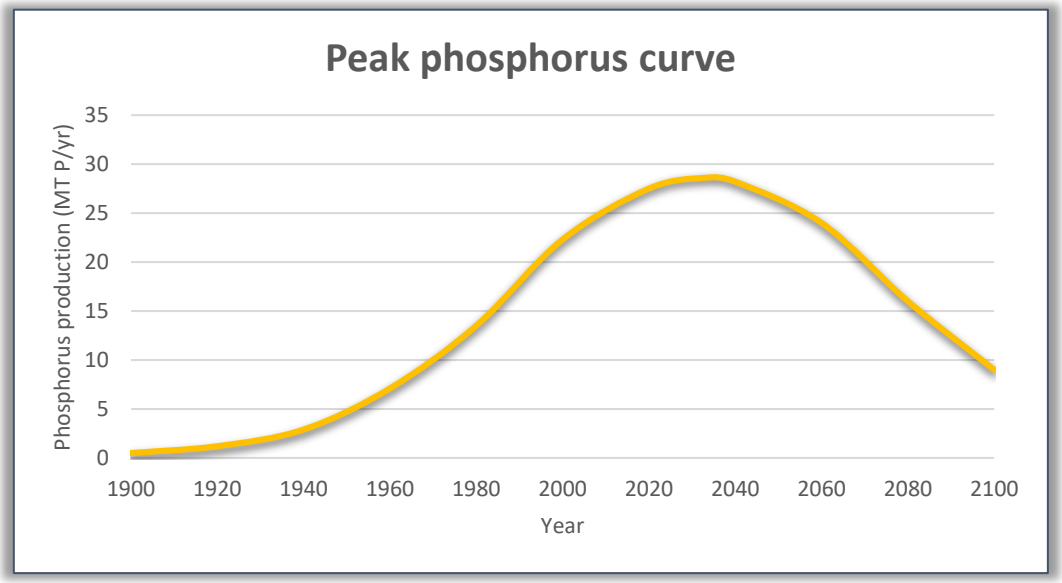

Figure 1-1: The phosphate production curve.
It indicates a peak production occurring around 2030 [5].

To meet the growing concern of P scarcity, the *European Union* has presented an action plan for circular economy. In brief, it aims at increasing the efforts in recycling and re-use of products to the benefit of the environment and economy [7, 8]. It is evident that the waste handling industry will be an important contributor to this measure. Recirculation and recovery of nutrients from wastewater, and especially finite resources like P, is highly relevant in this context. By recovering P as a product that can replace P rock in fertiliser production, the time until depletion can be extended [9]. The transition towards circular economy has already started some parts in the world. In Norway, the wastewater utility *IVAR* has made "Circular Economy" their principle in management [10], and are among the treatment plants that are developing their ability to recover nutrients.

1.2 Struvite for P recovery

1.2.1 Background

Struvite is a mineral with low solubility consisting of magnesium (Mg), ammonium and phosphate in equimolar concentrations ($MgNH_4PO_4 \cdot 6H_2O$, abbreviated MAP). As wastewater contains nutrients from urine and other sources, spontaneous struvite crystallization in wastewater utilities has been a common problem [11]. The occurrence is linked to turbulent flows often found in pipe connections, valves and pumps where pH is elevated due to the release of CO_2 [12, 13] . A lot of the research on struvite has therefore focused on mitigation strategies to prevent reduction of system efficiency from clogging and scaling [14]. Today, struvite is also a part of the solutions in resource recovery and pollution prevention of nutrients.

1.2.2 Advantages

Struvite has shown good capabilities as a product for P recovery. An advantage of recovering P as struvite, besides the fact that wastewater treatment plants (WWTPs) offer favourable conditions for precipitation, is that it has good fertilizer properties [15]. Compared to other P products, e.g. hydroxyapatite and other calcium phosphates (Ca-P), struvite release nutrients at a slower rate and has essential nutrients present in the same crystal [16, 17]. By extracting struvite from wastewater streams, we remove both nitrogen (N) and P, which both have an impact on the nutrient balance of receiving waters. Additionally, it can replace a part of imported P rock used in the fertilizer industry [9].

1.2.3 Magnesium addition

Most wastewater streams do not contain a high enough amount of Mg for efficient struvite production. To assure a supersaturation level of struvite that gives continuous crystal growth in wastewater streams, addition of magnesium ions is needed [18]. High molar ratios of Mg^{2+} to both Ca^{2+} and P are important to prevent low purity product and keep P recovery high [19, 20]. Several commercially available Mg salts exist. The most common sources are MgO, $MgCl_2$ and $Mg(OH)_2$, where the P recovery efficiency has been found to be the highest with MgO and lowest with $Mg(OH)_2$ [20]. The availability, solubility and reactivity of Mg are important parameters when selecting a source [21]. Alternative Mg sources exist, and these will be addressed in *Chapter 2.3.1*.

2. Theory and background

2.1 Properties of struvite

2.1.1 Basic stoichiometry

Struvite forms according to the chemical reaction [14],

$$Mg^{2+} + NH_4^+ + PO_4^{3-} + 6H_2O \rightarrow MgNH_4PO_4 \cdot 6(H_2O)$$

The precipitation process is separated into two stages: nucleation and growth. Nucleation is the formation of crystal embryos as constituent ions combine. This may be happen spontaneously (homogenous), in the presence of impurities (heterogenous) or due to seed crystals (secondary) [22]. Growth is the incorporation of constituents into the crystal lattice of the embryos to form detectable crystals [23]. These processes occur when the product of the concentrations of Mg^{2+}, NH_4^+ and PO_4^{3-} exceed the solubility product, K_{sp}, meaning the solution is supersaturated [14]. The solubility product can be expressed as the product of ion concentrations:

$$K_{sp} = [Mg^{2+}] \cdot [NH_4^+] \cdot [PO_4^{3-}]$$

2.1.2 Conditional solubility product

The precipitation process of struvite is largely controlled by pH, temperature and the presence of other ions (e.g. calcium) [24]. Therefore, for a specific reaction conditions, the conditional solubility product, K_{so}, should be used in thermodynamic calculations. It takes into account the ionic strength and ion activity of the struvite component ions as well as pH. The K_{so} can be calculated as:

$$K_{so} = a_{Mg^{2+}} \cdot a_{NH_4^+} \cdot a_{PO_4^{3-}}$$

With a_i being the activity defined as,

$$a_i = \gamma_i \cdot [C_i]$$

Where γ_i and $[C_i]$ are the activity coefficient and total concentration, respectively, of the ith ion in solution. This means that for $\gamma_i = 1$ we have $K_{so} = K_{sp}$ [11]. *Ohlinger* [25] found the minimum solubility product of struvite to be $10^{-13.26}$ (pK_{so}=13.26) at pH 10.2 when considering the

presence of three magnesium phosphate complexes ($MgPO_4^-$, $MgHPO_4$ and $MgH_2PO_4^+$). Magnesium phosphate complexes reduce the concentrations of Mg^{2+} and PO_4^{3-} available for struvite precipitation, hence, decreases the struvite precipitation potential (SPP) [25]. This pK_{so} has later been widely used as the pK_{sp} of struvite, e.g. in thermodynamic models like *Visual MINTEQ*.

2.1.3 Crystal morphology and growth

Struvite has an orthorhombic crystal structure, while the morphology depends on supersaturation and competing ions. Coffin-shaped crystals are common at low supersaturation (pH < 9.0), whereas dendrite and X-shaped crystals indicate higher growth rates at high supersaturation [12, 26-28]. Other commonly used shape descriptions found in the literature are needle-like and rod-like, which show similarities in terms of shape and appear at medium supersaturation levels (examples of these will be given in *Chapter 4.4*). The crystal length can range from only few to several hundred micrometres [29]. Crystal growth can be inhibited by competing ions, like calcium, and result in smaller crystals [30]. It has also been found that struvite crystal growth in fluidized bed reactors (FBR) is mainly a transport-controlled process that is dependant on fluid dynamics, and that growth rate can be related to the mixing energy [23, 31]

2.2 Conditions for efficient struvite crystallization in wastewater streams

2.2.1 Supersaturation

Struvite precipitation is possible when the supersaturation ratio (Ω) is greater than 1. Ω is defined as equation 1 [22, 32]:

$$\Omega = \frac{a_{Mg^{2+}} \cdot a_{NH_4^+} \cdot a_{PO_4^{3-}}}{K_{sp}} \quad (1)$$

The ion activities in the numerator of the equation above can be calculated from all equilibria equations for the different species of the ions. An example of a set of equations is given in *Table 2-1* for struvite precipitation in a typical animal waste treatment lagoon [14].

Table 2-1: A set of equilibrium equations for struvite component ions.
The equations are used for calculating the concentration of each struvite component ion in a solution..
The result can later be used to calculate the activity, a.

To be calculated	Equilibrium equation	pK From [25] and [32]*
$[\boldsymbol{Mg^{2+}}]$	$\frac{[Mg^{2+}]\cdot[OH^-]}{[MgOH^+]} = K_1$	2.56
	$\frac{[Mg^{2+}]\cdot[PO_4^{3-}]}{[MgPO_4^-]} = K_{Mg}$	4.8
	$\frac{[Mg^{2+}]\cdot[HPO_4^{2-}]}{[MgHPO_4aq]} = K_{Mg2}$	2.91
	$\frac{[Mg^{2+}]\cdot[H_2PO_4^-]}{[MgH_2PO_4^+]} = K_{Mg3}$	0.45
$[\boldsymbol{PO_4^{3-}}]$	$\frac{[H^+]\cdot[H_2PO_4^-]}{[H_3PO_4aq]} = K_{P1}$	2.15
	$\frac{[H^+]\cdot[HPO_4^{2-}]}{[H_2PO_4^-aq]} = K_{P2}$	7.2
	$\frac{[H^+]\cdot[PO_4^{3-}]}{[HPO_4^{2-}]} = K_{P3}$	12.25
$[\boldsymbol{NH_4^+}]$	$\frac{[H^+]\cdot[NH_3]}{[NH_4^+]} = K_N$	9.25*

To calculate the activity coefficient, γ_i, and consequently, K_{so} for ionic strength similar to that of a wastewater stream, Davies approximation to Debye-Hückels equation can be used. [14, 33]. When the activities are known, e.g. by using calculation software like *Visual MINTEQ*, the saturation index (SI) can be calculated. SI is a function of the ion activity product (IAP) and $K_{sp.}$ *Rahman* [34] define these as follows:

$$\mathrm{IAP} = a_{Mg^{2+}} \cdot a_{NH_4^+} \cdot a_{PO_4^{3-}} \tag{2}$$

$$\mathrm{SI} = \log(\Omega) = \log\left(\frac{\mathrm{IAP}}{\mathrm{K_{sp}}}\right) \tag{3}$$

When $IAP > \mathrm{K_{sp}}$, meaning SI > 0, the solution is supersaturated, and solids will precipitate [33]. It is possible to calculate saturation S_a from equation 4 where v is the number of ions in

the compound. For struvite, $v = 3$ [35].

$$S_a = \left(\frac{IAP}{K_{sp}}\right)^{\frac{1}{v}} \quad (4)$$

The molar ratio of the components of struvite is 1:1:1. Since the relative activities of Mg^{2+} and NH_4^+ to PO_4^{3-} can be lower in impure solutions and at different pH, an excess of these ions may be necessary to avoid limiting the precipitation and recovery of P [36].

2.2.2 Component ion molar ratios

Important factors for struvite crystallization and purity is the molar ratios of struvite components (Mg:P:N), and the molar ratios of struvite components to ions that may interfere with the precipitation process. Particularly magnesium-to-calcium (Mg:Ca), magnesium to-phosphorus (Mg:P) and phosphorus-to-calcium (P:Ca) molar ratios are important in this context. Ca^{2+} can replace Mg^{2+} in precipitation with phosphate and form calcium phosphates (Ca-P) (e.g. Monenite ($CHPO_4$), tricalcium phosphate ($Ca_3(PO_4)_2$, Hydroxyapatite ($Ca_5(PO_4)_3OH$) etc.). Studies show that the higher Mg:Ca and P:Ca molar ratio, the higher purity of struvite, and that these should be kept higher than ∼2:1 to prevent inhibition of formation and growth of struvite. Mg:Ca >1:1 has been found to avoid crystalline compounds of calcium phosphates, although amorphous forms are still possible. As long as Mg^{2+} and NH_4^+ are not limiting for precipitation, Ca^{2+} concentration determines the composition of the deposit. If Mg:P molar ratio is lower than 1, both Mg and Ca concentration impact deposit composition. [16, 19, 30, 37]. Calcium inhibition seems also to depend on NH_4^+ concentration. *Crutchik* [38] state that calcium inhibition is less likely in wastewaters with high ammonia concentrations (N:P ∼4). Additionally, a high N concentration can prevent the formation of newberyite ($Mg(PO_3OH)\cdot 3H_2O$) [39]

2.2.3 Optimum pH

The reaction pH is considered one of the most important process parameter for struvite precipitation [18, 40]. Based on many reported optimum pH levels from different studies, struvite has a high potential to precipitate in the pH range of 8.0 to 10,7 [14, 16]. *Ohlinger* [25] suggested a minimum struvite solubility occurring at pH 10,3-10,7, considering ionic strength and complexations. For wastewater streams, a fair assumption is that minimum solubility of

struvite occurs at pH between 8,9 and 9,3 [16, 29, 40, 41]. The importance of pH can also be seen from *Table 2-1*, as all of the equilibrium reactions are pH dependant. This is why pH control and adjustment is important in struvite reactors. Co-precipitation will also be determined by pH, as Ca-P generally need higher pH than struvite to be formed. *Hao* [42] found that at pH below 8,5 (in tap water with ~87 mg/L Ca^{2+}) Ca was not detected in the deposit, but increasing pH above this gave Ca compounds. They also conclude that at pH 8.0, it seems difficult to form relatively pure struvite in wastewaters containing Ca^{2+}.

2.2.4 Wastewater composition

Struvite crystallization is first of all a method to remove P from the liquid phase of wastewater streams. This is most common in WWTPs with enhanced biological P removal (EBPR). These plants are designed to make polyphosphate accumulating organisms (PAOs) take up more polyphosphate in the aerobic zone, than what they release in the anaerobic zone, giving a net removal of P. For P recovery by struvite crystallization, which also requires NH_4^+, the reject streams from the sludge dewatering step is suitable. By then, the water has gone through anaerobic digestion, where the dissolved P and N concentrations increase. Ammonium is released when protein is degraded, at the same time as Mg and P is released from PAOs and other bacteria through cell lysis [21, 25, 43, 44]. Besides the suitability regarding efficient struvite production, the motivation for removing nutrients from side streams has been to lower the nutrient load going back to the system when returning the reject stream to the influent [45].

2.2.5 Precipitation reactor

The struvite crystallization process usually takes place in reactors that are fluidized or mixed. A struvite reactor made for a pilot scale study in Japan is shown in *Figure 2-1*. Here, seawater was used for adding Mg and air was used for circulating and mixing the streams [46, 47]. Sodium hydroxide (NaOH) addition or CO_2 stripping can be used to adjust pH [44]. The changing diameters of the reactor helps the mixing, as it causes turbulent eddies [31]. Without further treatment, the struvite precipitate will be in the form of a crystalline powder. To produce struvite in a form that is more practical to handle, a binder can be added to the product before drying [48]. Additionally, a filtration step of the wastewater stream prior to entering the reactor could be necessary to lower TSS concentration, as this may lower the quality of the end product [49].

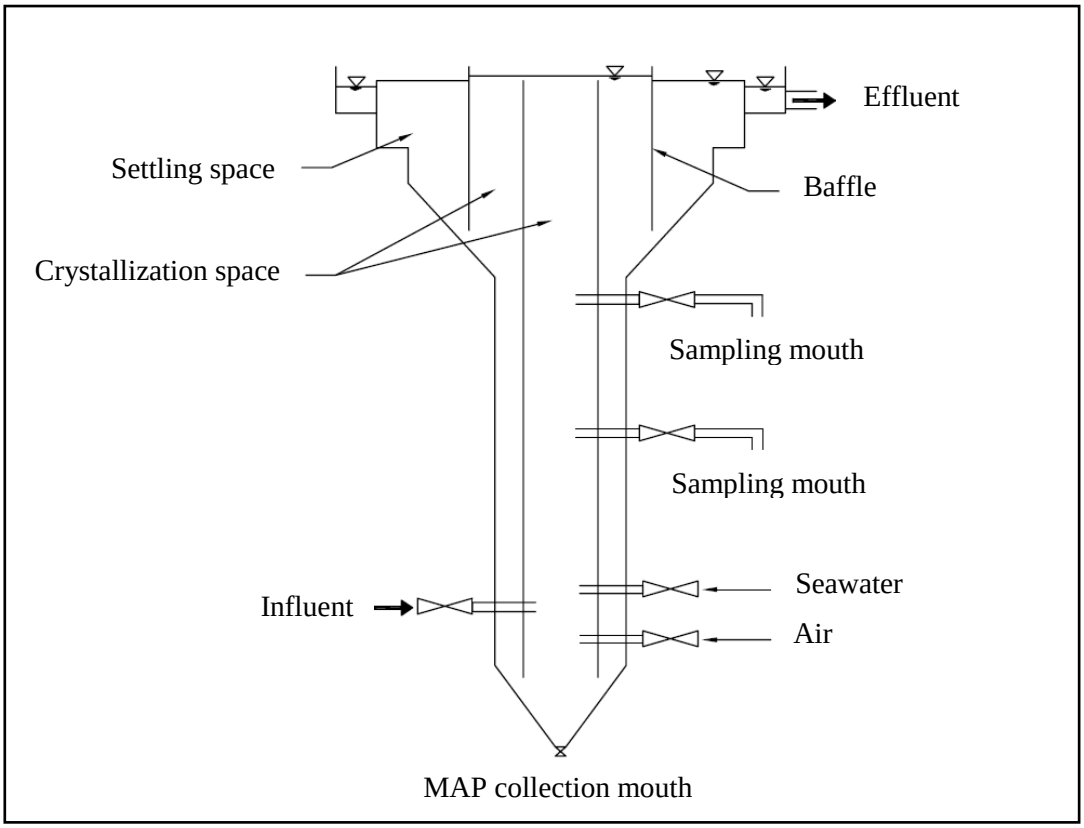

Figure 2-1: A pilot-scale struvite crystallization reactor. From Matsumiya [45].

2.3 Seawater as magnesium source

2.3.1 Economic and environmental benefit

The main purpose of investigating the performance of alternative Mg sources for struvite crystallization is the possibility to lower the cost of the production process. When using pure Mg salts the addition of Mg can contribute to up to 75% of the total production costs [50, 51]. Alternative sources have therefore been proposed and tested, like wood ash, bittern and NF brine. For WWTPs located near the coast the direct use of seawater is assumed to be a low-cost alternative as it is a free source of Mg that does not need to be transported over long distances [21, 38, 46]. Lowering the need of transport as well as replacing the use of manufactured chemical introduce a high level of sustainability to the process.

2.3.2 Potential for P recovery and product quality with seawater

Previous pilot- and lab-scale studies of struvite crystallization with seawater have shown promising results regarding recovery of P and product quality. In the experiments of *Liu* [51] and *Lahav* [52], high purity struvite could be obtained using seawater and brine as magnesium sources (see *Table* 2-2).

Table 2-2: Comparison of purity obtained using different magnesium sources.
The real and synthetic urine do not have detectable concentrations of Ca^{2+}, thus, the Mg:Ca molar ratio in the Mg source is the same as in the solution. In Lahav [52], no data on Ca^{2+} concentration in the supernatant side stream could be obtained.

Study	Mg source	Wastewater source	Mg:Ca molar ratio	Purity of struvite
***Liu* [51]**	$MgCl_2$	Real urine	Same as in Mg source	99.9 %
		Synthetic urine		99.7%
	Seawater	Real urine	5:1	95.6%
		Synthetic urine		92.8%
***Lahav* [52]**	NF brine	Sludge centrifuge supernatant	8.94:1*	> 95%
***Liu* [28]**	Seawater	Urine	4.3:1	~98%

*** No data for calcium concentration in the supernatant could be obtained. Mg:Ca is calculated from NF brine concentrations, assuming the contribution from the supernatant is low in comparison.**

An example of precipitation composition when adding seawater compared to $MgCl_2$ can be seen in *Table 2-3*. The main impurity substance in this result was calcium, which make up 1.39% of the precipitate. This is still considered a negligible effect on purity [28]. In the pilot study of *Matsumiya* [46], the precipitate had particles with N, Mg and P content close to the theoretical value of struvite. These results show that it is possible to obtain a product of high purity also when using seawater for magnesium addition.

Table 2-3: Struvite purity found from previous experiments.
Chemical composition of pure struvite and composition of precipitates obtained using different Mg sources, given in % of total weight..

		P	N	Mg	Ca	K	Al	Na
Theoretical value of struvite		12.63	5.71	9.9				
***Liu* [28]**	Pure struvite	5.71	5.71	9.79	-	-	-	-
	$MgCl_2$-struvite	5.42	5.42	9.52	0.71	0.13	<0.01	0.31
	Seawater-struvite	4.19	4.19	7.56	1.39	0.05	0.09	0.18
***Matsumiya* [46]**	Seawater-struvite	5.5	5.5	9.6	-	0.06	-	-

2.3.3 Concerns

While pure Mg sources do not add significant amounts of competitive ions and impurity to the solution, seawater contains a high amount of salts in addition to having a dilution effect [52]. *Lahav* [52] mentioned some possible side effects of using nanofiltration (NF) brine of seawater as Mg source instead of pure sources. These are also relevant for the use of unfiltered seawater:

i. Since Mg^{2+} concentration is much lower in brine (and seawater) than when using pure sources, it can result in blending and dilution of the wastewater stream, causing TAN and total inorganic orthophosphate concentrations at the entrance of the precipitation reactor to decrease. This reduces the struvite precipitation potential (SPP).
ii. Seawater contains other salts than magnesium, like sulphates, chlorides and sodium ions, and other ions present in lower concentrations. This can form ion pairs that reduce the SPP, resulting in a need to keep pH at a higher level to get a given P removal efficiency.
iii. Ca^{2+} present in seawater may cause the formation of Ca-P, like $Ca_3(PO_4)_2$, $Ca_5(PO_4)_3(OH)$ etc., which reduce the purity and value of the struvite product.

Additionally, there are concerns about the increased salinity of the wastewater main stream if the return stream from the struvite reactor contains seawater [53]. The impact of a continuous side stream feed of seawater to biological processes is not well understood, as previous research either focus on shock loads or much higher salinity levels than what we expect from struvite crystallization processes.

2.4 Objectives

This Master's thesis aims at assessing the feasibility of seawater as an alternative magnesium source for P recovery by struvite crystallization. This includes an assessment of the recoverability of P, analysis of final product characteristics and cost estimations. The main objective is to find out whether seawater can replace pure magnesium sources, and if so, how it will affect the struvite crystallization. It also addresses how to optimize process parameters for efficient struvite precipitation.

2.5 Limitations

2.5.1 Concerns of seawater to be included in the assessment

This study only considers what is happening inside a struvite reactor. It is not taking into consideration the possible effect of introducing seawater to the main stream of a biological treatment plant. Therefore, it is not a full assessment of all aspects of seawater as magnesium source, but it will tell us something about the performance of seawater regarding recovery of P and end product quality, which, together with cost, are important factors when deciding which magnesium source to use.

2.5.2 Wastewater composition

A chemical composition of the nutrients P and N in the reaction medium was chosen based on concentrations in the reject water of the Norwegian wastewater treatment plant HIAS, located in Hamar. This plant and its reject water composition are assumed to be representative for a WWTP where P recovery by struvite precipitation is possible. Our results will be relative to these concentrations, and might not be transmissible to all other reject water characteristics.

2.5.3 Reference magnesium source

In this study, we assume that $MgCl_2$ is a representative salt for the purpose of comparing the performance of seawater to pure magnesium sources. It has good reaction kinetics with the same or better performance as other magnesium salts, and is assumed to be a good reference for comparing seawater performance. The drawback of using $MgCl_2$ is that it also adds a lot of Cl^- to the solution, meaning the impact of Cl^- from seawater is damped when we compare to $MgCl_2$ as opposed to using for instance $Mg(OH)_2$.

2.5.4 Basis for estimating struvite production

It was discovered quite early in the experiments that measuring ammonium nitrogen concentrations for estimating struvite precipitation was more difficult than magnesium and phosphorus. This can be due to spectrophotometry tests of NH_4-N being more difficult to handle in a correct way, or that NH_4^+ can volatilize as NH_3 during the experiments. It was attempted to avoid this by operating the struvite reactor with nitrogen atmosphere, but an effect of this was not detected. Struvite precipitation estimations are therefore mostly based on phosphorus and magnesium removal, although NH_4-N removal in theory would give a better picture of struvite precipitation, as it is not as prone to precipitate as other compounds.

2.6 Accuracy of results and sources of error

Since there exist a numerous amount of unknown error intervals when using different instruments and laboratory equipment, few confident intervals of results are given in this study. Some possible sources of error are:

- Pipetting errors due to human errors or inaccurate calibration of equipment
    - Affects initial and final concentration measurements
- Errors in weighing of salts for preparation of stock solutions and reject waters
    - Affects initial concentrations, thereby the calculated recovery
- Precipitated solids sticking to surface of laboratory equipment
    - Affects the measured yield of solids
- Volatilization of ammonium
    - Affects the molar ratio of ammonium, phosphorus and magnesium

At an early stage of experiments, samples were washed with *Milli-Q* water and/or 70% ethanol saturated with struvite. This may have caused solid species other than struvite to dissolve.

Measures were taken to avoid these errors as much as possible, and multiple experiments were run to be more certain about the results. They are still taken into consideration in the discussion and conclusion of this study.

2.7 Project structure

This master project has consisted of 3 main elements for the sake of determining how seawater will perform as a magnesium source for struvite precipitation. These elements are

1) Laboratory experiments
2) Thermodynamic equilibrium calculations
3) Cost estimations

The progress of work and main aspects and experimental conditions for the project is summarized in the illustration on the next page. The planning of experiments was a dynamic process that was continuously developed based the results achieved and the insight into the challenges of seawater for struvite precipitation. Chapter 3 presents experiment design and materials used in experiments and calculations. Chapter 4 presents the results of experiments and thermodynamic calculations, whereas Chapter 5 contains cost estimations.

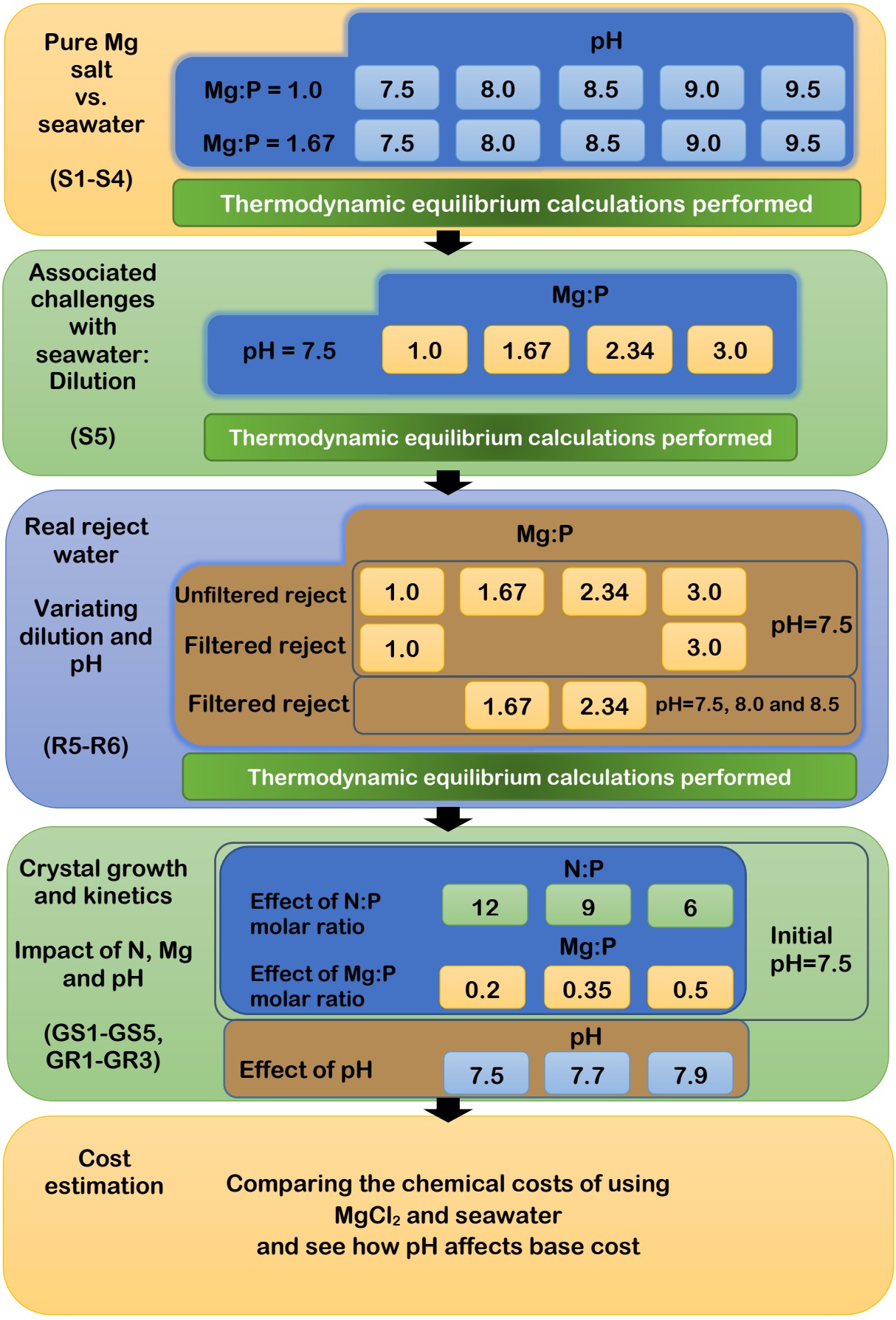
Pure Mg salt vs. seawater
(S1-S4)
pH
Mg:P = 1.0
7.5
8.0
8.5
9.0
9.5
Mg:P = 1.67
7.5
8.0
8.5
9.0
9.5
Thermodynamic equilibrium calculations performed
Associated challenges with seawater: Dilution
(S5)
Mg:P
pH = 7.5
1.0
1.67
2.34
3.0
Thermodynamic equilibrium calculations performed
Real reject water
Variating dilution and pH
(R5-R6)
Mg:P
Unfiltered reject
1.0
1.67
2.34
3.0
Filtered reject
1.0
3.0
pH=7.5
Filtered reject
1.67
2.34
pH=7.5, 8.0 and 8.5
Thermodynamic equilibrium calculations performed
Crystal growth and kinetics
Impact of N, Mg and pH
(GS1-GS5, GR1-GR3)
N:P
Effect of N:P molar ratio
12
9
6
Mg:P
Effect of Mg:P molar ratio
0.2
0.35
0.5
Initial pH=7.5
pH
Effect of pH
7.5
7.7
7.9
Cost estimation
Comparing the chemical costs of using
MgCl2 and seawater
and see how pH affects base cost

3. Materials and methods

3.1 Elaboration of laboratory activities and analysis

The experiments were designed at lab-scale with a 1 L reactor operating in batch mode. The liquid introduced to the reactor resembled a typical reject stream from dewatering of anaerobically digested bio-P sludge, as this is the most relevant wastewater stream for struvite crystallization. The amount of Mg source added to the reactor was based on the struvite molar ratio of Mg to P, experiments conducted prior to this study and recommendations given in the literature. Based on the objective of this thesis, the experiments were designed to:

a. Compare the performance of seawater and one pure Mg source under different struvite supersaturation values (pH).
b. Manipulate parameters that are assumed to affect the performance of seawater as Mg source (Mg:P molar ratio, pH and type of reject water)

By performing both a. and b. it was possible to detect whether the following side-effects of using seawater occurred:

- Ca^{2+} in seawater can compete with Mg^{2+} to precipitate with PO_4^{3-} and form calcium phosphates (Ca-P).
- Seawater constituents might lower the saturation and purity of struvite.
- The dilution of wastewater from seawater addition will impact the recoverability of P and struvite precipitation.

To find out whether the possible side effects are occurring in the experiments, the following calculations were conducted:

1. Calculations of how much recovery of P and Mg was achieved by controlling or measuring initial concentrations and analyzing the final concentrations. N recovery was also included where necessary.
2. Analysis of product properties such as particle size distribution, yield, morphology and phase recognition by scanning electron microscope (SEM) and X-ray diffraction.
3. Utilization of a thermodynamic equilibrium calculation software to validate the experiments, increase the understanding of ion interaction in the solutions, and do equilibrium calculations for other cases that might contribute to the understanding of the performance of seawater.

A cost estimation was included in order to estimate the economic benefit of using seawater.

3.2 Laboratory equipment and procedures

All used chemical reagents are of analytical grade from *Merck*. *Milli-Q* water (18.2 MΩ cm^{-1}) was used for all purposes. The lab-scale crystallization system consisted of a 1 L glass beaker and a mixer. Temperature was regulated by a water bath and maintained at $20 \pm 0.1^{\circ}$. This temperature was chosen based on the side stream temperature of a bio-P plant in Norway. After each experiment the reactor content was filtered with a vacuum filtration to retrieve the solids for analysis. In this process, some samples (S1-S3) were washed with *Milli-Q* water saturated with struvite and/or 70% ethanol saturated with struvite. The ion concentrations in the filtrate were measured with spectrophotometry using cuvettes (*Hach DR Lange 1900; LCK303, LCK326, LCK350* and *LCK349*). Precipitates were dried at room temperature before weighing. Solid phases were characterized by powder X-ray diffraction (XRD) (*D8 Advance DaVinci, Bruker AXS GmBH*) in the range of 5−75°. SEM analyses were performed using a *Hitachi S-3400N*, and particle size analysis were done by laser diffraction using a *Beckman Coulter LS230*. The *LS230* was operated at different modes depending on the particle properties. It was run at a pump speed ranging from 40% to 55%, while PIDS (Polarization Intensity Differential Scattering) ranged from 7% to 15%. The background media was 70% ethanol saturated with struvite. For pH adjustments, 1 M NaOH and 0.1 M HCl was used. The pH was constantly measured by a combined glass electrode with KCl reference electrolyte. For characterization of seawater and for ion concentration measurements of NH_4^+, Mg^{2+} and Ca^{2+} in crystal growth experiments, ion chromatography (*Metrohm*) with a ±5% accuracy was used.

3.3 Preparation of reject water

3.3.1 Synthetic reject water

Stock solutions of 0.5 M sodium dihydrogen phosphate ($NaH_2PO_4 \cdot 2H_2O$) and 3.0 M ammonium chloride (NH_4Cl) were prepared from their corresponding crystalline solids. Synthetic reject water was prepared from these according to the composition of reject water from dewatering of bio-P sludge at a WWTP in Norway. The final composition of the synthetic reject water can be seen in *Table 3-1*. Conductivity was measured with a *HQ440D* from *Hach*.

Table 3-1: Composition of synthetic reject water after preparation

Synthetic reject water		
pH	~6.6	
Conductivity	5160 µS/cm	
TDS*	~3300 ppm	
	mmol /L	**mg/L**
PO_4-P	4.25	137.1
NH_4-N	53.85	754.3
Na^+	4.25	101.7
Cl^-	53.85	1909.0

***From the conductivity calculator of Lenntech BV [54]**

3.3.2 Real reject water

Real reject water was obtained from *IVAR Central WWTP North Jæren* (*SNJ*), from the thickening of bio-P sludge. The thickening step is located after a few hours residence time under anaerobic conditions in a sludge storage tank. The time from taking the reject water out from the treatment plant to delivery in Trondheim was about 20 hours, during which no temperature control was possible. It was kept in a refrigerator at ~1-4°C during the experimental period of about 2 weeks. A characterization was performed, and the result can be seen in *Table 3-2*. Solids measurements were performed as described in *Richardsen* [55]. Ion concentrations were measured with spectrophotometry within 1 day after delivery, and then repeated after 3 days to detect any changes. The ion concentrations were found to be stable during this time. These low concentrations of soluble P and N are not common for this type of side stream, but is a result of recent transition to bio-P at *SNJ*. The Mg concentration is also high for this type of wastewater. It is assumed to be due to seawater intrusion, as *SNJ* is located near the coast. This means that other seawater constituents may also be present. These were partly identified from ion chromatography (IC) of crystal growth experiment samples, from which an estimation of seawater intrusion was made (See *Appendix 1*).

Table 3-2: Composition of unfiltered reject water from SNJ.
It includes only measured values, except TS, which is calculated as the sum of TDS and TSS.

Unfiltered reject water	
Conductivity [µS/cm]	1744
pH	~7.0
	Concentration [mg/L]
TS	2.047
TDS	1.272
VSS	0.621
PO_4-P	26.55
NH_4-N	46.87
Mg^{2+}	41.6
Tot-P	37.55
Soluble COD	468
Total COD	1838

In order to have comparable results to experiments with synthetic reject water, the concentrations of P and N were adjusted using salts of sodium dihydrogen phosphate ($NaH_2PO_4 \cdot 2H_2O$) and ammonium chloride (NH_4Cl) to reach 754.3 mg/L NH_4-N and 137.1 mg /L PO_4-P. The composition re-adjustment was performed prior to each experiment and the result is shown in *Table 3-3*. The real reject water was used in two modes:

1) Original reject with suspended solids and

2) Filtered with 1.2 µm filter.

The reason behind using 1) was to investigate the effect of suspended solids on the process, while 2) was to make retrieval of precipitated struvite possible for further analysis since the suspended solids in reject water made it difficult to separate the struvite in a lab-scale reactor.

Table 3-3: Composition of real filtered reject water after P and N adjustment

Adjusted and filtered reject water			
Conductivity	~6600 µS/cm		****
pH	~6.5		Measured
Ion concentrations:	**mmol/L**	**mg/L**	
PO_4-P	4.25	137.1	*
NH_4-N	53.85	754.3	*
Mg^{2+}	1.71	41.6	Measured
Na^+	~17.4	~400	**
Cl^-	50.5-66.6	1790-2360	*/***
Ca^{2+}	~1.0	~40	**
K^+	~1.0	~40	**

***** **Calculated from a salt addition of 2.702 g/L NH_4Cl and 0.557 g/L $NaH_2PO_4 \cdot 2H_2O$**

****** **From ion chromatography of growth experiment sample GR1/GR3 and estimated seawater composition. See *Appendix 1*.**

******* **Maximum value is based on an assumption that seawater intrusion make out 3% of the reject water. See *Appendix 1*.**

******** **Calculated with conductivity calculator and conductivity convertor from *Lenntech BV* [54, 56]. See *Appendix 1*.**

3.4 Seawater characterization

Seawater was obtained from the Trondheim fjord via *NTNU SeaLab*, where seawater is pumped from a depth of 70 meters, about 800 meters from land, and filtered through a sand filter (estimated removal of particles of sizes >70µm). It was kept in a refrigerator at ~1-4°C during the experimental period of about 3.5 months. Annual variations of seawater properties measured by *NTNU SeaLab* shows a pH variation of 7.9-8.3 and salinity of ~33 ppm. The ionic composition of sampled seawater used in this study was defined by IC for cations and anions. Measurements was performed in nine replicates for cations and two replicates for anions to ensure quality of data. Resulting mean and standard deviation can be seen in *Table 3-4*, although with bicarbonate concentration from external reference, as it could not be measured. Ion concentrations and Mg:Ca molar ratio are reasonable compared to previously reported seawater compositions [57] .

Table 3-4: Seawater composition

Seawater properties and composition		
Conductivity	31600 µS/cm	
pH	7.9-8.3	
	Ion Concentration [mg/L]	**Standard deviation**
Anions		
Cl^-	16085	1237
SO_4^{3-}	2740	42
NO_3^-	160	14
HCO_3^{2-}	140*	-
Br^-	80	0
Cations		
Na^+	10570	178
Mg^{2+}	1276	34
Ca^{2+}	447	31
K^+	393	18

*** From *Cotruvo* [57].**

3.5 Design of experiments

3.5.1 Comparison of $MgCl_2$ and seawater at changing supersaturation (S1-S4)

In these experiments, the recovery of P and Mg at different pH, and by using both a pure Mg source and seawater, were studied. Only synthetic reject water was used for this purpose. No dilution from any of the sources was considered, meaning the initial concentrations of N and P are the same as if only reject water was present in the reactor. When pure Mg source was used, the prepared amount of 0.5 M $MgCl_2 \cdot 6H_2O$ stock solution was added with burette after pH adjustment of the reactor content. In experiments with seawater, the $NaH_2PO_4 \cdot 2H_2O$ part of the synthetic reject water was added with burette after pH adjustment, as this was more practical than adding large amounts of seawater. Total volume of reject and magnesium source was 1 L. Molar ratio of magnesium-to-phosphorus (Mg:P) was set to 1.0 and 1.67, where 1.0 represents the molar ratio found in struvite. 1.67 was picked due to previous studies with Ca-P and struvite by Ph.D.-candidate Sina Shaddel, whose results for $MgCl_2$ as Mg source are included in this

study. The pH was kept constant during the experiments. Nitrogen (N_2) gas was connected to achieve nitrogen atmosphere in the reactor. This was in order to avoid pH change due to dissolution of CO_2. A two-blade impeller was used for mixing at 200 revolutions per minute (rpm). This rpm was found be high enough to achieve homogenous mixing and avoid aggregation, and low enough to avoid crystal break and too high nucleation rate. The setup can be seen in *Figure 3-1*. *Table 3-5* shows the experimental conditions for series S1 to S4.

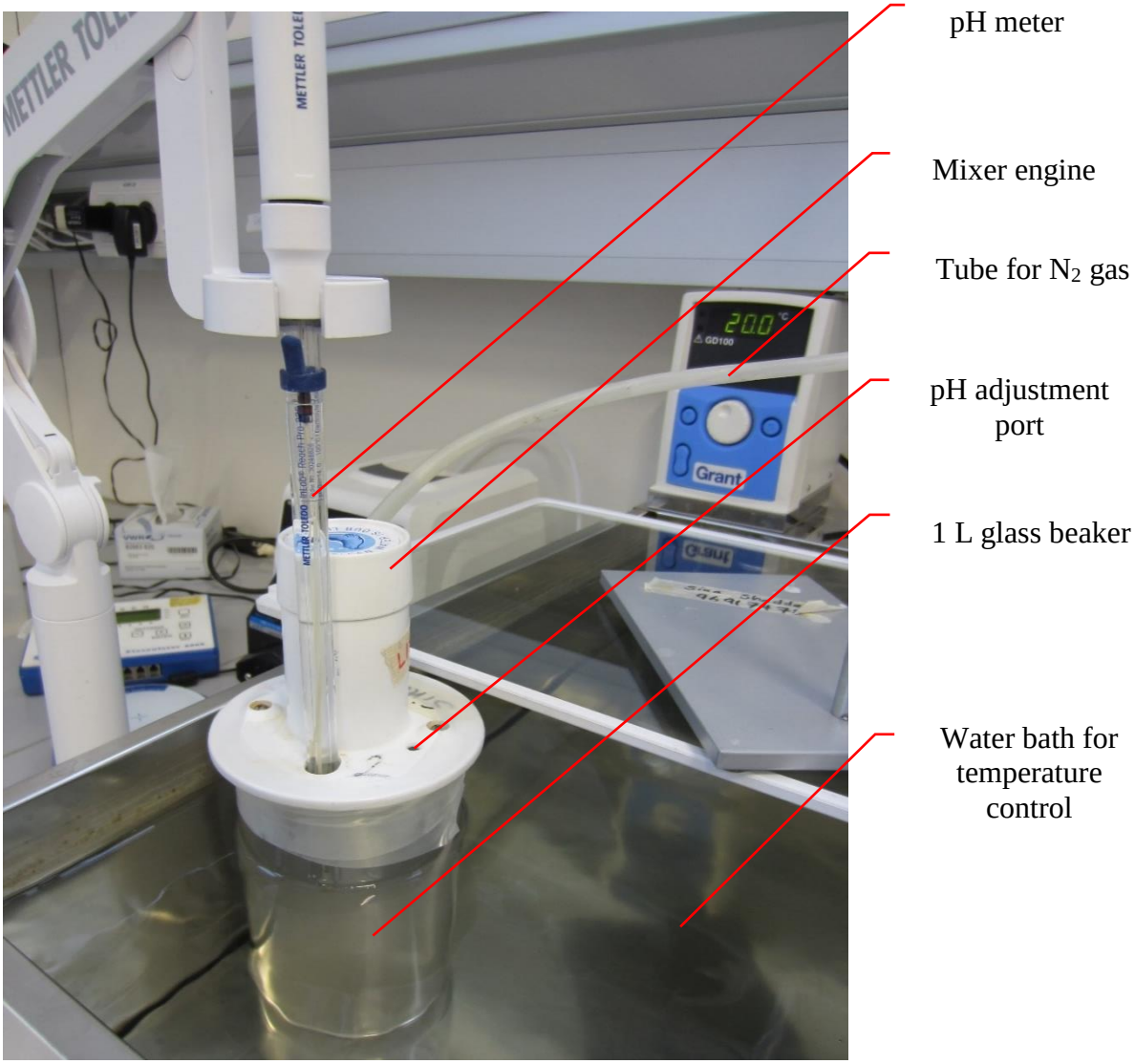

Figure 3-1: Experimental setup of lab-scale struvite reactor

Table 3-5: Experimental conditions of S1-S4.

	Mg source	pH	Mg:P Molar ratio	Initial concentration [mg/L]		Seawater amount in reactor [%]
				PO_4-P	NH_4-N	
S1	$MgCl_2$	7.5, 8.0, 8.5 , 9.0 and 9.5	1.0	137.1	754.3	-
S2	Seawater		1.0	137.1	754.3	8.4
S3	$MgCl_2$		1.67	137.1	754.3	-
S4	Seawater		1.67	137.1	754.3	14.1

The mixer operated for 60 minutes from the time when all struvite constituents had been added. About 14 mL of sample was taken at the end of the experiment and filtered through a 0.2 µm syringe filter. Cuvette tests for PO_4-P, NH_4-N and Mg^{2+} were performed on the filtrate. The content of the reactor was analyzed as described in *Chapter 3.2*, where the vacuum filtration was performed using a 0.2µm filter.

3.5.2 Dilution effect of seawater at different Mg:P molar ratios and pH (S5, R5, R6)

In these experiments, the recovery of P, Mg and N at different Mg:P molar ratios and pH were investigated while considering the dilution effect of seawater. This means that the initial concentration of P and N is lowered as the seawater amount is increased to rise the Mg:P molar ratio. Experiments were conducted using both synthetic and real reject water. Since the real reject water contains some magnesium, less seawater was needed to have the same Mg:P as in the experiments with synthetic reject water. *Milli-Q* water was therefore added in order to achieve the same dilution. The total volume of solution was 1 L. The experimental setup was similar to that of experiment S1-S4, although without supply of N_2 gas (Figure 3-1). This was found not to affect the result. Both filtered and unfiltered real reject water was used in these experiments. Filtered reject water made it easier to analyze the precipitate, as the content of particulate matter in the unfiltered reject water was high. In series S5 and R5, the dilution effect at pH 7.5 was investigated for Mg:P molar ratio of 1.0 up to 3.0 with a step size of 0.67. In series R6, an additional effect of pH was studied for Mg:P of 1.67 and 2.34. The pH was kept constant during the 1 hour duration of experiments. The mixer operated at 200 rpm, for reasons described in *Chapter 3.5.1*. *Table 3-6* shows the experimental conditions for series S5 and R5, and *Table 3-7* shows the experimental conditions for R6.

Table 3-6: Experimental conditions for S5 and R5.
Initial concentrations are calculated for S5, whilst it was measured with spectrophotometry for R5u and R5f prior to experiment started. SW=Seawater

	Mg source	Reject water type	pH	Mg:P molar ratio (measured)*	Initial concentration [mg/L]		Seawater amount in reactor [%]
					PO_4-P	NH_4-N	
S5	SW	Synthetic	7.5	1.0	126.4	695.7	7.8
				1.67	120.2	661.2	12.3
				2.34	114.5	630.0	16.5
				3.0	109.4	602.1	20.2
R5u	SW	Real unfiltered	7.5	1.0 (0.86)	121.0	702.7	4.8
				1.67 (1.65)	118.9	688.5	9.5
				2.34 (2.13)	114.7	635.0	13.8
				3.0 (3.26)	110.5	616.8	17.6
R5f	SW	Real filtered	7.5	1.0 (0.93)	128.5	725.3	4.8
				1.67 (1.50)	120.7	685.9	9.5
				2.34 (2.16)	117.4	658.7	13.8
				3.0 (2.76)	111.2	630.3	17.6

***Numbers in parenthesis are based on measured initial P and Mg concentrations. These are not necessarily more accurate then targeted molar ratios, but are included because the basis for these numbers are also the basis for recovery calculations in these experiments. However, only the targeted molar ratio is used as reference in the presentation of results.**

Table 3-7: Experimental conditions for R6.
Initial concentrations are calculated for pH 8.0 and 8.5, whilst it was measured by spectrophotometry for pH 7.5 prior to experiment started. SW=Seawater.

	Mg source	Reject water type	Mg:P molar ratio	pH	Initial concentration [mg/L]		SW amount in reactor [%]
					PO4-P	NH4-N	
R6a	SW	Real filtered	1.67	7.5	120.7	685.9	9.5
				8.0	120.2	661.2	
				8.5			
R6b	SW	Real filtered	2.34	7.5	117.4	658.7	13.8
				8.0	114.5	630.0	
				8.5			

3.5.3 Study of crystal growth kinetics

In these experiments, the change in pH and concentration of P, Mg and Ca was measured during growth of struvite crystals. The purpose was to find out how different parameters affect the kinetics of crystal growth. Experiments were conducted with both synthetic and real reject water, and only seawater was used as Mg source. Mixing was performed by a combined 4-blade/2-blade impeller with three baffles. The mixer operated at 150 rpm, slightly lower than the other experiments. This was to avoid nucleation and breaking of crystals. Total volume of reject water and seawater was set to 1L without any dilution from seawater. Initial pH was adjusted prior to adding 0.7 grams of pure struvite seed crystals (*Alfa Aesar*, > 98% struvite) sieved at 63µm. Experiments with synthetic reject water were run with nitrogen atmosphere. Duration of mixing was 1 hour with drifting pH (no pH adjustment). 9 samples were taken from 1 to 18-20 minutes and filtered with 0.2µm syringe filters to measure ion concentrations. No analysis of the precipitates is included in these experiments.

3.5.3.1 Effect of N:P and Mg:P molar ratios using synthetic reject water (GS1-GS5)

In experiments GS1, GS2 and GS3 the effect of N:P molar ratio was studied at an initial pH of 7.5 and an Mg:P molar ratio of 0.2. Preliminary experiments confirmed that secondary nucleation will not occur under these conditions, but they will allow the growth of seed crystals. In series GS4 and GS5 the effect of Mg:P molar ratio was studied, at a constant N:P molar ratio of 6 and initial pH of 7.5. The result of GS3 is also relevant for this series of experiments. Experimental conditions are summarized in *Table 3-8*.

Table 3-8: Experimental conditions for GS1-GS5.

	Molar ratios		Initial concentration [mg/L]		Seawater amount	Initial
	N:P	Mg:P	PO_4-P	NH_4-N	in reactor [%]	S_a *
GS1	12	0.2	137.1	754.3	1.7	1.45
GS2	9	0.2	137.1	565.7	1.7	1.36
GS3	6	0.2	137.1	371.9	1.7	1.23
GS4	6	0.35	137.1	371.9	3.0	1.43
GS5	6	0.5	137.1	371.9	4.2	1.55

*** Calculated from *Visual MINTEQ* and equations 3 and 4.**

3.5.3.2 Effect of pH on growth kinetics using real reject water (GR1-GR3)

In experiments GR1, GR2 and GR3, the effect of pH on growth kinetics was studied using real filtered reject water. Since the reject water already contained Mg, only around 1% seawater was needed to achieve Mg:P molar ratio of 0.5. It is therefore not possible to make concrete comments about the effect of seawater in these experiments. The seawater intrusion to the WWTP where the reject water was sent from still makes it relevant to consider. Experimental conditions are summarized in *Table 3-9*. Only pH is changed between the experiments.

Table 3-9: Experimental conditions for crystal growth experiments (GR1, GR2, GR3). Experiments are run with real filtered reject water and seawater as magnesium source

	pH	Molar ratios		Initial concentration [mg/L]		Seawater amount in reactor [%]
		N:P	Mg:P	PO_4-P	NH_4-N	
GR1	7.5	6	0.5	137.1	371.9	~1.0
GR2	7.7	6	0.5	137.1	371.9	
GR3	7.9	6	0.5	137.1	371.9	

3.6 Thermodynamic equilibrium calculations

3.6.1 Model properties

The software used for thermodynamic equilibrium calculations was *Visual MINTEQ* ver. 3.1, a free equilibrium speciation model used for calculating equilibrium composition of dilute aqueous solutions. It can for instance calculate activity, saturation indexes, mass distribution among dissolved species and solid phases and help the user predict the outcome of simultaneously occurring chemical reactions. *Visual MINTEQ* was used for comparing results of the experiments to theoretical thermodynamically calculated results, calculating activity and supersaturation, studying which complexes are formed and which compounds are oversaturated in our solution. It was also used for calculations of other cases than what is covered in our experiments. *Visual MINTEQ* uses a $\log K_{sp} = -13.26$ for struvite, which is equivalent to the K_{sp} mentioned in *Chapter 2.1.2*.

3.6.2 Setup of the model

Simulations were run for all experiments with synthetic reject water (S1-S5) and filtered reject water (R5f, R6a and R6b). Initial concentrations of all known ions were put into the components list of the model. Ion concentrations used can be seen in *Appendix 2*. This includes all ion contribution from the Mg sources, pH adjustment and constituents of the synthetic and real reject water. The ionic compositions of seawater and real reject water were not fully characterized. This was a part of the uncertainty in the model. The pH was fixed to the same value as in the experiments. For P, N and Mg recovery calculations we assumed that struvite was the only crystal that would precipitate, as the kinetics is faster than for other oversaturated phases, like hydroxyapatite [52]. *Visual MINTEQ* does not consider kinetics, only thermodynamics, which makes it necessary to define the dominant precipitating phase. *Appendix 3* contains calculated saturation indexes (SI) of oversaturated compounds in S1-S4. Thermodynamic equilibrium calculations were performed as a part of the analysis of experimental results. All references to theoretical recovery and yield in this study are from calculations with *Visual MINTEQ*, based on input values from *Appendix 2*.

3.7 Cost estimation software

The software used for cost simulations was developed by Oded Nir at the Israel Institute of Technology, and is available from:
https://www.researchgate.net/publication/286456042_Struvite_program.
Further descriptions of properties, limitations and setup of this software is given in *Chapter 5*.

4. Results and discussion

4.1 Recovery and production of solids

The recovery of soluble P, N and Mg was calculated as the absolute change in concentration by the equation:

$$Recovery\ [\%] = \frac{C_{initial} - C_{final}}{C_{initial}} \cdot 100\%$$

Where $C_{initial}$ is the concentration of the ion in the 1L reactor at the beginning of the experiment. C_{final} is the concentration in 1 L that was measured with spectrophotometry at the end of the experiments (after 60 minutes of mixing). The concentration was corrected for any volumes added from pH adjustment.

Estimations of struvite production (yield) based on molar removal of P, Mg or N was calculated as;

$$Yield\ [mg/L] = (M_{initial} - M_{final}) \cdot MW_{struvite} \cdot 1000 mg/g$$

Where $M_{initial}$= Initial concentration if ion in mol/L, M_{final}= final concentration of ion in mol/L and $MW_{struvite}$=the struvite molar weight (245.41 g/mol).

Weight of produced solids, either achieved in experiments, estimated from molar removal of ions or calculated with *Visual MINTEQ* (theoretical) are given in milligram per litre of reactor content (the total volume of reject water and magnesium source), unless stated otherwise.

4.1.1 Comparison of $MgCl_2$ and seawater at changing supersaturation (S1-S4)

4.1.1.1 Achieved and theoretical recovery

No dilution was taken into account in these experiments, meaning only the effect of seawater constituents contributed to any difference between the Mg sources. 5 experiments at constant pH values between 7.5 and 9.5 were conducted. In *Appendix 4*, the resulting P and Mg recovery with minimum and maximum values from two replicates of experiment series S2 are given. *Figure 4-1* and *4-2* show the P recovery at different pH at Mg:P of 1.0 and 1.67 respectively for $MgCl_2$ and seawater. Results show that the two sources are performing well, and that it is

possible to achieve high P recovery values (>90%) with both sources and Mg:P molar ratios. The recovery is, however, deviating between the two sources at low pH values in both cases. It could be that, when pH is low, the additional effect of high ionic strength in seawater lowers the supersaturation to such an extent that seawater can no longer achieve the same P recovery as $MgCl_2$. A consequence is that P recovery increase more for seawater than $MgCl_2$ when pH is changed from 7.5 up to 9.5. Figures in *Appendix 4* also show more uncertainty in the measurements at pH 7.5 regarding P and Mg recovery, indicating that the solution is sensitive to small errors in experimental or environmental conditions.

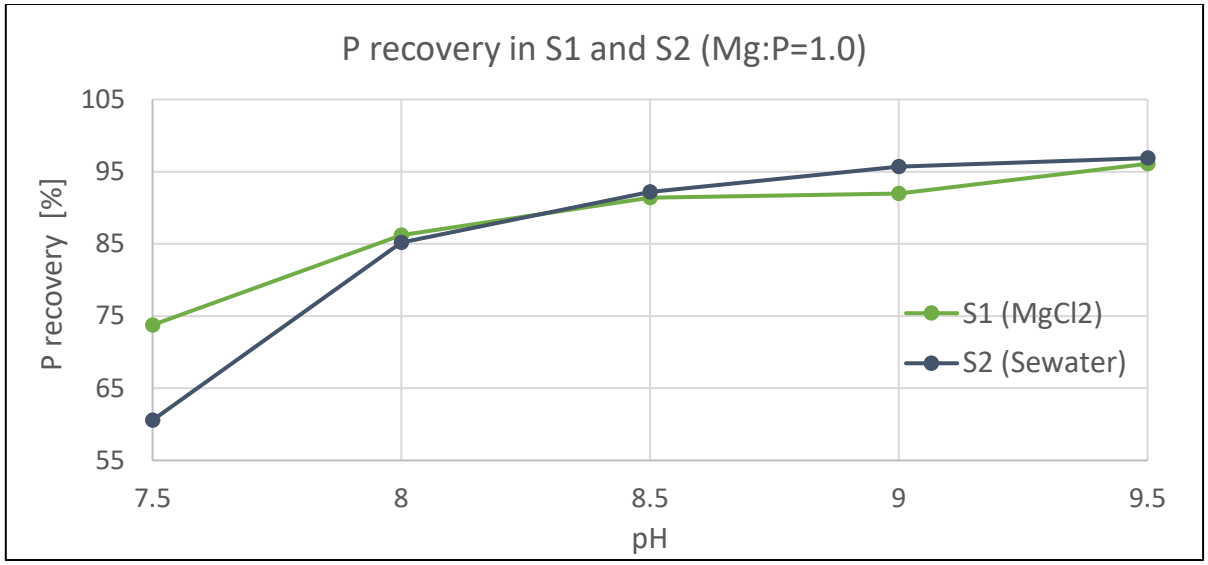

Figure 4-1: P recovery [%] for S1 and S2.

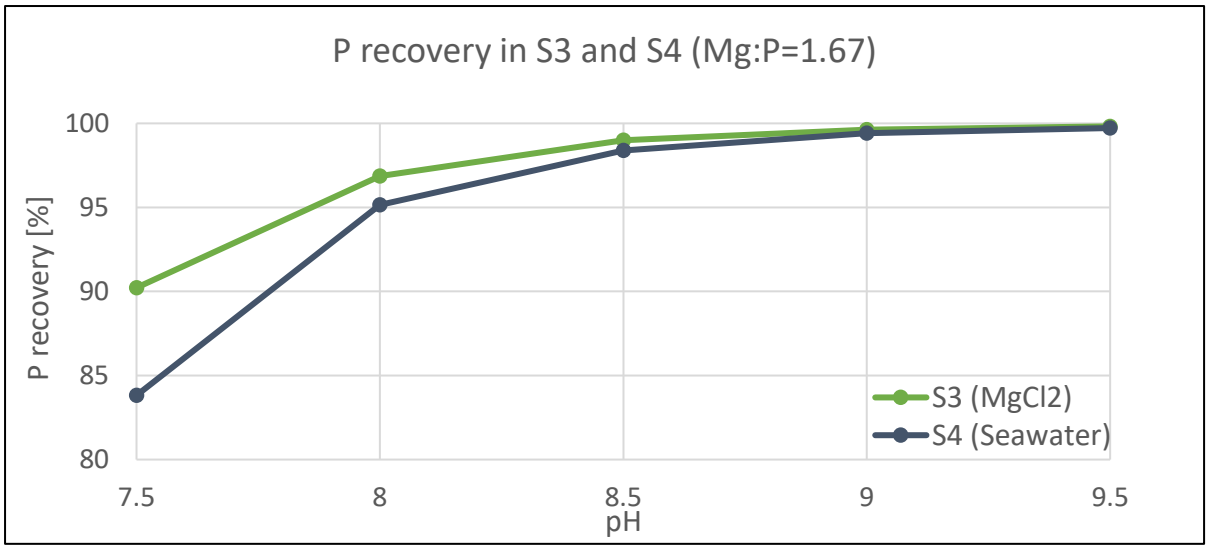

Figure 4-2: P recovery [%] for S3 and S4.

Figure 4-3 B shows that when we use seawater at Mg:P of 1.0 (S2), we are not reaching the theoretical P recovery at pH 7.5, which could be a sign that equilibrium is not yet established in our experiment. At higher pH, however, actual P recovery is higher than theoretical one, meaning there could be other solids precipitating in addition to struvite, as theoretical calculations only allow solids to precipitate as struvite. P recovery is also slightly higher with seawater than $MgCl_2$ in this case (Figure 4-1). Besides co-precipitation, this can also be due to errors in the procedure of the experiments with $MgCl_2$, as actual P recovery with $MgCl_2$ is lower than the theoretically calculated P recovery (Figure 4-3 A). In S3 and S4, P recovery is very

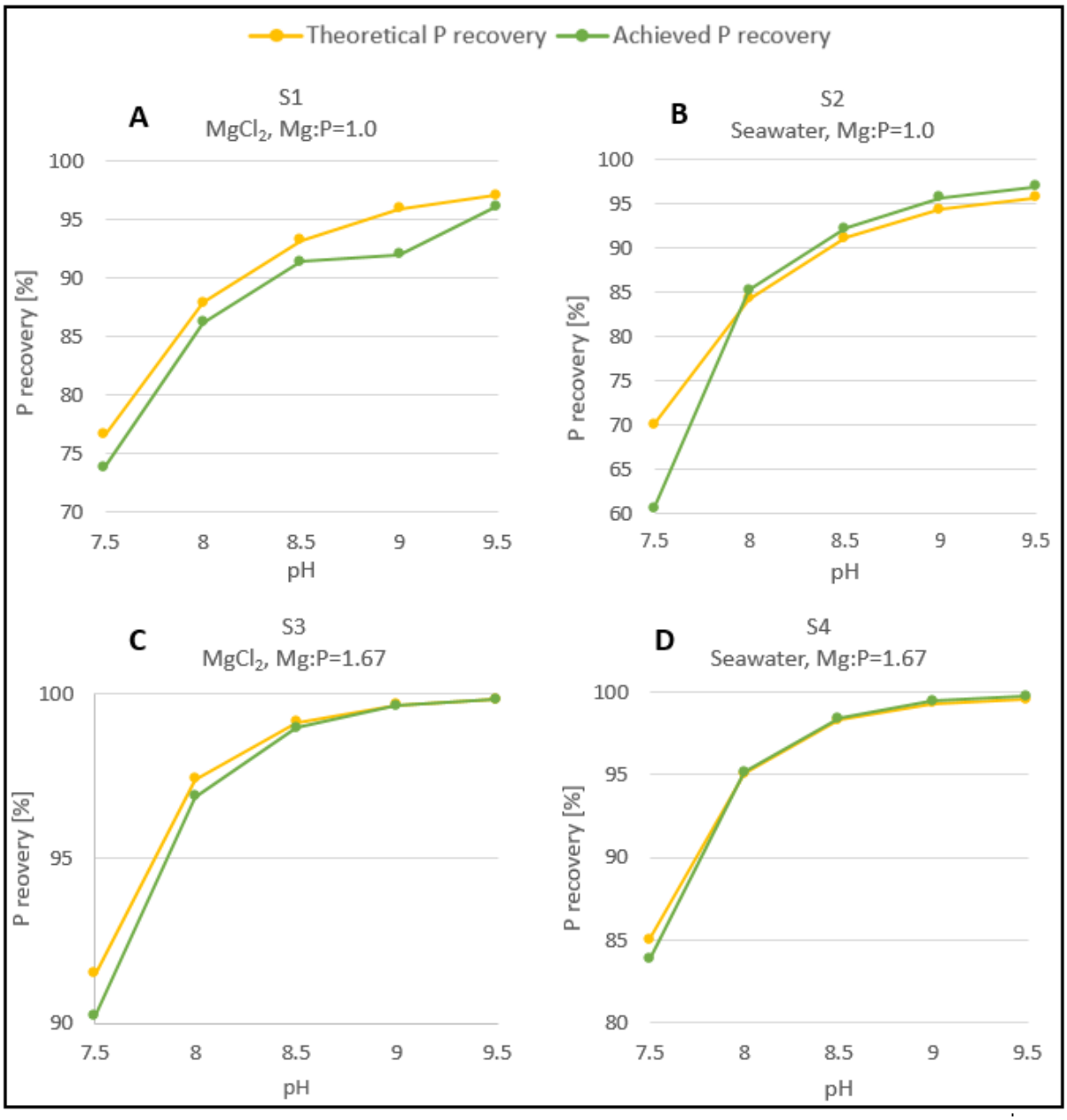

Figure 4-3: Theoretical and achieved P recovery [%] for S1 (A), S2 (B), S3 (C) and S4 (D).

close to theoretical values (Figure 4-3 C and D), meaning the deviation in recovery seen at low pH values in *Figure 4-1* and *4-2* could in fact show that low pH is more critical for P recovery when we use seawater than $MgCl_2$.

4.1.1.2 Production of solids

Figure 4-4 shows that the production of solids at Mg:P=1.0 was about the same for the two Mg sources, although slightly higher for seawater at pH ≥ 8.0. The grey line shows the calculated yield of solids from seawater based on the average molar removal of P and Mg if all solids are assumed to be struvite. It shows that the solids we are able to retrieve from the reactor is overall lower than what we produced according to removal. This makes it difficult to say what is causing a higher yield from seawater compared to $MgCl_2$, as the difference might have other causes than the reaction conditions. Errors due to handling of solids will undoubtedly be a contributor to the total error in yield measurements. Solids are observed sticking to the surface of the reactor, impeller, and particle size instrument and filtering equipment Also, since we are filtering the solids, some small particles might be lost through the filter paper.

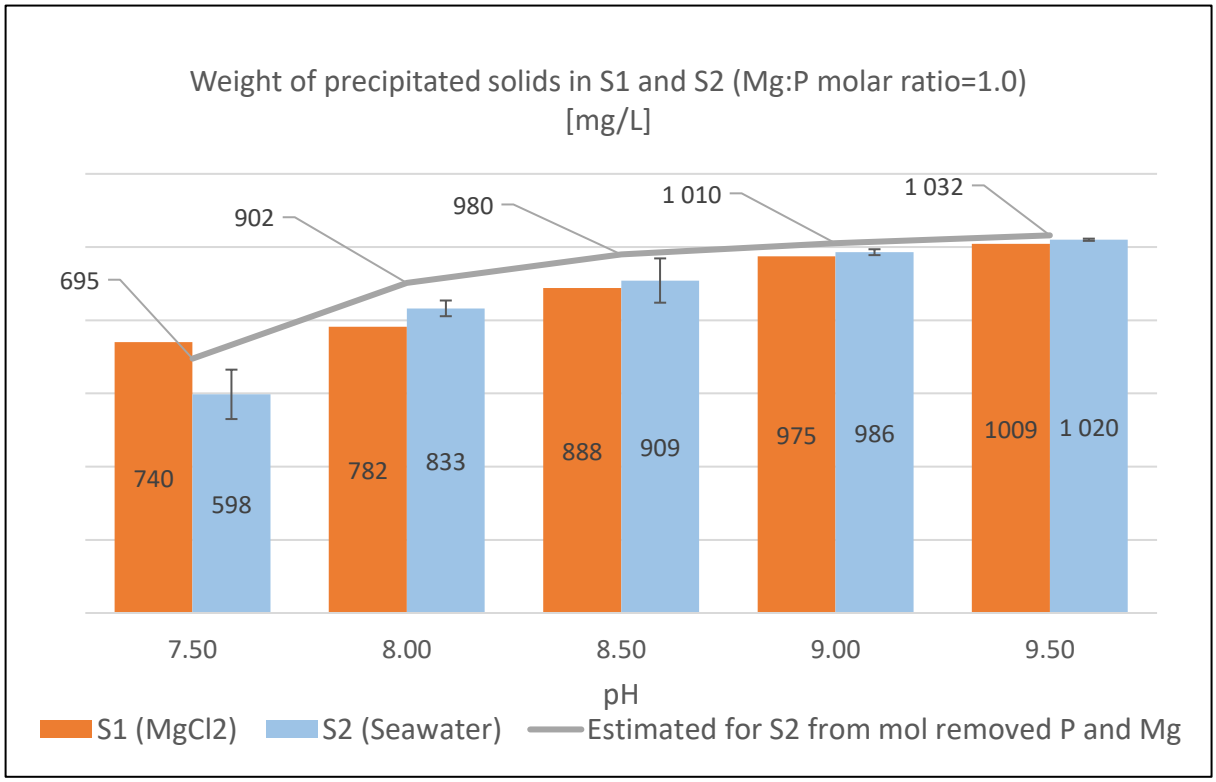

Figure 4-4: Weight of precipitated solids [mg/L] from S1 and S2.
It includes the estimated yield of struvite from average molar removal of P and Mg in S2. The deviation bars of S2 is based on minimum and maximum values from two replicates of the experiments.

There is a chance that other solids, like Ca-P has precipitated in S2, but this can not explain the weight deviation between both the Mg sources (S1 and S2) as well as the deviation between the weighed and estimated yield in S2. If a part of the precipitated solids is a compound with higher molar weight than struvite, then the blue bars should be higher than both the grey line and the orange bars, if no solids are lost. This is based on an assumption that no co-precipitation occurs when using $MgCl_2$ (Only $Mg_3(PO_4)_2$ and struvite are oversaturated in S1). On the contrary, if these solids have lower molar weight than struvite, the blue bar should be lower than the grey line, but not higher than the orange ones. We have already seen that P recovery in S1 was lower than theoretical value, meaning the orange bars should have been higher. Since the difference between the weighed and calculated yield for seawater is up to 70 mg, we can not easily conclude about any of these effects.

An additional comparison of theoretical and achieved Mg recovery could reveal if Ca-P has precipitated in the experiments with seawater. In *Figure 4-5 A*, we see that Mg recovery is below the theoretical for S2, which is the same experiment as where P recovery was higher than theoretical for pH >7.5. Together with observations in *Figure 4-4*, this could indicate that Ca-P with higher molar weight than struvite is precipitating, causing Mg recovery to be lower and the weight of solids to be higher than predicted. The graph in *Figure 4-5 B* is harder to interpret as results at pH 9.5 obviously has a larger error. However, actual Mg recovery at three pH

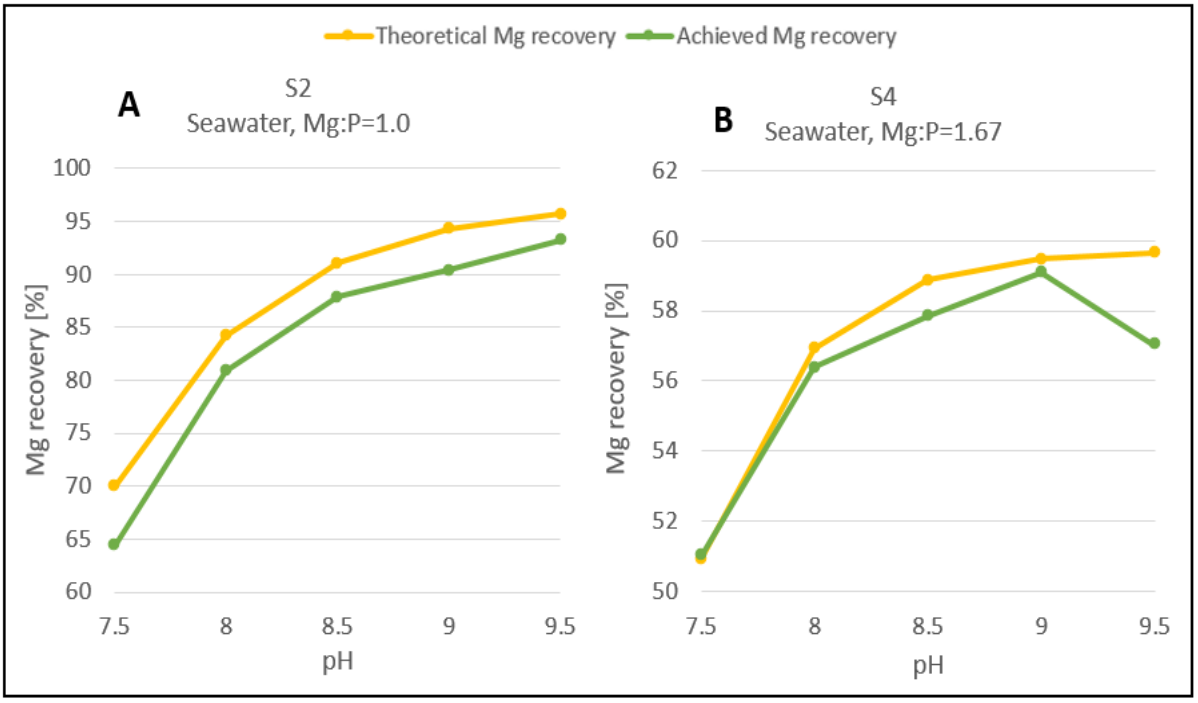

Figure 4-5: Theoretical and achieved Mg recovery [%] in S2 and S4.

values show that we are probably closer to theory than when Mg:P is 1.0.

If we assume that Mg recovery is only a result of struvite precipitation, then the mol/L removed Mg should be the same as mol/L precipitated struvite. Calculating struvite precipitation from mol/L removed P could give wrong yield as some P might precipitate as Ca-P. *Figure 4-6* shows a calculation of struvite solids based on molar removal of P (blue bars) and Mg (orange bars), in addition to the actual weight of retrieved solids from the reactor (grey bars). Since we are certain that some solids are lost during handling, the grey bars show slightly lower weights than what was produced in the reactor. Still, the grey bars are about the same as or higher than the orange bars at pH 9.0 and 9.5. This is in theory only possible if something that is not containing Mg and is heavier than struvite actually precipitated. In practice, this can be due to error in measurements of Mg. At lower pH values, we can not be sure if the grey bars would be higher than the orange ones if all lost solids were added.

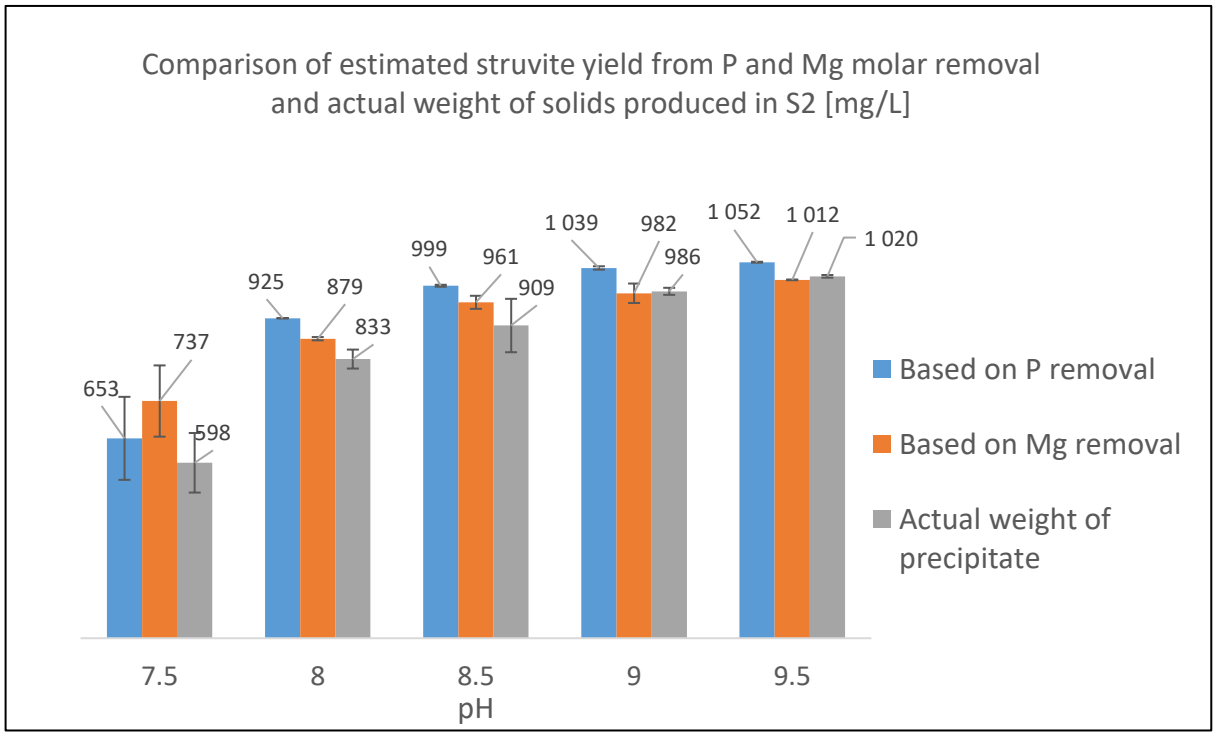

Figure 4-6: Estimated and achieved yield [mg/L] in experiment S2.
The grey bar shows the actual weight of retrieved solids in the experiment. The blue and orange bars show estimated struvite production based on molar removed P and Mg respectively. Deviation indicators show minimum and maximum values achieved in two replicates of the experiment.

As seen in *Chapter 2.2.2*, there exist some critical molar ratios of Mg:Ca and P:Ca that determine the potential for Ca-P to precipitate. An estimate is that both of these molar ratios should be higher than 2:1 to avoid co-precipitation, although this will also depend on other factors, like pH and N:P molar ratio. Seawater is the only contributor to Ca^{2+} when we use synthetic reject water. *Table 4-1* shows the initial Mg:Ca and P:Ca molar ratios in S2 and S4. These are above what we may call critical limits. When struvite is precipitating in the experiments, these molar ratios decrease, giving final molar ratios as given in *Table 4-2*. Final Mg:Ca is far below the critical value for Mg:P=1.0, whereas an Mg:P of 1.67 gives an excess of Mg that is large enough to keep Mg:Ca close to the critical level during the whole experiment. This means that, according to Mg:Ca molar ratio, there is a bigger chance for Ca-P to precipitate when Mg:P is 1.0, which can explain why P recovery is higher and Mg recovery is lower than theoretically possible with seawater for Mg:P=1.0 and not for Mg:P=1.67. P:Ca molar ratio is also lower than critical value, and very low for Mg:P=1.67. The effect of this is less documented in the literature.

Table 4-1: Initial Mg:Ca and P:Ca molar ratios in S2 and S4.

	Intitial Mg:Ca	Initial P:Ca
Mg:P=1.0 (S2)	4.7	4.7
Mg:P=1.67 (S4)	4.7	2.8

Table 4-2: Final Mg:Ca and P:Ca molar ratios in S2 and S4.

	Mg:P=1.0 (S2)		Mg:P=1.67 (S4)	
pH	**Final Mg:Ca**	**Final P:Ca**	**Final Mg:Ca**	**Final P:Ca**
7.5	1.860	1.469	2.304	0.456
8.0	0.914	0.696	2.051	0.137
8.5	0.605	0.369	1.981	0.046
9.0	0.548	0.187	1.924	0.016
9.5	0.317	0.142	2.021	0.008

4.1.1.3 Possible complexations and co-precipitants

According to thermodynamic equilibrium calculations, there are several complexes formed and oversaturated compounds with a potential to precipitate when we use seawater. This is mainly because seawater contains Ca^{2+}, which can form complexes with phosphate and precipitate as Ca-P, but also due to Na^{+}. Some solids are amorphous, while others have crystal structure. Since the thermodynamic model does not consider kinetics, it can not predict which solids will precipitate during a given time. In *Appendix 3*, and overview of oversaturated compounds and their corresponding SI values are given. *Table 4-3* gives an overview of the molecular weights of these solids.

Table 4-3: Molecular weight of oversaturated compounds in S2.

Compound	Molecular weight [g/mol]
Struvite	245.41
Brushite ($CaHPO_4 \cdot 2H_2O$)	172.09
Hydroxylapatite (HAP) ($Ca_5(PO_4)_3OH$)	502.31
$Ca_3(PO_4)_2$	310.17
$Ca_4H(PO_4)_3 \cdot 3H_2O$	500.28
Monenite $CaHPO_4$	136.06
$Mg_3(PO_4)_2$	262.86
Dolomite $CaMg(CO_3)_2$	136.41

Table 4-3 shows that there are several compounds with higher molar weight than struvite, supporting the possibility of Ca-P occurring in solids from experiments. Struvite generally has faster kinetics than hydroxylapatite and amorphous Ca-P, which makes reaction time an additional factor to consider. If our experiments were run for less than 20-30 minutes, we could most likely exclude hydroxylapatite from our solids [52]. Hydroxylapatite (HAP) takes a long time to crystalize as it is formed out of precursors like amorphous calcium phosphate (ACP) (e.g $Ca_3(PO_4) \cdot xH_2O$), octacalcium phosphate (OCP) and brushite. It is therefore more likely to find the precursors than HAP in our solids [58, 59]. For a 1 hour experiment it is difficult to find clear evidence in the literature of possible solid phases that can precipitate. Precipitation of Ca-P is determined by temperature, P and Ca concentrations, ionic strength, pH and the presence of other ions. Brushite has been found to be the first Ca-P to precipitate at 25°C at pH

5.3-6.8, but is probably less likely to form at constant experimental pH values of 7.5-9.5. Amorphous Ca-P (ACP) is more likely to precipitate at high pH than crystalline Ca-P [60].

The most abundant forms of complexes in S1 and S2 found with *Visual MINTEQ* are shown in *Figure 4-7* and *4-8*. They show that the main difference between using $MgCl_2$ and seawater is the availability of HPO_4^{2-}, which is bound to more Ca^{2+} and Na^{+} when we use seawater.

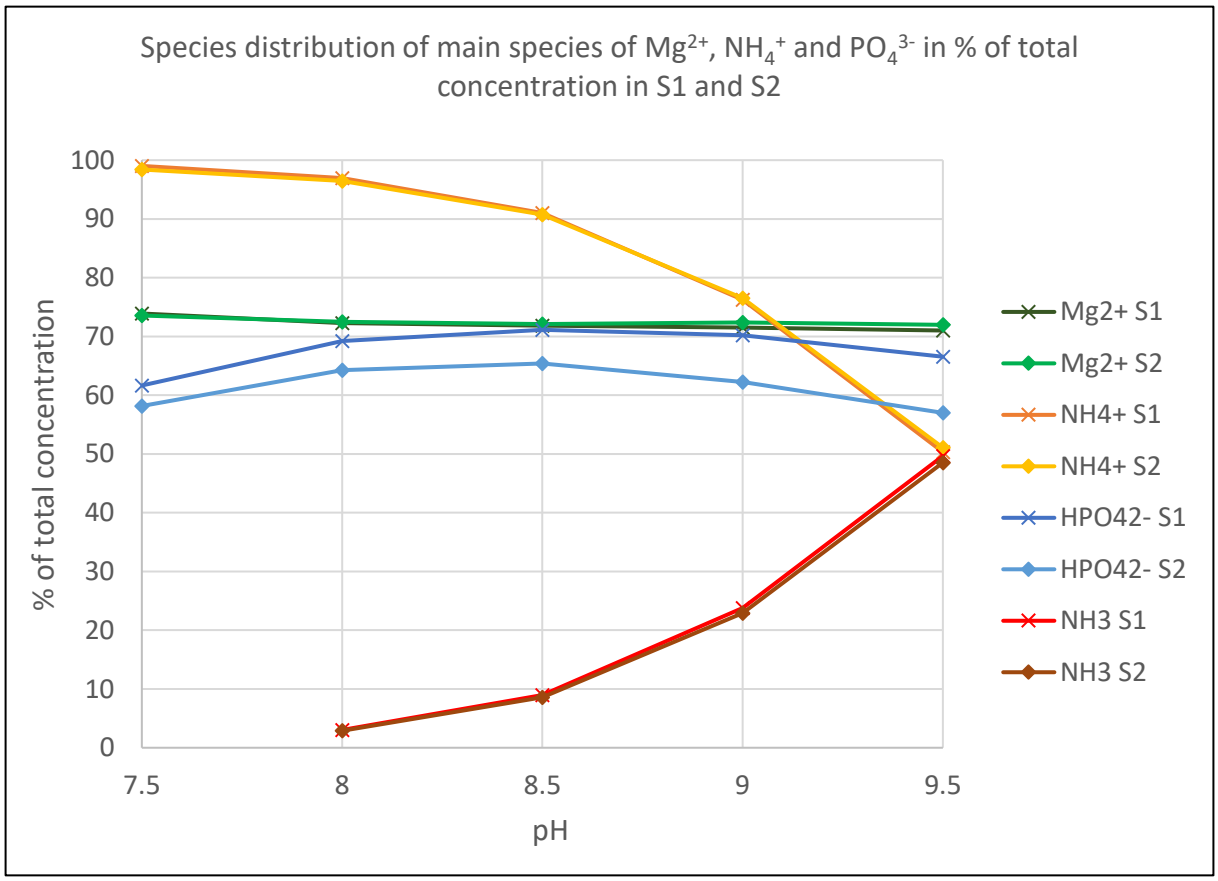

Figure 4-7: Species distribution of struvite components in percent of total concentration. For solutions in S1 and S2. Calculated with Visual MINTEQ.

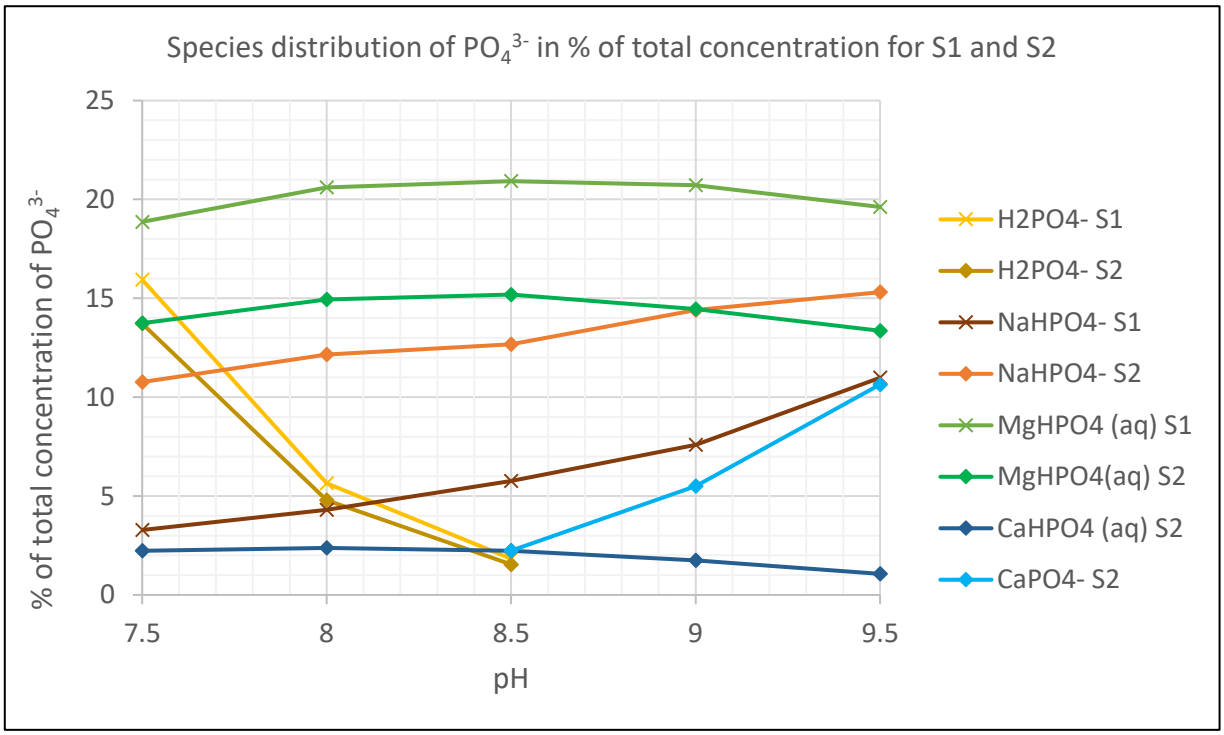

Figure 4-8: Species distribution of PO_4^{3-} in percent of total concentration in S1 and S2..
It includes the most abundant complexes formed (excluding HPO_4^{2-}). Calculated with Visual MINTEQ.

Complexation due to the presence of Na^+ and Ca^{2+} affects the activity of struvite ions. *Figure 4-9* shows that the activity of the three struvite components are lower when we use seawater. PO_4^{3-} is the ion with the lowest ratio with 83%-76% of the activity found when using $MgCl_2$ when Mg:P is 1.0, and 80%-69% when Mg:P is 1.67. The drop from pH 8.5-9.5 can be related to the presence of $CaHPO_4$ (aq), which is increasing rapidly from this point (light blue line in *Figure 4-8*). The activities of Mg^{2+} and NH_4^+ with seawater are approaching the activities when using $MgCl_2$ as pH increase. At the same time, saturation (S_a) has a slower increase with pH when seawater is used (*Figure A3.1* in *Appendix 3*), meaning the combined effect of change in activities makes seawater more inconvenient at higher pH values compared to $MgCl_2$. Still, both the theoretical and achieved P recovery deviated more between the two sources at lower pH values. This may be due to the supersaturation being higher than necessary to recovery all available P at high pH values, such that adequate supersaturation is obtained also with seawater, although slightly lower than the pure Mg source. At low pH, smaller differences in supersaturation are critical for P recovery, and the ionic strength of seawater might introduce this sensitivity to the solution.

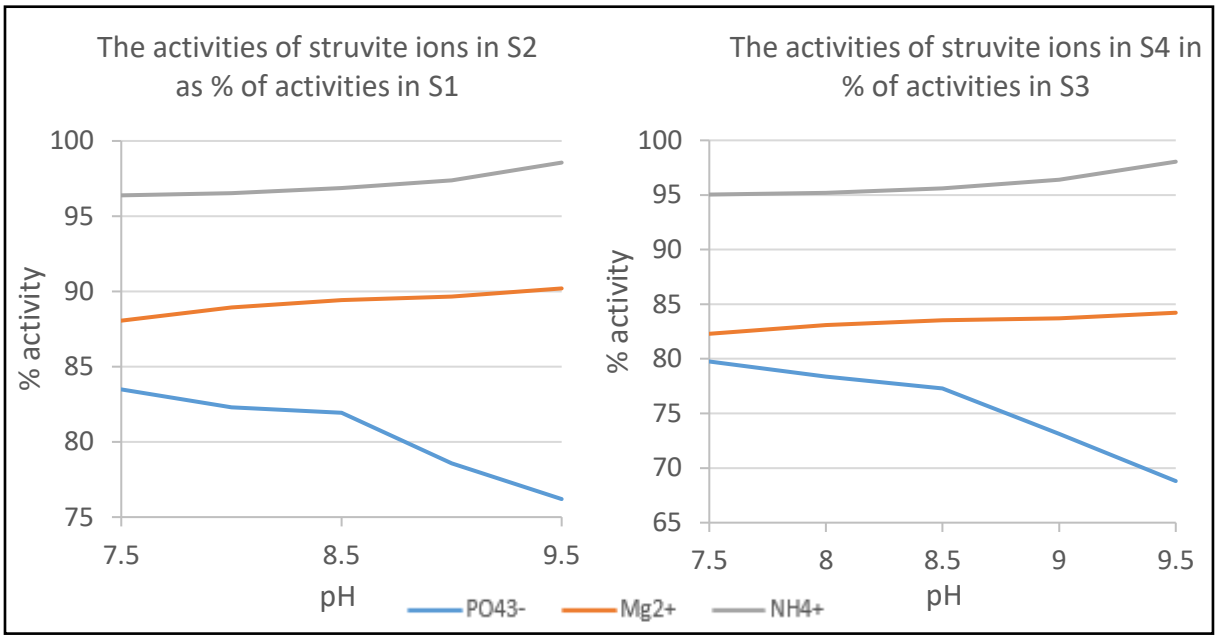

Figure 4-9: Ratio of activities of struvite ions in S2 to S1 [%].
Ratio of activities found with seawater at Mg:P=1.0 (left) and Mg:P=1.67 (right) in % of activities found when using $MgCl_2$. Calculated with Visual MINTEQ.

4.1.2 Dilution effect of seawater at different Mg:P molar ratios (S5 and R5)

4.1.2.1 Achieved and theoretical recovery in S5

These experiments consider the dilution from seawater at four Mg:P molar ratios at a constant pH of 7.5. *Table 4-4* shows the final concentrations of P and N, and the recovery of Mg for series S5. It is clear that as we are adding more seawater, and lowering the concentration of P, the recovery of Mg will be lower, as the theoretical molar ratio of Mg:P for struvite precipitation is 1:1. The final concentration of N shows that high N recovery is not achievable with struvite. *Figure 4-10* shows that the increase in P recovery is higher as Mg:P is raised from 1.0 to 1.67, than for increases at higher Mg:P molar ratios. One reason can be that for higher Mg:P, an increase of supersaturation by increasing Mg concentration is not enough to compensate entirely for a lowering of supersaturation when diluting the reject water and increasing the ionic strength. When Mg:P increases, so does the amount of seawater in the reactor, giving a higher proportion of seawater constituents, and lower initial P and N concentrations.

Table 4-4: Final P and N concentration and Mg recovery of S5 (pH=7.5).

Mg:P	Final PO_4-P [mg/L]	Final NH_4-N [mg/L]	Mg^{2+} recovery [%]
1	54.2	664.1	54.6
1.67	26.7	618.6	46.9
2.34	21.9	603.7	35.6
3.0	17.2	595.5	22.4

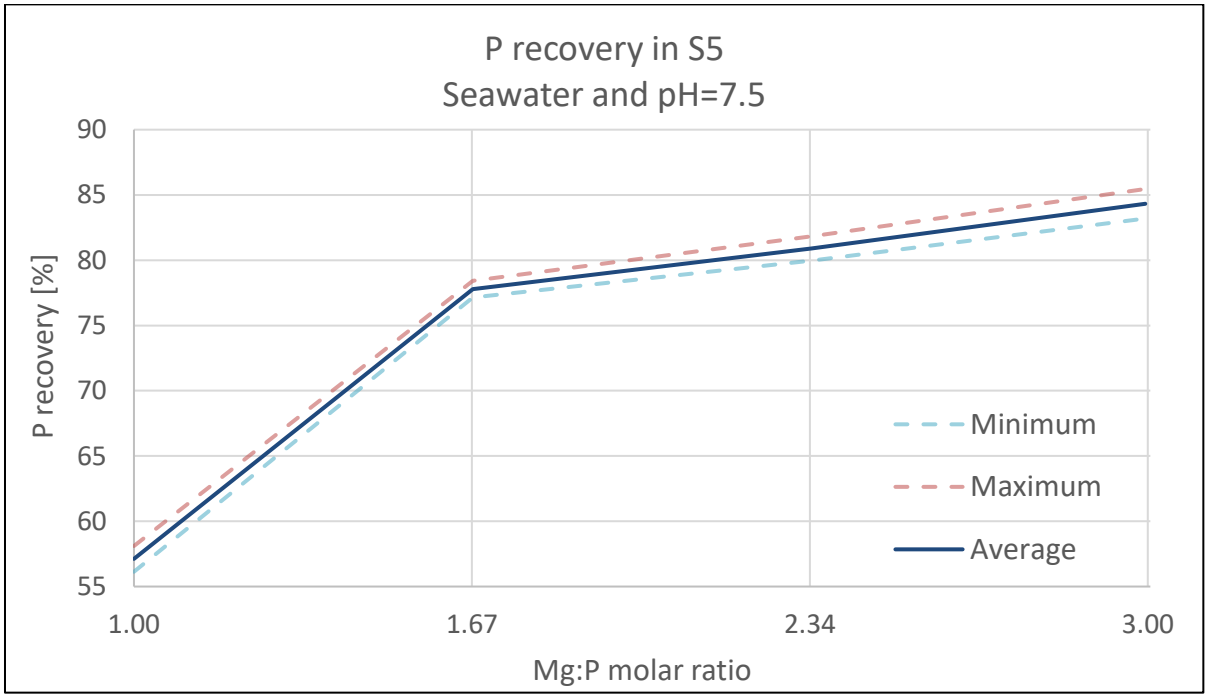

Figure 4-10: P recovery [%] in S5.
Includes minimum and maximum values obtained in two replicates of the experiments.

Thermodynamic equilibrium calculation of S5 shows that up to an Mg:P molar ratio of 3.0, P recovery is lower than theoretical value (Figure 4-11 A). The deviation between theoretical and achieved P recovery is the greatest for Mg.P=1.0, which again shows that low supersaturation experiments are more sensitive to additional impact of seawater constituents. The calculation also shows that as we are increasing Mg:P we get higher P recovery up to a certain point. Beyond Mg:P of 3.0 we will most likely only see an insignificant increase in P recovery, if it increases at all.

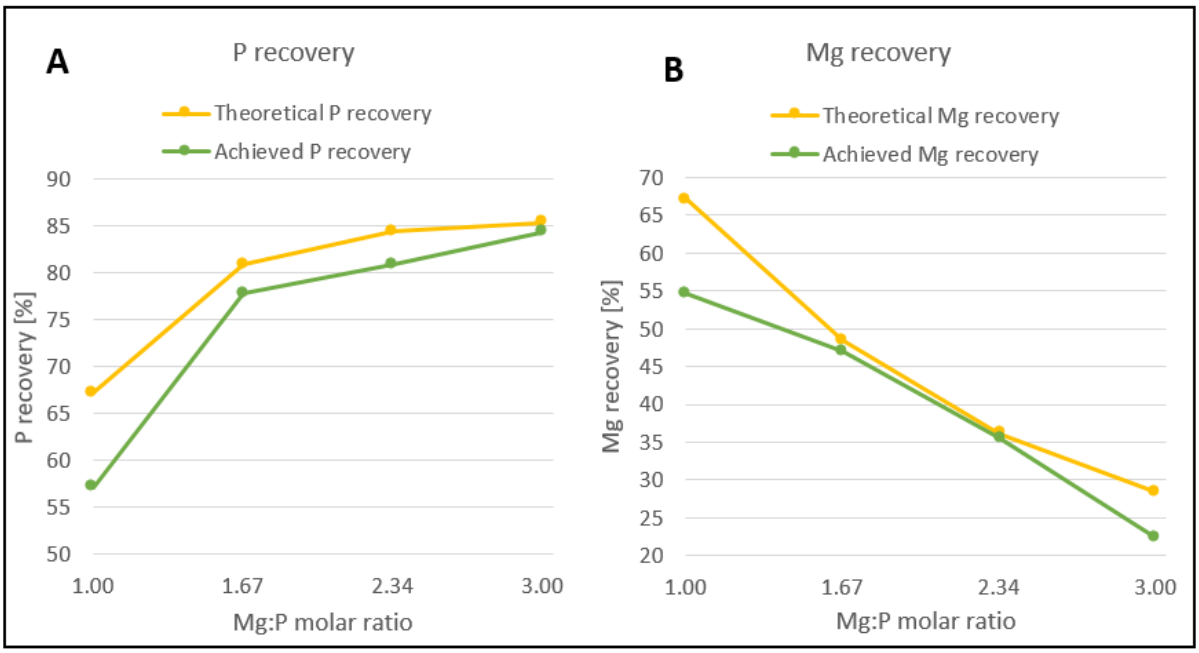

Figure 4-11: Theoretical and achieved P and Mg recovery [%] in S5.

4.1.2.2 Production of solids in S5

Figure 4-12 shows the theoretical and achieved solids production per litre of reactor solution, as well as estimations of produced struvite based on molar removal of P and Mg. We can see that actual yield (yellow line) is below theoretical value, but they follow the same trend. The actual yield also follows the same trend as estimated yield based on molar P recovery (orange line), while estimated yield based on Mg recovery deviates from the other trends at Mg:P=3.0. We see that Mg recovery also deviate from theoretical value at Mg:P of 3.0 and 1.0 (Figure 4-11 B). The same can be seen for P recovery at Mg:P of 1.0, where the explanation might be that supersaturation is too low for equilibrium to be established. We do, in fact, have lower supersaturation at Mg:P=1.0 in S5 than at pH 7.5 in experiment series S2, where the combined effect of ionic strength and low pH seemed to cause very low supersaturation. In S5, we are diluting P and N concentrations, meaning supersaturation is even lower. At Mg:P=3.0, P recovery is closest to theory, while Mg recovery drops in comparison. At the same time, weight of produced solids is higher than what Mg recovery indicates. This is either caused by errors in ion concentration measurements of Mg, or it is a sign that Ca-P is precipitating.

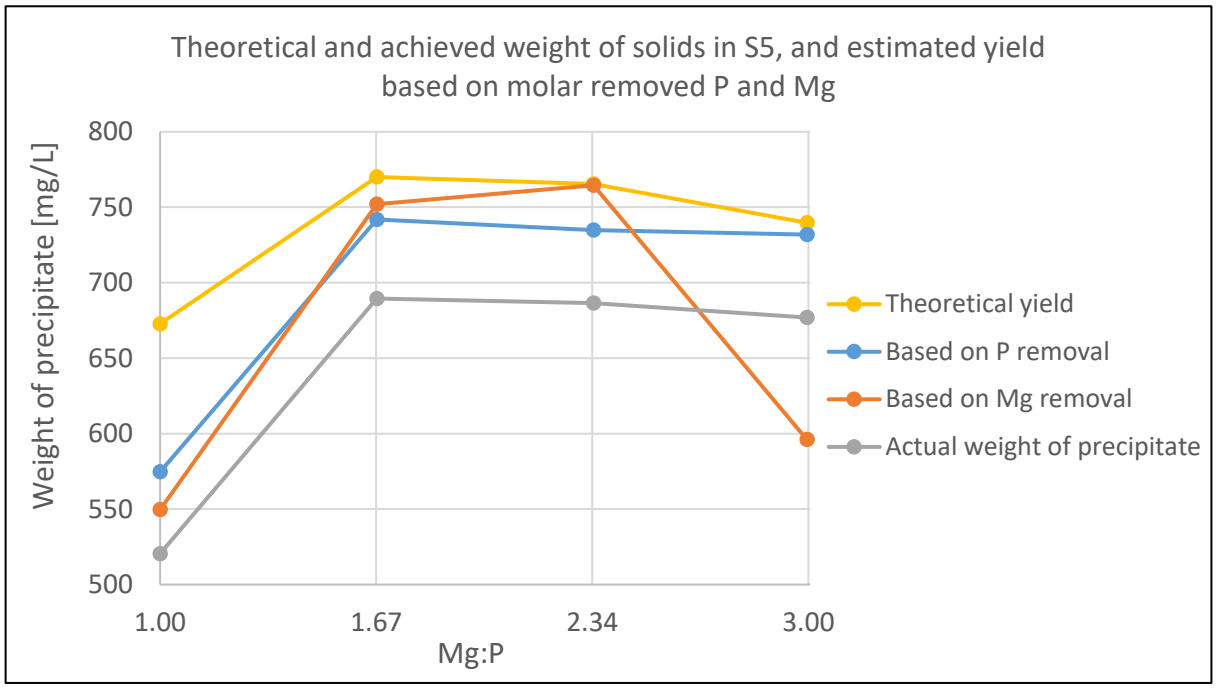

Figure 4-12: Theoretical, estimated and achieved yield [mg/L] in S5. Theoretically calculated yield of struvite, actual weight of solids from experiment series S5 and estimated yield of struvite from molar removal of P and Mg in S5.

Since increasing Mg:P molar ratio with dilution means a higher Ca:P molar ratio when we use seawater, it is important to consider it in these experiments. *Table 4-5* shows that the final Mg:Ca molar ratio is not below 2:1 at any Mg:P, but it is also not that high that we are certain that Ca-P will not precipitate. Final P:Ca molar ratio is also very low, and this combination makes it more probable that Ca-P can precipitate towards the end of each experiment. It is, however, not clear which combination of molar ratios will favour the formation of Ca-P the most.

Table 4-5: Initial and final Mg:P, Mg:Ca and P:Ca molar ratios in S5.

Mg:P	Initial Mg:Ca	Final Mg:Ca	Initial P:Ca	Final P:Ca
1.0	4.7	2.12	4.7	2.01
1.67	4.7	2.48	2.8	0.62
2.34	4.7	3.01	2.0	0.38
3.0	4.7	3.63	1.6	0.24

Table 4-6 shows the saturation index for all oversaturated compounds in the S5 solution. The number of compounds is lower than in S2 (Table 4-3), and saturation indexes are also generally lower. This is expected, as we are diluting the solution at low pH. By increasing Mg:P molar ratio, we also increase SI for all compounds except struvite, which only increase up to Mg:P of 2.34. The SI of struvite is almost the same for Mg:P of 1.67 and 3.0, meaning the peak SI should appear close to Mg:P of 2.34.

Table 4-6: Oversaturated compounds in S5.

Saturation indexes at different Mg:P molar ratios for oversaturated compounds				
Compound	**1.0**	**1.67**	**2.34**	**3.0**
Ca3(PO4)2 (am2)	1.225	1.574	1.759	1.866
Ca3(PO4)2 (beta)	2.216	2.665	2.851	2.958
Ca4H(PO4)3:3H2O(s)	1.786	2.22	2.443	2.566
CaHPO4(s)	0.287	0.374	0.412	0.429
CaHPO4:2H2O(s)	-	0.066	0.104	0.12
Hydroxyapatite	9.881	10.492	10.825	11.022
Struvite	0.9	0.955	0.966	0.957

4.1.2.3 Achieved recovery in R5

The experiments with real reject started with the reject including suspended solids. The effect of suspended solids has been studied by doing the same experiments with unfiltered and filtered reject water. The comparison of results with and without filtration of reject water showed marginal differences in recovery of P and Mg (Figures 4-13 and 4-14), showing that suspended solids has no substantial effect on ion interaction for struvite precipitation. However the final product in case of precipitation with suspended solids was a mixture of crystals and solids. This lower the purity of product. Results indicate that the two types of reject waters have the same supersaturation, even though real reject water contains more impurities than synthetic. In this discussion, it is important to notice that the amount of added seawater is slightly lower when using real reject water, compared to synthetic, as seen from *Table 3-6*. There is, however, signs of seawater already being a part of the reject water. The concentration of Ca^{2+} in the reject water was calculated to be around 40 mg/L. Together with measured initial concentrations of P and Mg, this gives initial Mg:Ca and P:Ca molar ratios in experiments of R5 as shown in *Table 4-*

7. The Mg:Ca is likely to be halved at Mg:P=1.0 during the experiment (as seen in *Table 4-5*), giving Mg:Ca below 2:1. Calcium inhibition could potentially be a problem in these experiments.

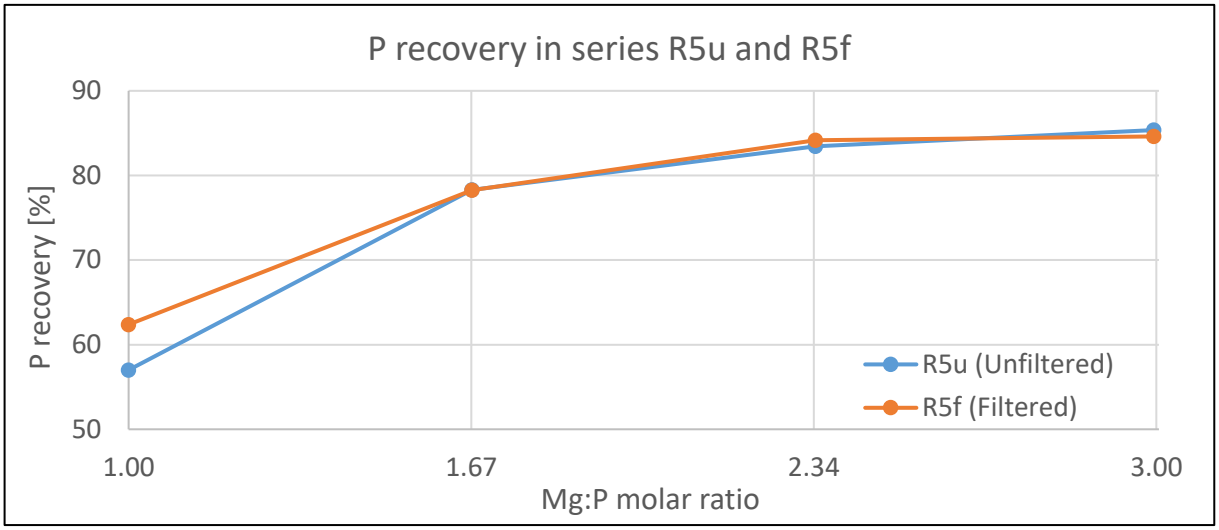

Figure 4-13: P recovery [%] in R5u and R5f. pH=7.5

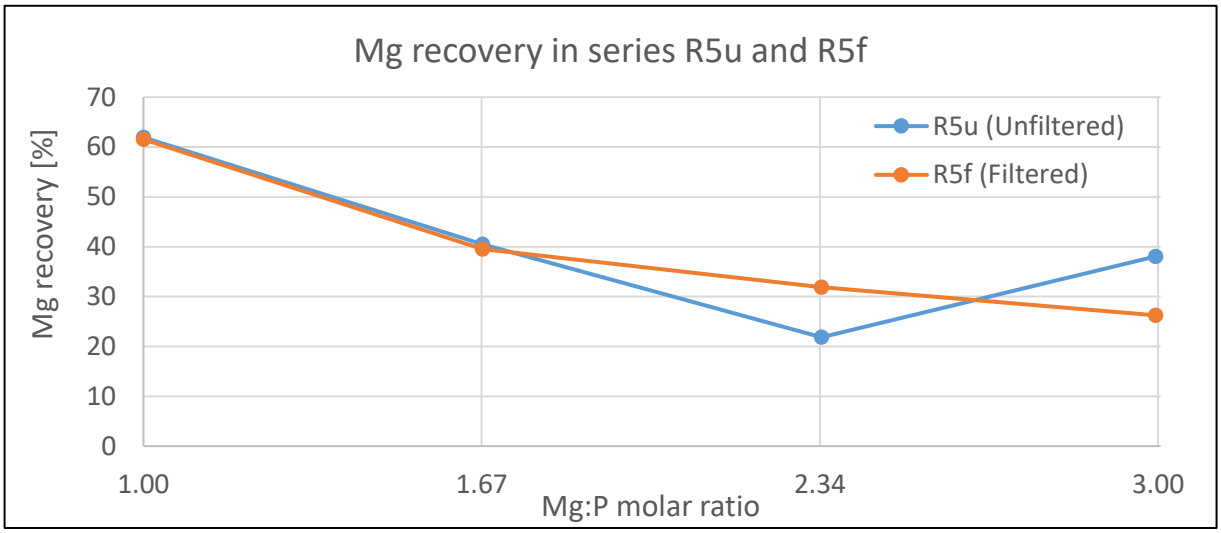

Figure 4-14: Mg recovery [%] in R5u and R5f. pH=7.5.

Table 4-7: Initial molar ratios of Mg:P, Mg:Ca and P:Ca in R5.

Mg:P	Mg:Ca	P:Ca
1.0	2.47	2.77
1.67	3.15	2.00
2.34	3.38	1.58
3.0	3.90	1.30

4.1.2.4 Production of solids and theoretical recovery in R5

The average molar removal of P, Mg and N in R5u and R5f is shown in *Table 4-8*, together with estimated struvite production. The ideal case for molar ratio of recovered ions is 1:1:1 - the molar ratio in struvite -, but deviation might occur due to internal factors, like lower ion activity with respect to pure system, or external factors, like cuvette test errors, pipetting errors etc. The estimated struvite production is calculated from the two most reasonable values of molar recovery, based on a molecular weight of struvite of 245.41 g/mol. The production is given in mg per liter of reactor content (mg/L react.) and mg per liter of reject water (mg/L reject). We can see that the production of solids per liter of reject water is increasing more compared to production per liter of reactor content. This shows that although P recovery is not increasing much for high Mg:P molar ratios, we are still able to produce more struvite from each unit of reject water.

Table 4-8: Recovery [mmol/L] of P, N and Mg, and estimated struvite production in R5. Values are based on average molar removal in R5u and R5f. Estimated struvite production is given in mg /L reactor content and mg/L reject water.

Mg:P molar ratio	P recovery [mmol/L]	N recovery [mmol/L]	Mg recovery [mmol/L]	Estimated Struvite production [mg/L react.]	Estimated Struvite production [mg/L reject]
1.0	2.41	1.95*	2.22	568	597
1.67	3.03*	2.47	2.44	603	666
2.34	3.14	2.99	2.16*	752	872
3.0	3.04	3.87*	3.51	804	973

***Not included in the calculation for estimated struvite production**

Figure 4-15 shows that the weight of produced solids in synthetic (S5) and real reject (R5f) are almost the same, like the similarity in P recovery also indicates. Comparing this to the estimated weight of struvite based on molar removal of P and Mg shows that P recovery (blue line) gives a better picture of the actual production than Mg recovery (orange line). This is because Mg recovery is below theoretical value in these experiments (see *Figure 4-16*). P recovery, on the other hand, is very close to theoretical recovery (see *Figure 4-17*), and struvite yield estimated from molar P removal matches very well the theoretical struvite production (blue and yellow lines in *Figure 4-15*).

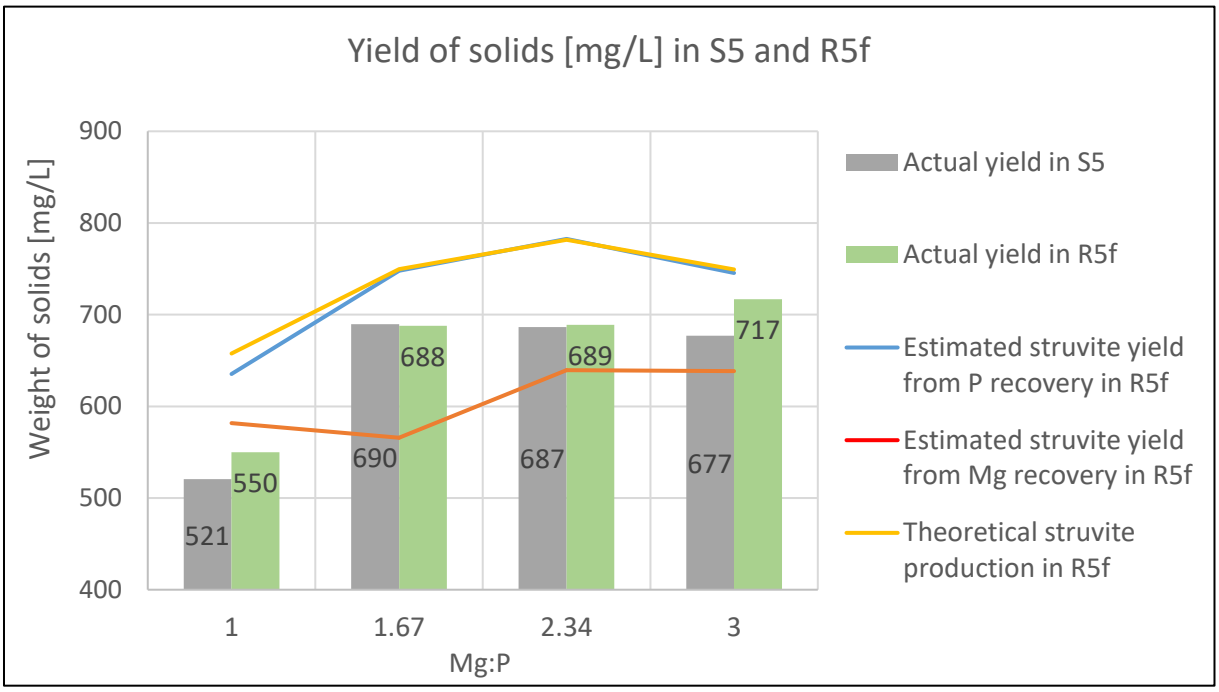

Figure 4-15: Yield of solids [mg/L] from S5 and R5f.
Dry solids weight of solids produced in S5 and R5f, estimated struvite precipitation based on molar removal of P and Mg in R5f, and theoretical struvite production in R5f.

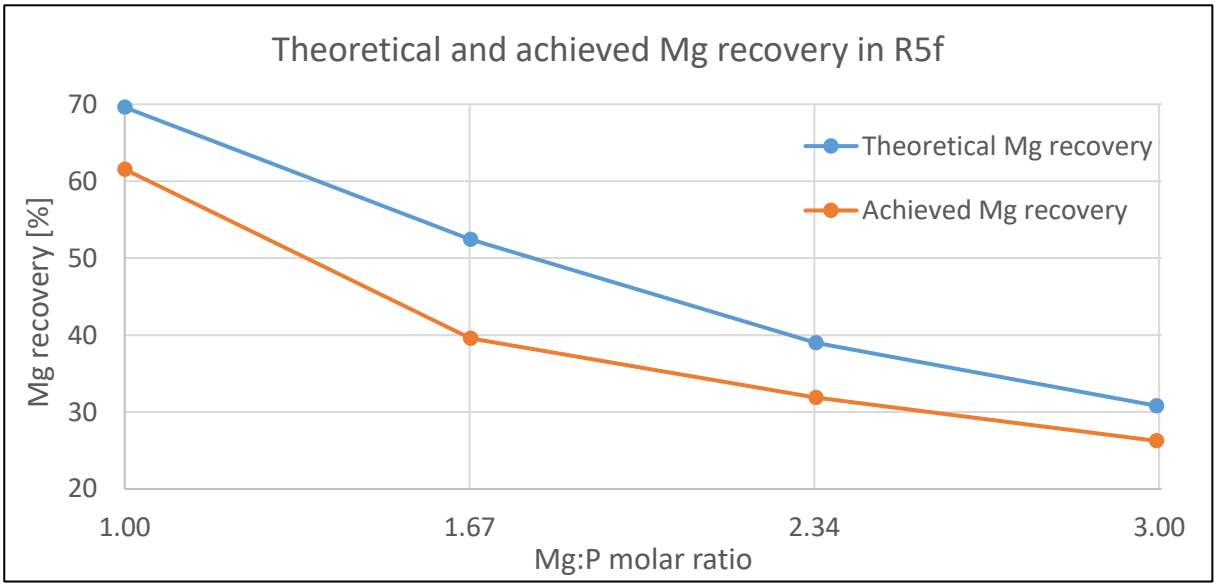

Figure 4-16: Theoretical and achieved Mg recovery [%] in R5f. pH=7.5.

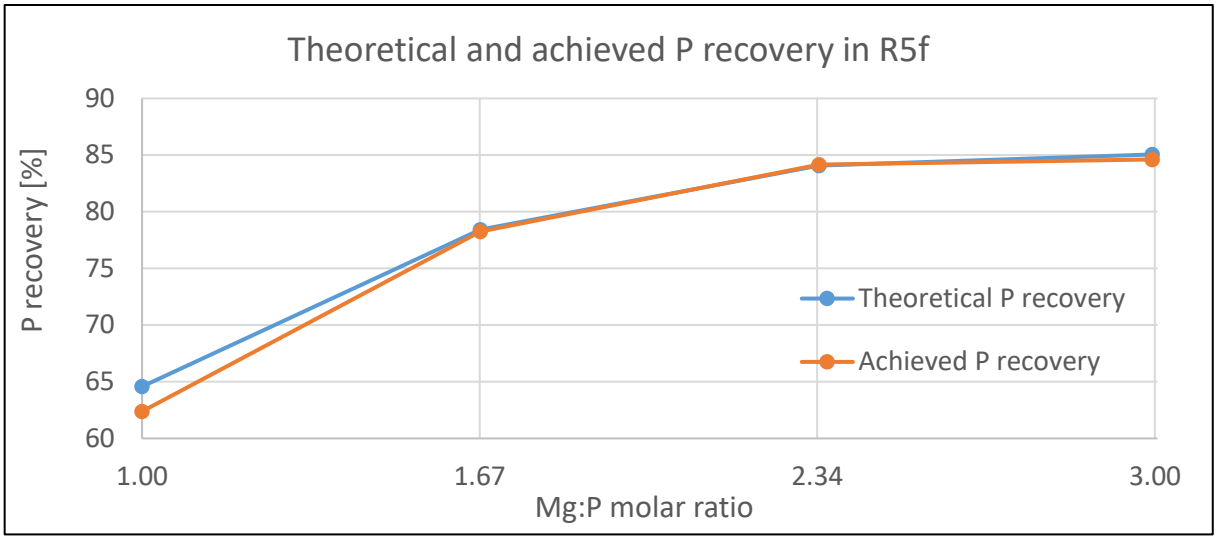

Figure 4-17: Theoretical and achieved P recovery [%] in R5f. pH=7.5.

Since the actual yield of solids was higher than the estimated yield of struvite based on Mg removal, there are either errors in Mg measurements or solids containing P and not Mg that have precipitated alongside struvite. This will be further discussed when solids are analyzed in *Chapter 4.3*.

4.1.3 Dilution effect of seawater at different Mg:P molar ratios and pH (R6)

4.1.3.1 Achieved and theoretical recovery

In these experiments, pH was elevated to 8.0 and 8.5 for the case of filtered reject water at Mg:P 1.67 (R6a) and 2.34 (R6b) with dilution from seawater. Results at pH 7.5 are included from experiment series R5f. A P recovery higher than 90% was achieved for pH 8.0, at Mg:P molar ratios of both 1.67 and 2.34, as seen in figure 4-18. Almost 85% recovery could be achieved at pH 7.5 at Mg:P=2.34. The results indicate that it is possible to increase recovery only by increasing the magnesium concentration, and this effect is greater at lower pH. When Mg:P is increased from 1.67 to 2.34 at pH 7.5, the P recovery is increased by 6-7%, whilst at pH 8.5, the difference is less than 1%. This can be due to phosphate becoming the limiting substance for precipitation at Mg:P of 2.34 and 3.0

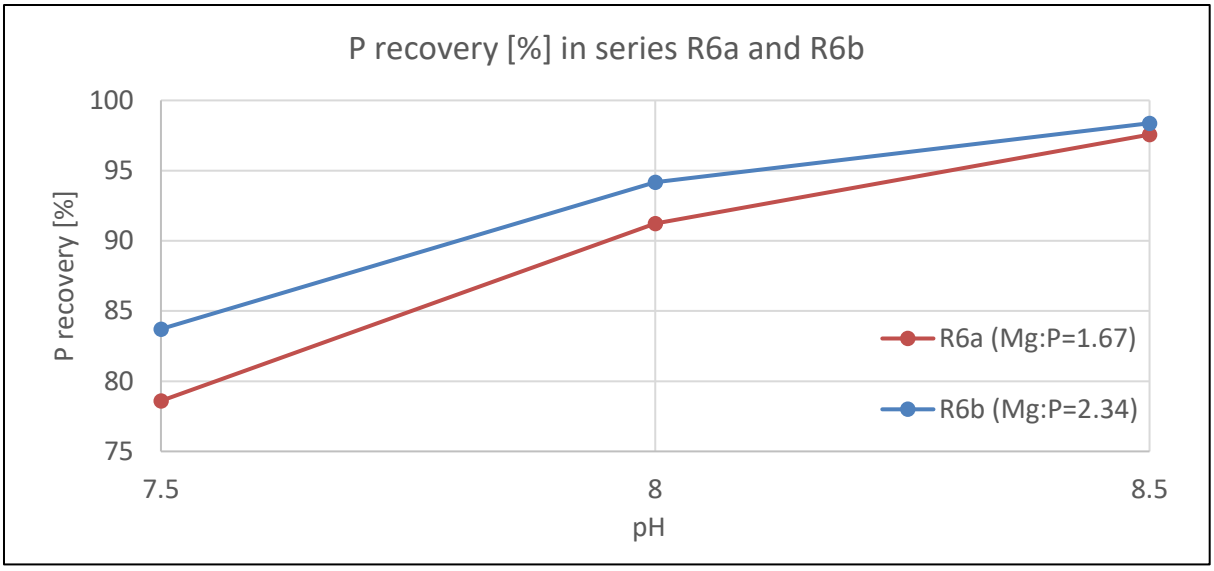

Figure 4-18: P recovery [%] in R6a and R6b.

Perhaps the best contribution to the assessment of seawater as Mg source compared to a pure source is when we compare the two sources under the condition that seawater is diluting the reject water and $MgCl_2$ is not. *Figure 4-19* shows that at Mg:P=1.67, $MgCl_2$ is performing better than seawater, although they both give P recovery higher than 90% for pH > 8.0. Here, $MgCl_2$ is used in synthetic reject water, while seawater is used in real reject water. The performance is more different at lower pH, as observed in other experiments. This result shows that we can not expect seawater to give the same P recovery as a pure source, but it still gives acceptable results.

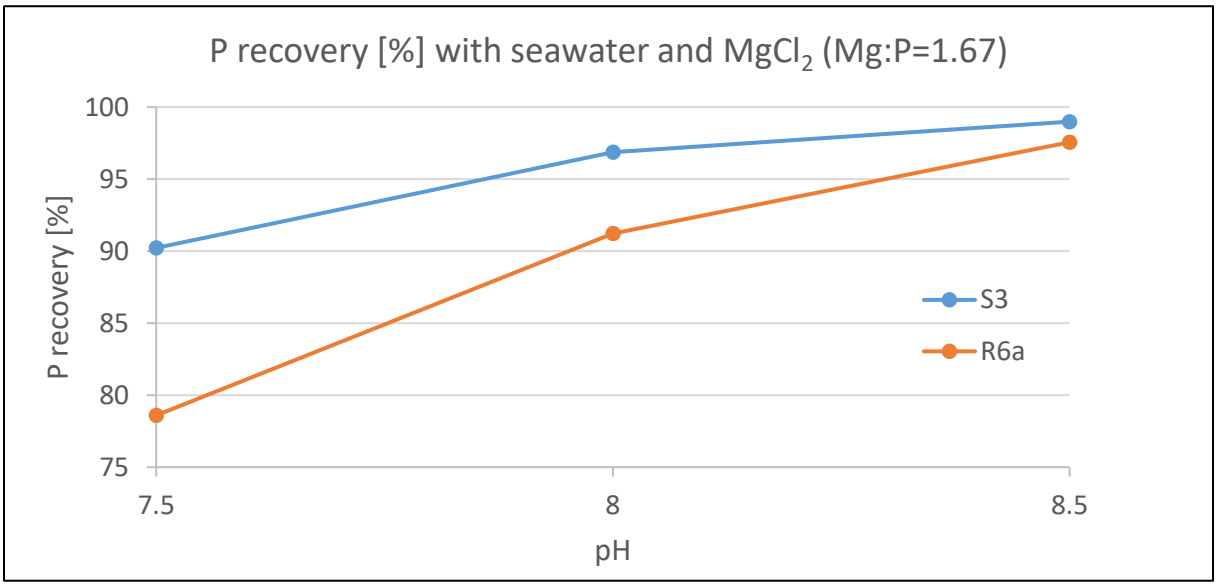

Figure 4-19: P recovery [%] in R6a compared to series S3.

4.1.3.2 Production of solids

The solids that precipitated in these experiments were filtered, dried at room temperature and weighed, and the result can be seen in *Figure 4-20* and *Figure 4-21*. It shows that more precipitate was produced at pH 8.5 than 8.0. Although the yield from the solution mix of reject water and seawater decreases with increasing Mg:P molar ratio, the solids production increases per unit of reject water introduced to the reactor. This means that although seawater has a dilution effect, we can still produce more struvite by increasing Mg:P molar ratio.

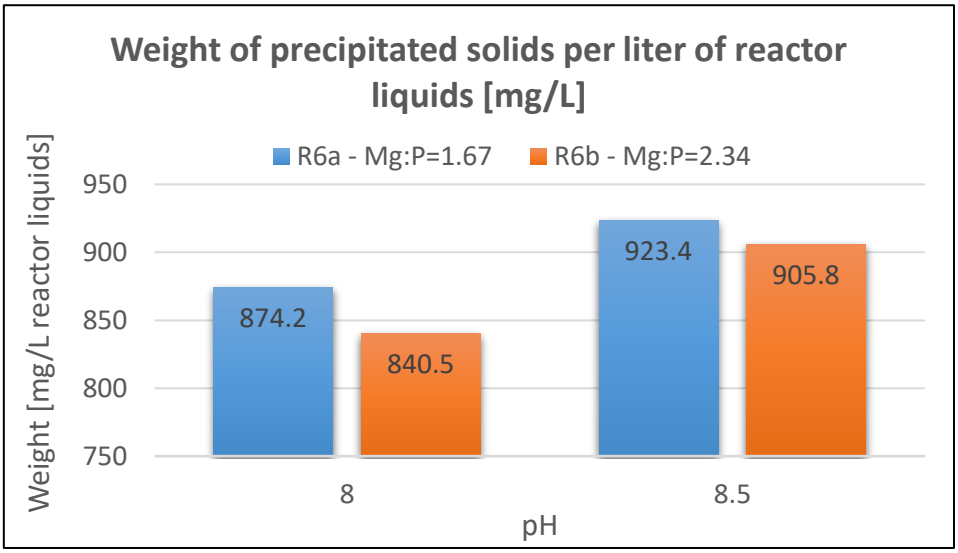

Figure 4-20: Weight of precipitated solids in R6a and R6b. Given in mg per litre of reactor liquids.

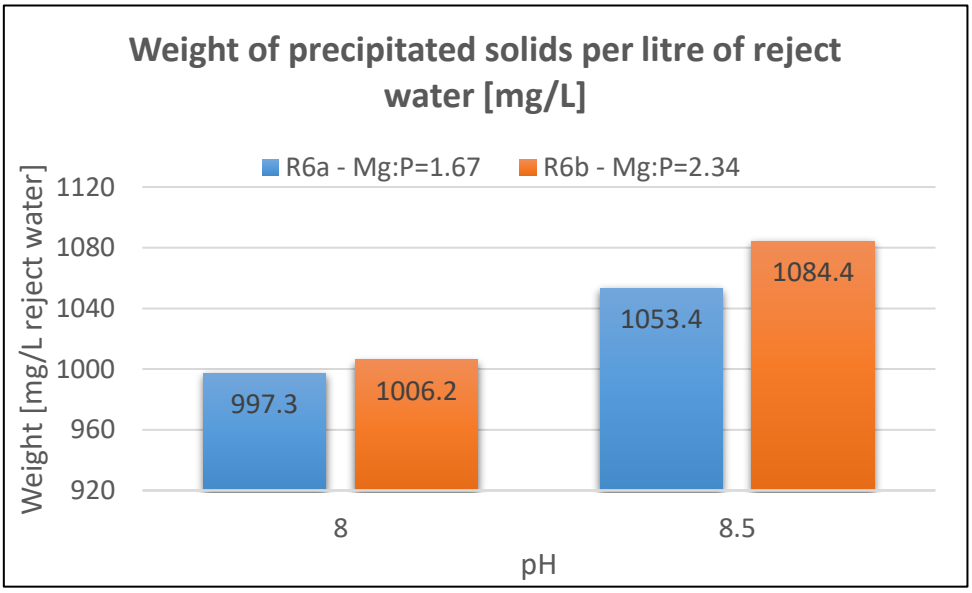

Figure 4-21: Weight of precipitated solids in R6a and R6b. Given in mg per litre of reject water

The achieved production of solids per litre reject water is close to theoretical values when we compare *Figures 4-21* and *4-22*. Although it seems like the effect on yield from increasing Mg:P is larger at pH 8.5 than 8.0 from the experiment results, the theoretical calculations show that the increase of yield is higher at low pH. This means that increasing Mg:P molar ratio at lower pH values is more efficient than increasing it at higher pH. This correlates well with how P recovery is affected by Mg:P, as seen in *Figure 4-18*.

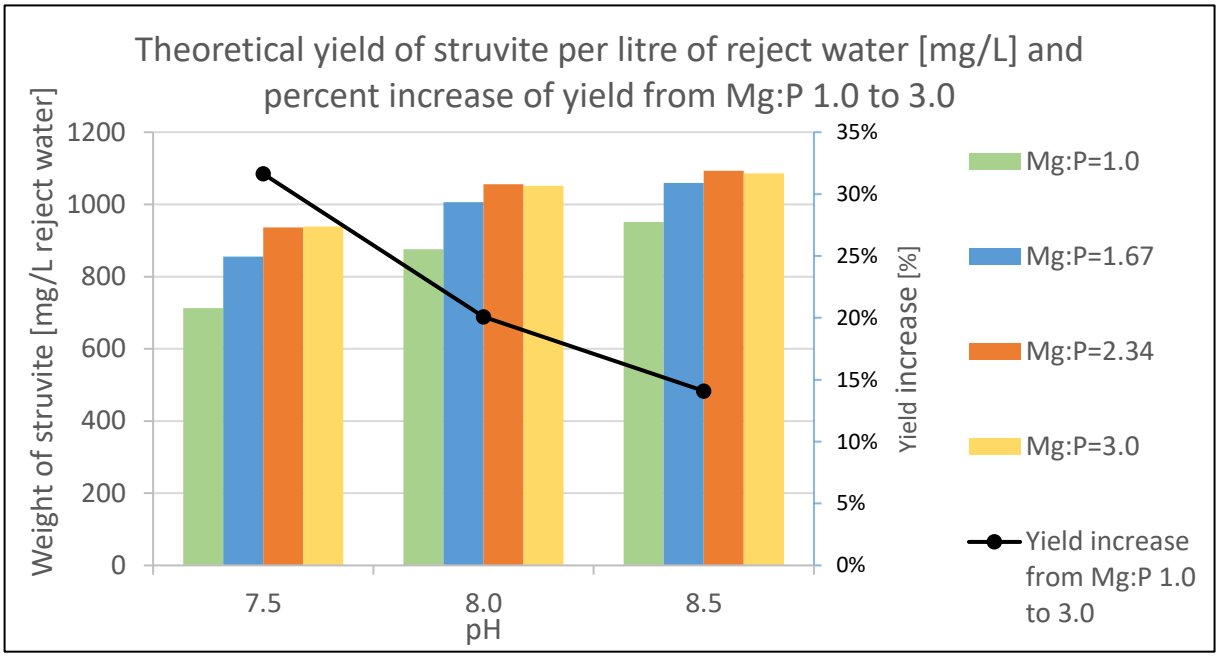

Figure 4-22: Theoretical struvite yield at different pH and Mg:P molar ratios. Given in mg per litre of reject water. It includes the percent increase (black line) of theoretical yield between Mg:P=1.0 and Mg:P=3.0. Compositions of reaction liquids used in Visual MINTEQ corresponds to those of experiment series R5 and R6.

4.1.3.3 Reaction kinetics

The speed of reaction is important, as a struvite reactor should have a specific hydraulic retention time (HRT). In our experiment, the time for stable pH was registered, meaning the time until reactions are finished and we reached equilibrium between solid and soluble phases. The reference for stable pH was the *Mettler Toledo* pH meter, which has a" stable pH" indicator.

At the lowest pH, the reactions are quite slow, and even though the pH meter indicates a stable pH, it keeps changing very slowly, almost until 60 minutes have past. *Table 4-9* shows the time from the experiment started until pH was stable in R6a and R6b. It shows that increasing pH

also increase the rate of reaction leading to struvite crystallization. The same was observed for all experiments. Mg:P molar ratio is not affecting the rate of precipitation to the same extent.

Table 4-9: Time [min] from experiment started until stable pH is obtained.

Time until stable pH (until end of reaction) [min]			
Mg:P	**pH=7.5**	**pH=8.0**	**pH=8.5**
1.67 (R6a)	35-40	16	10-12
2.34 (R6b)	35	20	4

4.2 Additional thermodynamic calculations

It was noticed in *Chapter 4.1.2.2* that SI of struvite had a peak appearing at an Mg:P molar ratio around 2.34 for experiment S5 (pH=7.5, seawater as magnesium source and synthetic reject water). To see if the same trend also appear for other P and N concentrations (220 mg P/L and 1200 mg N/L, with N:P still at 12), another thermodynamic equilibrium calculation was made with the same seawater characteristics, dilution and pH as in S5. The only difference, except increasing P and N, was that we excluded the contribution of Cl^- from the NH_4Cl salt, which is a big part of total Cl^- in the reactor. This was in order to make the model closer to a real case. This is also why SI for struvite is deviating between *Figure 4-23* and *Table 4-6*. We observe in *Figure 4-23* and *4-24* that the maximum SI occurs at Mg:P ~2.0 for [P]=137 mg/L and Mg:P~1.3 for [P]=220 mg/L. The seawater amount is in both cases around 15%. It could be a sign that there is an optimum amount of seawater occurring around this point. It also seems like the higher the [P], the lower is the optimum Mg:P. It can be explained from the ionic strength, as activity of struvite component ions gets lower when the concentration of other ions increase. Seawater is the only contributor to ionic strength in the case of synthetic reject water in the calculation, except for some Na^+ from the phosphate salt. This also emphasize that the contribution of Cl^- from the NH_4Cl salt is affecting our results.

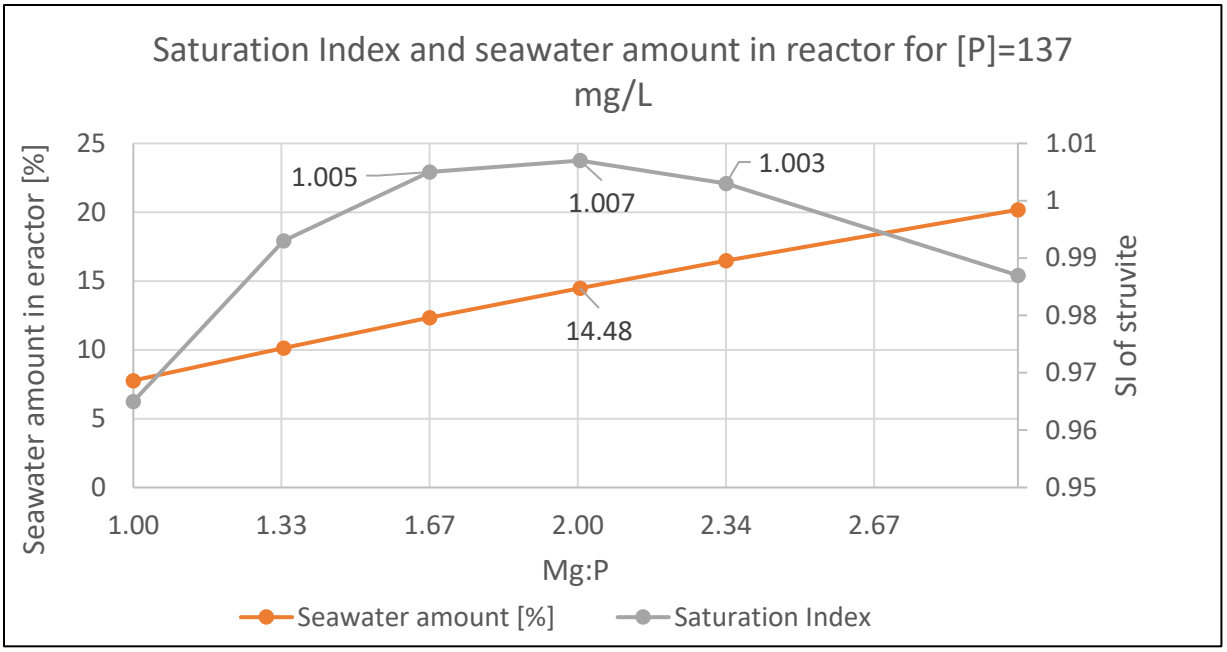

Figure 4-23: Visual MINTEQ calculations of SI of struvite and corresponding seawater amount. The amount of seawater is given as percent of total volume in the reactor. Reaction conditions corresponds to experiment S5, only with less Cl^- in the solution.

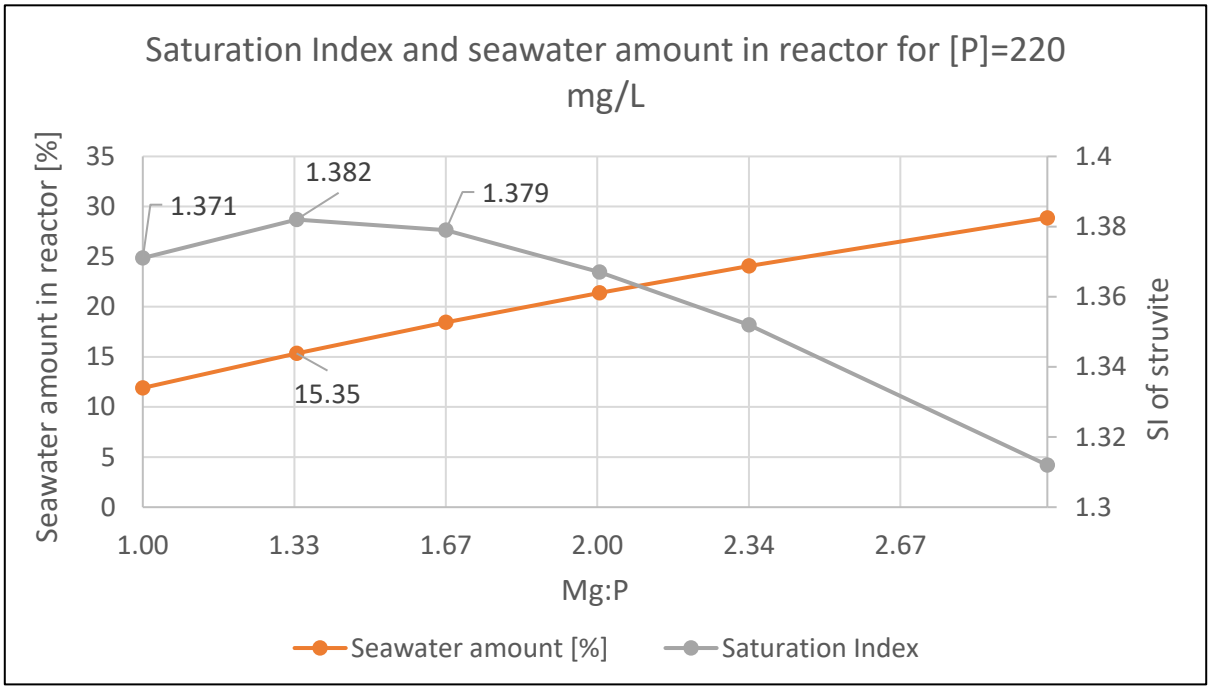

Figure 4-24: Visual MINTEQ calculations of SI of struvite and corresponding seawater amount. The amount of seawater is given as percent of total volume in the reactor. Reaction conditions corresponds to experiment S5, only with higher P and N concentrations and less Cl^- in the solution.

4.3 Phase characterization

The purity of products can be studied by using X-ray diffraction (XRD), which utilize the diffraction angle and lattice spacing in crystals to identify the composition of crystalline materials. The result is a diffraction pattern that can be identified by comparing it to known compounds, like in *Figure 4-25* and *Figure 4-26*. Here, the reference struvite diffraction pattern is of 98% struvite from *Alfa Aesar* by *Thermo Fischer Scientific*. We can see that for both synthetic and real reject water, at different Mg:P and pH, the diffraction patterns are almost identical in the way that the position of peaks are the same as the reference along the 2-theta axis (X-axis). The intensity of each peak (hight) is also matching well, at least for the smaller peaks. To determine whether the solids contain amorphous compounds (like ACP), the sharpness and halo formation (graph is elevated from the baseline) should be studied [59, 61]. *Figure 4-27* shows examples of XRD patterns of possible co-precipitants. Here, crystallized compounds, like brushite (in green) and stoichiometric hydroxylapatite (in black) have well-defined peaks and no halo, whereas ACP (in blue) has no distinct peaks and forms a halo.

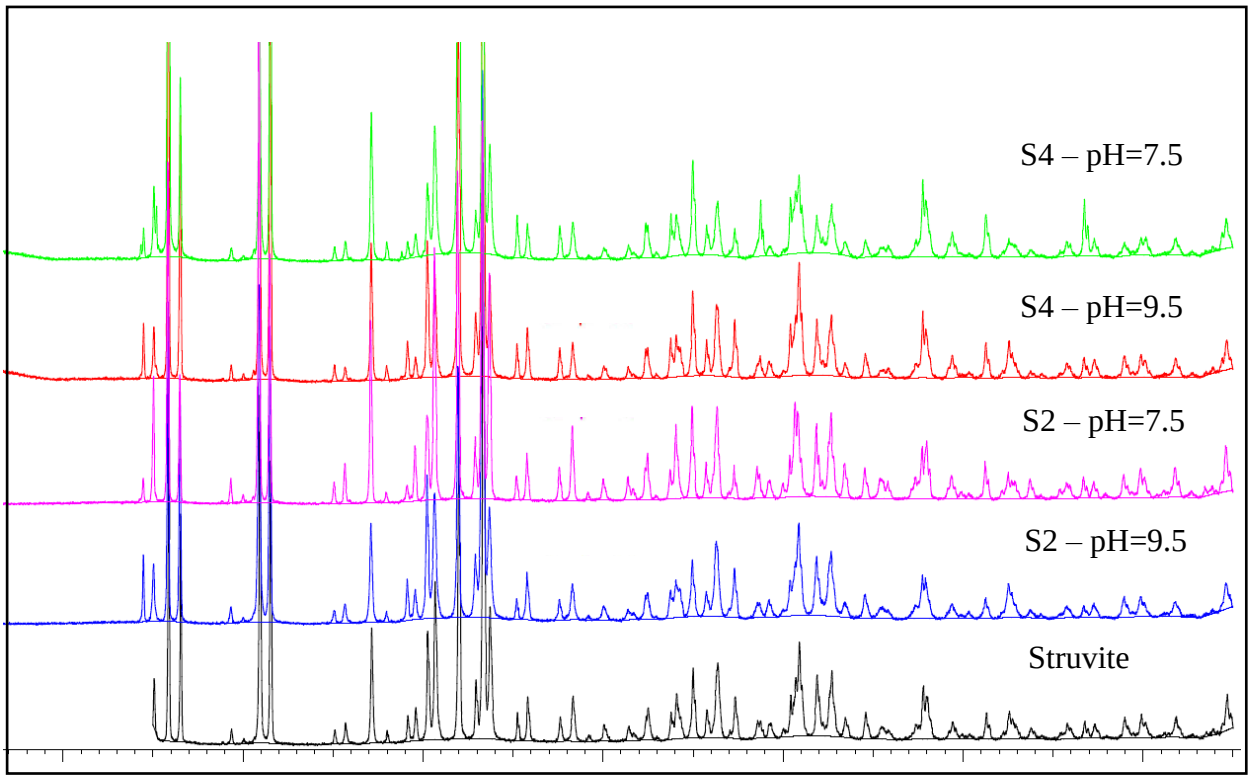

Figure 4-25: XRD patterns of pure struvite and solids obtained in S2 and S4.
Pure struvite (black), S2-pH 9.5(blue), S2-pH 7.5 (pink), S4-pH 9.5 (red) and S4-pH 7.5 (green)

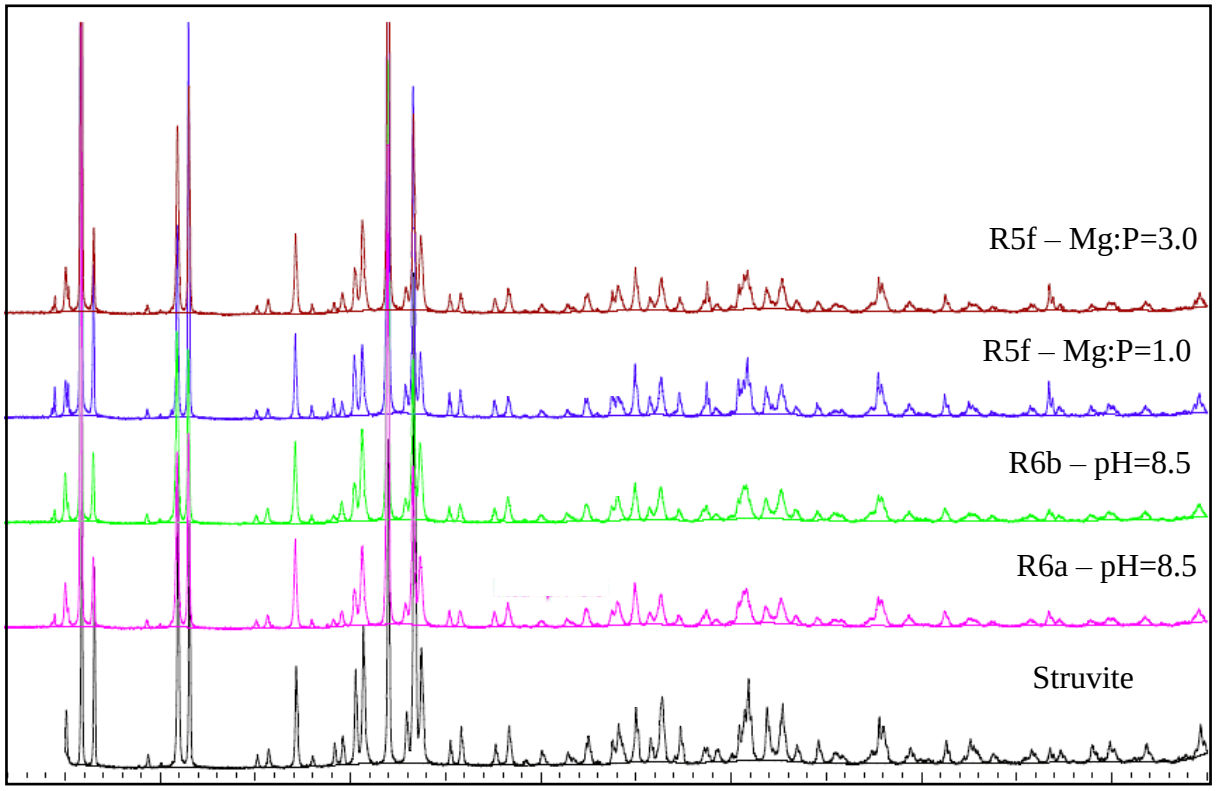

Figure 4-26: XRD patterns of pure struvite and solids obtained in R6a and R5f. Pure struvite (black), R6a-pH 8.5 (pink) R6b-pH 8.5 (green), R5f-Mg:P=1.0 (blue) and R5f-Mg:P=3.0 (brown)

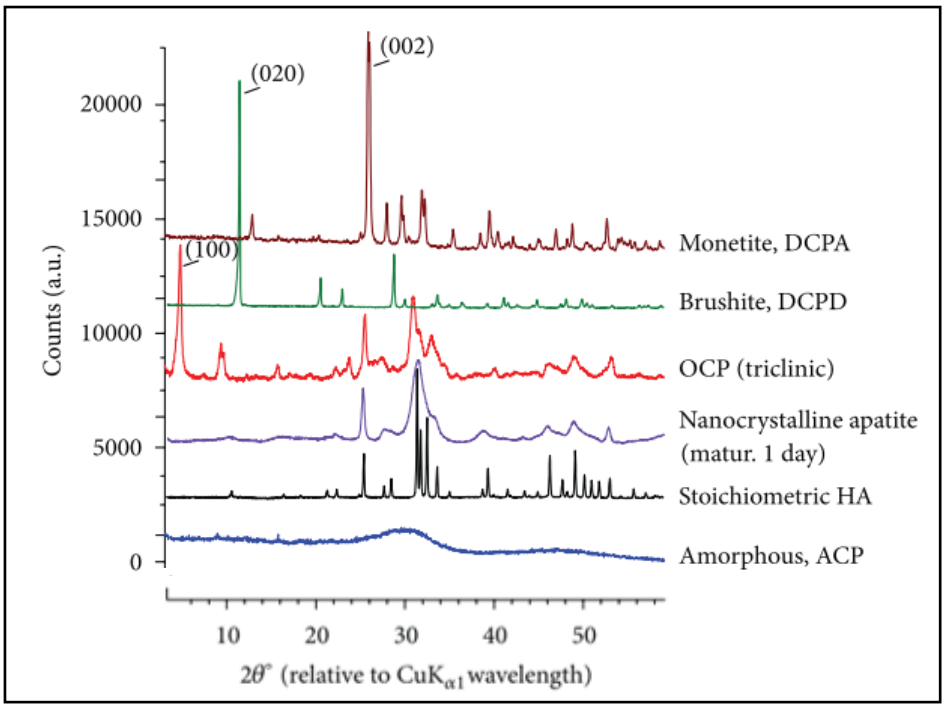

Figure 4-27: XRD patterns for different crystalline and amorphous compounds. All patterns except for ACP are offset along the intensity axis (Counts) for the purpose of comparison. Counts are therefore relative to the baseline of each graph. Figure is taken from Drouet [59].

The XRD patterns of the solids obtained in the experiments show defined peaks. All solid samples have baselines ranging from 100 to 400 counts, no matter if the samples are washed and filtered or not, meaning no halo is forming. The only solid samples from this study that indicated formation of other crystalline compounds with XRD was in solids produced in S2 (Synthetic reject water mixed with seawater at Mg:P=1.0) at pH 7.5 and 8.5, that were not washed or filtered. *Appendix 6* shows that at three 2Theta values (11.688, 32.678 and 45.473 along $CuK_{\alpha 1}$), peaks that do not match with the reference struvite appear. One of them, at 11.688 may correspond to the main peak of brushite, as seen in *Figure 4-27*. The second one (32.678) is in an area where most other Ca-P have several peaks, including struvite. It is sometimes difficult to distinguish Ca-P from struvite and to identify which Ca-P has formed because their typical peak placements tends to coincide. Observing only one small peak of a substance means that very little of the solid is present in the sample, and that identification of the solid is very uncertain.

Possible sources of error in the XRD results can be that the amount of solid that is analysed is small compared to the total amount of precipitate. We are only using around 5% of the total amount of product for XRD, meaning co-precipitates might not be a part of the sample. The range of 5−75° could also be too narrow to detect all possible solids. However, the most probable Ca-Ps have their main intensity peaks within a range of 10-40 on the 2-theta axis - which is the same as for struvite - meaning they should be possible to detect if present in amounts high enough. If there are co-precipitates in our products, the amounts are below what we are capable of detecting and identifying with XRD.

4.4 Crystal morphology and size

4.4.1 Comparison of $MgCl_2$ and seawater at changing supersaturation (S1-S4)

4.4.1.1 Particle size measurements

Analysis of crystals produced from both Mg sources in synthetic reject water at different pH values were conducted based on particle size measurements and images taken with scanning electron microscope (SEM). When we use $MgCl_2$ as Mg source we expect certain crystal morphologies and sizes at different supersaturations. The pH is known to be an important factor as it has a great impact on supersaturation level, and it is easy to distinguish between crystals formed under different conditions. There are many different ions and particles that might affect

the saturation of struvite when we use seawater. It is therefore interesting to compare crystals formed with pure Mg salts and seawater. For particle size results, the median size from the volume distribution is used (Dv50) as well as the particle size that 90% of the total volume of particles are smaller than (Dv90). These values, as well as the standard deviation and variance are calculated by the software connected to the *LS230*. We can see from *Table 4-10* and *Table 4-11* that particle size is dropping as pH increase. This is likely to be due to increased nucleation rate as supersaturation increase [11]. When nucleation rate is high, we may get a higher number of crystals, making all of them smaller as there is a limitation in struvite components present. It is important to keep in mind that particle size is not necessarily the same as crystal size. A particle can consist of several crystals in the form of aggregates. Some particle size measurements also showed strange values, and the size trend with pH is not clear for experiment series S3 and S4 (Table 4-11). The change in particle size with pH is somewhat smaller with seawater than $MgCl_2$. *Figure A3.1* in *Appendix 3* shows that saturation in the seawater mix is increasing less with increasing pH compared to experiments with $MgCl_2$. This could also be the reason why the change in particle size is slightly less.

Table 4-10: Particle size of samples from S1 and S2 (Mg:P=1.0).
Both the median and the Dv90 (in parenthesis) is given.

	S1 - $MgCl_2$		S2 - SW	
pH	**Median (Dv90) [µm]**	**Standard deviation /variance**	**Median (Dv90) [µm]**	**Standard deviation/ Variance**
7.5	93.3 (159.3)	1.709 / 2.921	91.7(145.3)	1.589 / 2.526
8.0	96.1 (137.8)	1.663 / 2.767	81.8 (137.1)	1.618 / 2.617
8.5	50.9 (122.4)	2.817 / 7.938	68.4 (97.6)	1.514 / 2.293
9.0	32.4 (61.9)	2.598 / 6.751	43.7 (78.8)	2.746 / 7.538
9.5	27.8 (64.2)	2.607 / 6.796	32.7 (73.0)	2.847 / 8.107

Table 4-11: Particle size of samples from S3 and S4 (Mg:P=1.67).
Both the median and the Dv90 (in parenthesis) is given.

	S3 - $MgCl_2$		S4-Seawater	
pH	**Median, (Dv90) [µm]**	**Standard deviation/ Variance**	**Median, (Dv90) [µm]**	**Standard deviation/ Variance**
7.5	85.7 (133.4)**	1.612 / 2.599	85.7 (152.4)	1.596 / 2.546
8.0	93.7 (142.4)	1.720 / 2.957	72.9 (106.2)	1.479 / 2.188
8.5	43.6 (106.1)**	2.669 / 7.123	58.8 (115.6)	2.343 / 5.483
9.0	60.1 (159.8)	2.788 / 7.771	48.1 (112.6)	2.797 / 7.824
9.5	24.6 (62.5)**	2.555 / 6.528	41.6 (125.6)*	3.050 / 9.302

***** **Particle size distribution is not well defined.**
****** **Conducted by PhD. candidate Sina Shaddel**

4.4.1.2 Crystal Morphology

The morphologies obtained in the experiments match well with expected morphologies within each pH value. *Figure 4-28* shows typical coffin-shaped crystals for both Mg sources at pH 7.5. At pH 8.5, the $MgCl_2$ gives distinct elongated or rod-like crystals, whereas seawater particles are mostly aggregates of more compact crystals. This can be a sign that supersaturation is lower when using seawater although at same pH as with pure Mg source. For pH 9.5 we can see the same dendrite shape for both cases, but the crystals are larger in the seawater case, as the table above also indicated. Experiences from the particle size measurements showed that less aggregation occurs at high supersaturation, making particle size analysis more representative for crystal size.

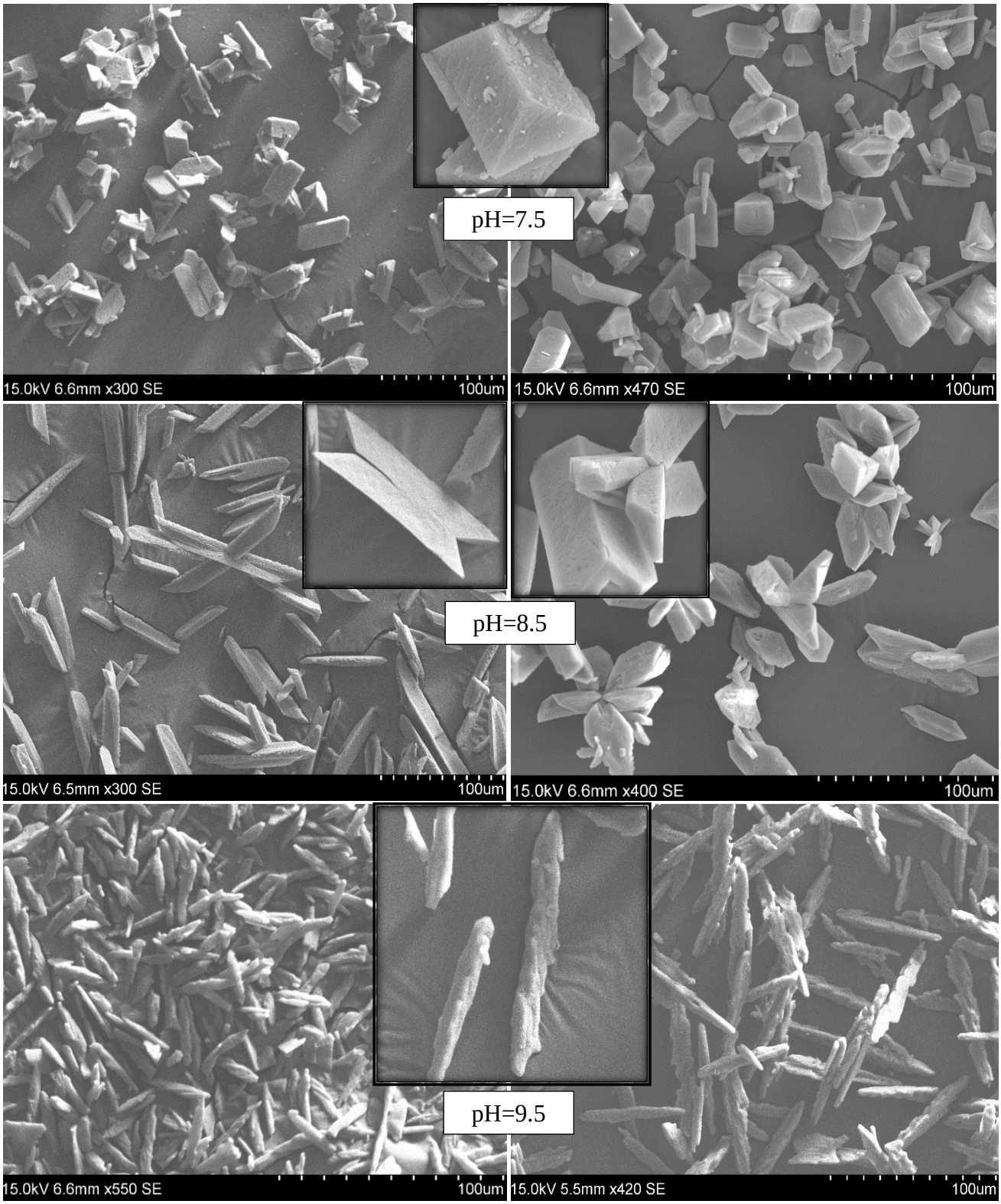

Figure 4-28: SEM images of struvite.
Precipitated with $MgCl_2$ (left) and seawater (right), at Mg:P=1.0 and pH of 7.5 (upper row), 8.5 (Middle row) and 9.5 (bottom row). The images show typical morphologies for different pH levels, coffin-shaped at low pH, via needle like to dendrite at high pH.

In experiment S2, it was found that P recovery was higher than theory, at the same time as Mg recovery was lower, and one possible explanation is that Ca-P is precipitating along with struvite. From XRD results in *Figure 4-25* and SEM images of these experiments given at the right side in *Figure 4-28*, it is without a doubt mostly struvite crystals that are formed during the experiments. By closer examination of the SEM images traces of solids attaching to the surface of the struvite crystals were observed (*Figures 4-29* and *4-30*). The sizes are in the range of 1-5μm, meaning they are very small compared to the median size of particles in these

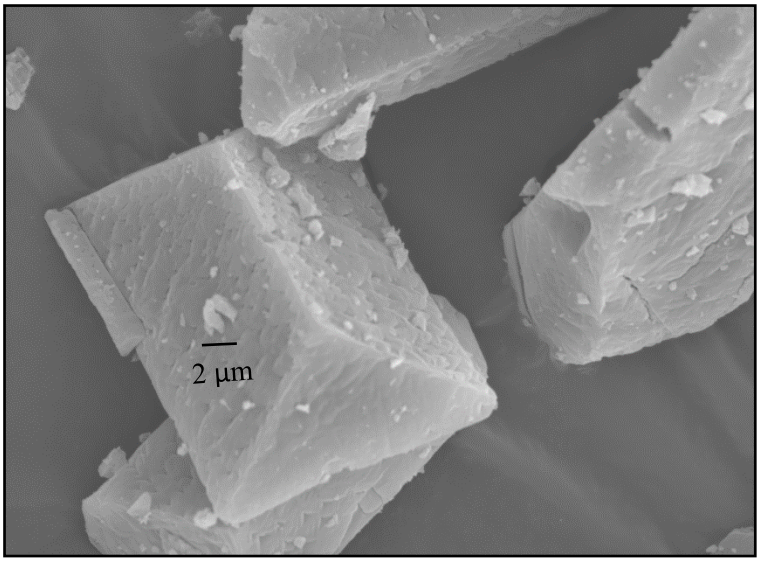

Figure 4-29: SEM image showing possible co-precipitant. From solids obtained in S2 at pH 7.5

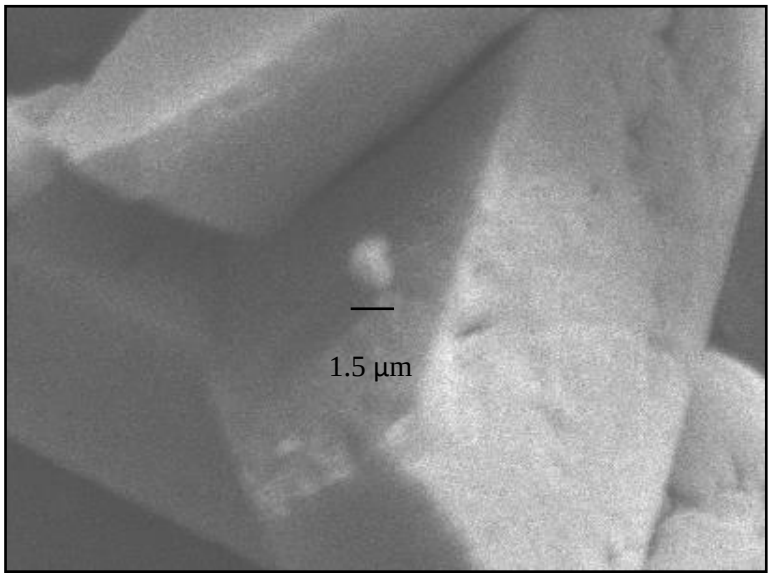

Figure 4-30: SEM image showing possible co-precipitant. From solids obtained in S2 at pH 8.0

experiments. Since the filtering of the seawater we use only removes larger particles (>70µm), we can not be sure that these trace elements did not originate from the seawater, rather than being a result of co-precipitation during the experiments. If so, pre-treatment of seawater could be necessary to remove all sources of impurity in the struvite produced. For Mg:P molar ratio of 1.67, no clear sign of co-precipitants could be seen with SEM (See *Appendix 7*).

4.4.2 Dilution effect of seawater at different Mg:P molar ratios and pH (S5, R5 and R6)

4.4.2.1 Particle size measurements

The effect of dilution with seawater on particle size and morphology has been studied for both synthetic and real reject water. Additionally, we have compared the results of using different types of reject water. An interesting observation is that with increasing Mg:P molar ratio, the particle size seems to decrease in synthetic reject water, while it is slightly increasing for real reject water (Table 4-12). One explanation can be that as Mg:P molar ratio rises, the supersaturation in the synthetic case is increasing, giving higher nucleation rate and formation of a higher amount of crystals. In real reject water, the supersaturation is not increasing the same way, perhaps due to complexations with reject water constituents. However, since the P recovery in these two experiment series were almost the same, supersaturation should not be very different. Increasing pH also did not change particle size substantially for experiment series R6 (Table 4-13). The reasons could be the same as mentioned above.

Table 4-12: Particle size of samples from S5 and R5f (pH=7.5).
Both the median and the Dv90 (in parenthesis) is given, meaning the particle size that 90% of the total volume of particles are smaller than .

	S5		R5f	
Mg:P	**Median (Dv90) [µm]**	**Standard deviation / Variance**	**Median (Dv90) [µm]**	**Standard deviation / Variance**
1.0	86.1 (132.6)	1.530 / 2.342	28.4 (47.2)	2.042 / 4.169
1.67	83.3 (130.0)	1.523 / 2.319	29.2 (48.0)	2.097 / 4.397
2.34	80.4 (126.2)	1.526 / 2.328	29.9 (50.3)	2.264 / 5.126
3.0	75.1 (121.6)	1.583 / 2.505	30.4 (51.4)	2.264 / 5.125

Table 4-13: Median particle size and Dv90 (in parenthesis) in R6a and R6b.

Median particle size and Dv90 [µm]			
Mg:P	**pH=7.5**	**pH=8.0**	**pH=8.5**
1.67 (R6a)	29.2(48.0)	31.7 (51.0)	30.8 (48.8)
2.34 (R6b)	29.9 (50.3)	34.3 (53.9)	32.3(51.4)

4.4.2.2 Crystal morphology

Figure 4-31 shows that crystal morphology of solids produced in experiment series S5 is not changing from the coffin-shape seen at low supersaturation values. The same is observed for experiment series R5 (Figure 4-32). The low change in particle size with Mg:P molar ratio and pH found in *Chapter 4.4.2.1* can also be seen from these SEM images. While products of experiments with synthetic reject water are white powders, the real filtered reject water gave grey precipitate when dried. With unfiltered reject water, the precipitate was almost black due to other reject water components

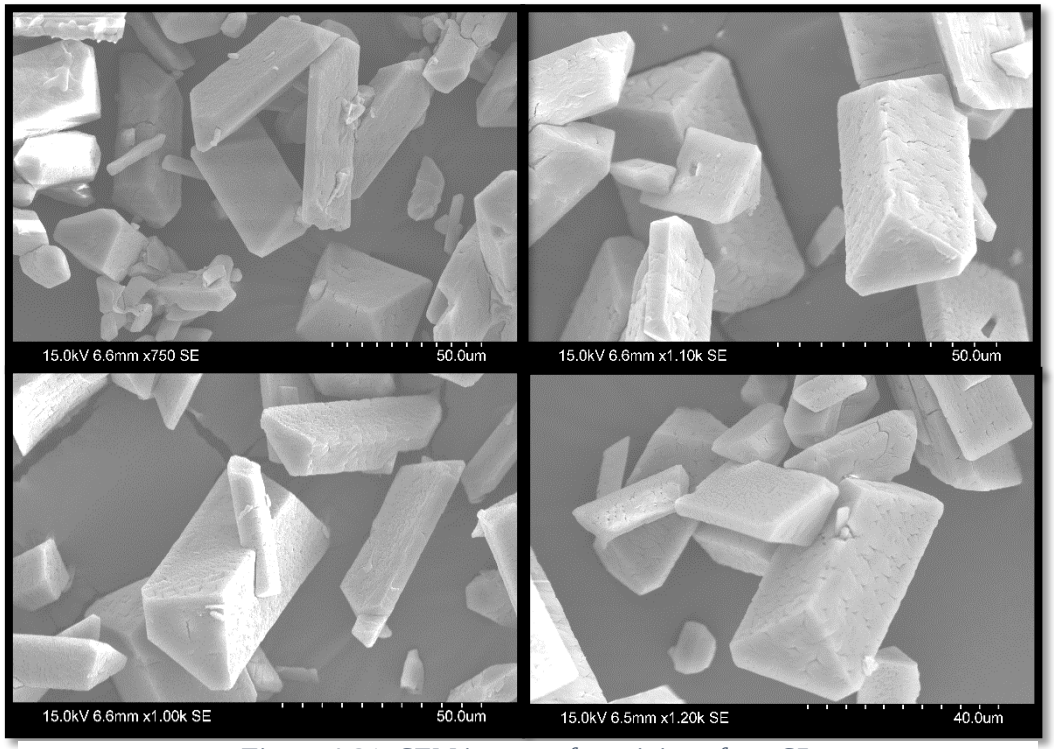

Figure 4-31: SEM images of precipitate from S5.
From experiments at Mg:P of 1.0 (upper left), 1.67 (upper right), 2.34 (bottom left) and 3.0 (bottom right).

.

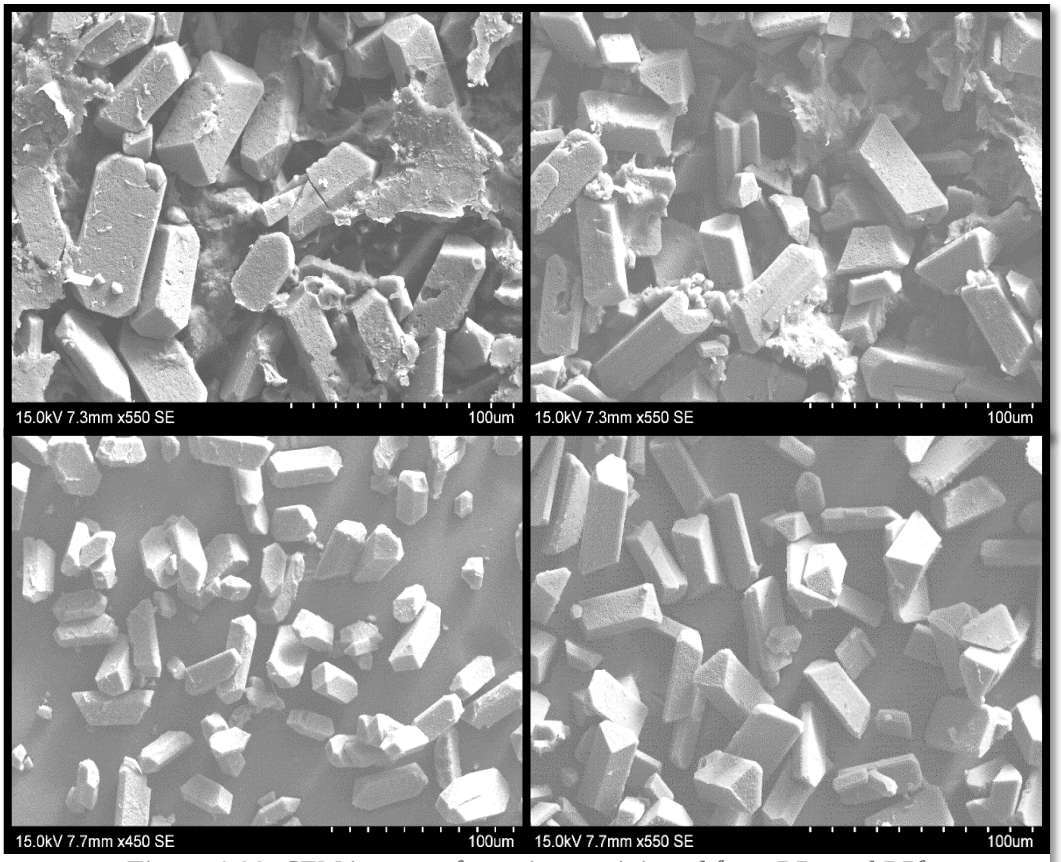

Figure 4-32: SEM images of struvite precipitated from R5u and R5f. Solids produced from real unfiltered (upper row) and filtered (bottom row) reject water at pH=7.5, and Mg:P of 1.0 (left column) and 3.0 (right column).

The morphology of crystals produced in experiment series R6 is also not changing much with pH and Mg:P but there is a slight change from coffin-shaped to more elongated and less compact particles at Mg:P=2.34 and pH 8.5 (Figure 4-33). Calculations with Visual MINTEQ also showed that this is where the saturation is highest.

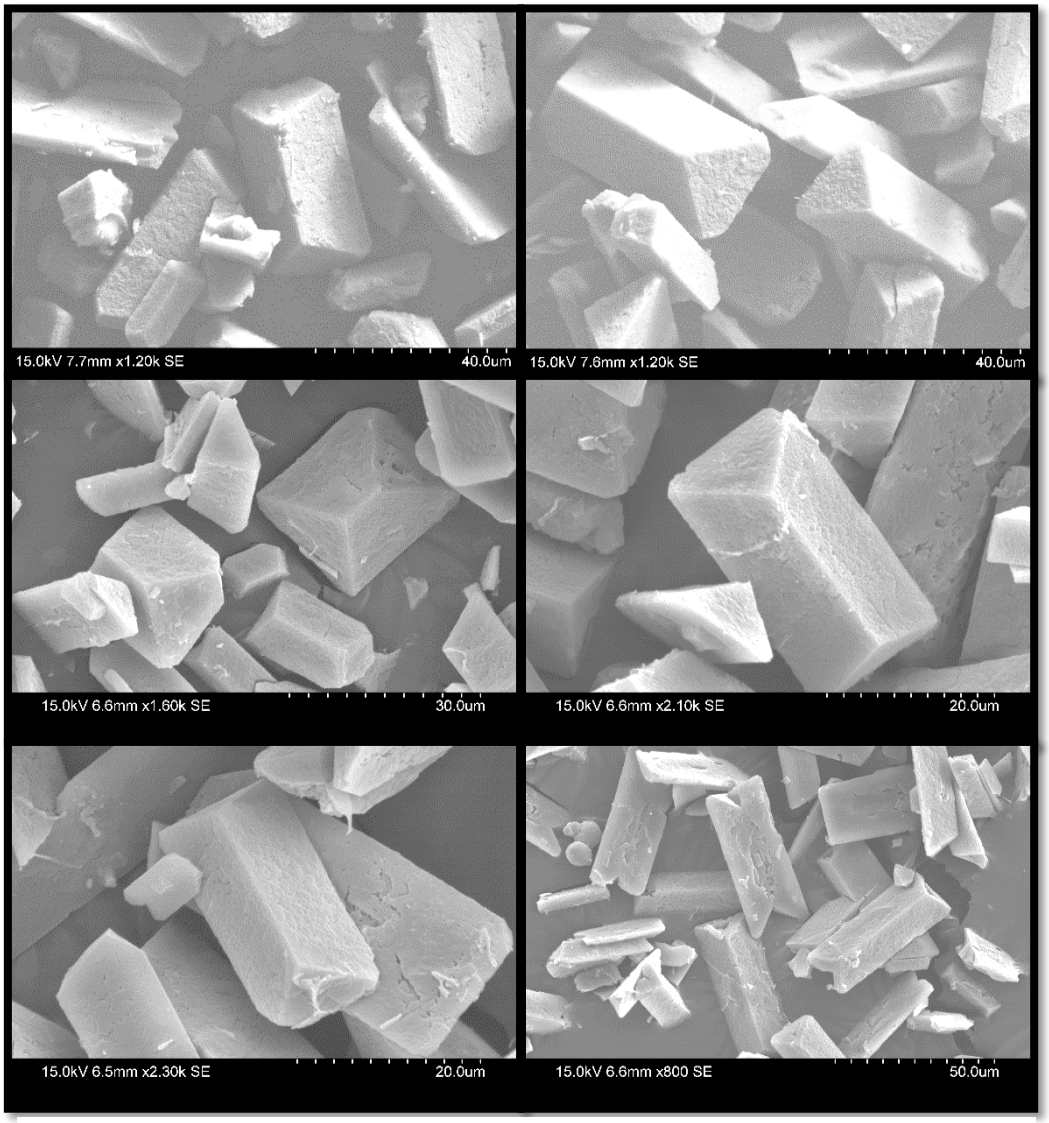

Figure 4-33: SEM images of solids obtained in R6a (left) and R6b (right). For experiments at pH of 7.5 (upper row), 8.0 (middle row) and 8.5 (bottom row). The images show that morphologies are similar except for Mg:P 2.34 (R6b) at pH 8.5, where crystals are emerging towards more elongated and x-shaped.

4.4.2.3 Purity

There are signs of other co-precipitants when we use seawater in real filtered reject water. At pH 8.5, some spherical shaped solids were found in experiment series R6a (Figure 4-34) and R6b (Figure 4-35). The amounts are not large enough to be detected with XRD, and it is difficult to find examples in the literature of crystals having this type of morphology without it being a result of microbial activity or synthesis. Again, we can not exclude that these particles originated from the seawater.

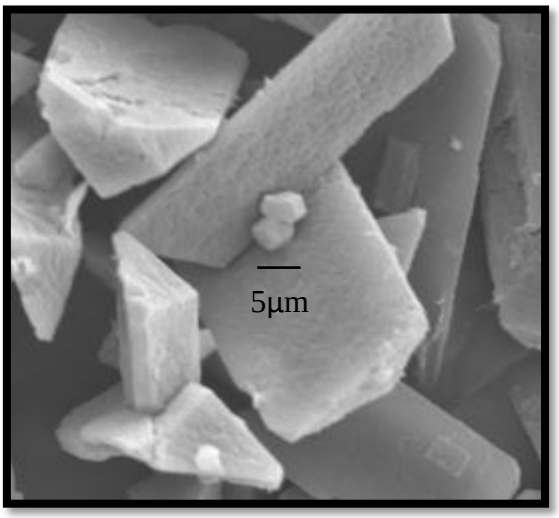

Figure 4-34: SEM image of possible co-precipitant.
From R6a (Mg:P=1.67) at pH 8.5

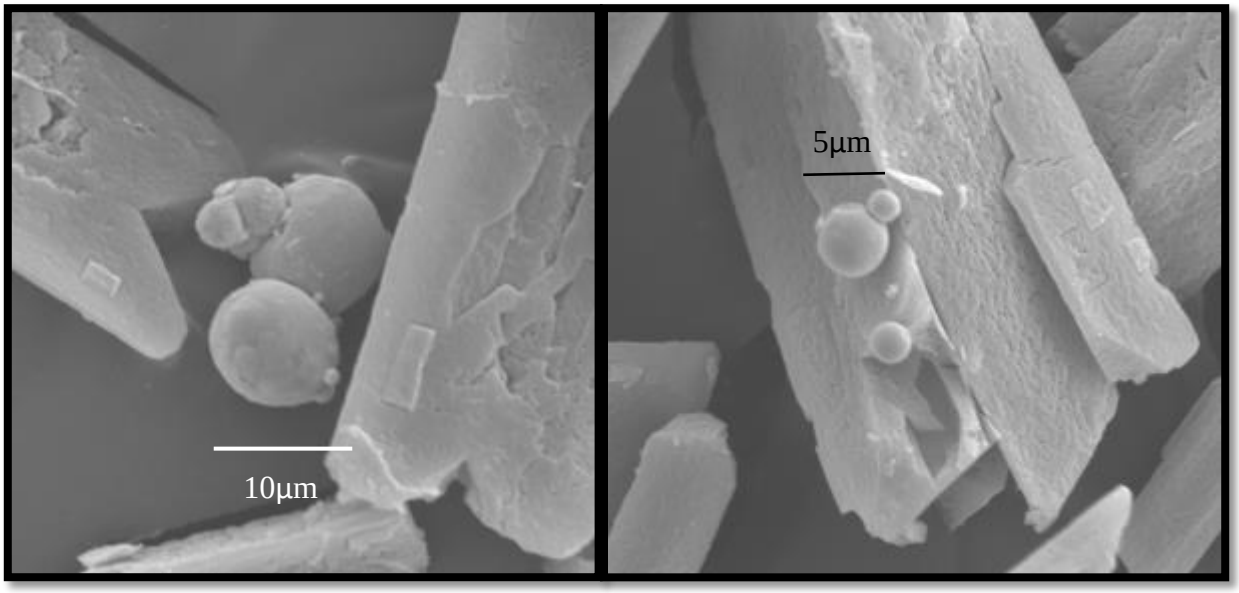

Figure 4-35: SEM image of possible co-precipitant.
From R6b (Mg:P=2.34) at pH 8.5

4.4.3 Additional comments to analysis

4.4.3.1 Impact of solids handling on analysis

There is a big difference between solid samples that were retrieved by filtration and the ones that were just left to dry directly from the reactor. Filtration was performed using a 0.2μm filter and washing was done with solutions saturated only with struvite. *Figure 4-36* shows a sample from S2 that was neither filtered nor washed, as opposed to the samples pictured in *Figure 4-28.* It may look like a fair amount of the precipitate is another compound than struvite. Still, XRD analysis showed no sign of either other crystalline or amorphous compounds in this specific sample, meaning the particles surrounding struvite crystals are not necessarily co-precipitants. One would think that when we wash our samples with something that is saturated only with struvite, it can dissolve other solids. However, none of the samples of S5, R5 or R6 were washed, and there were no significant amount found of anything else than struvite by XRD or SEM analysis. The same applies for the sample pictured below, although it looks like co-precipitation has occurred. This shows that the characteristics of the solids from struvite production is influenced by post-treatment processes.

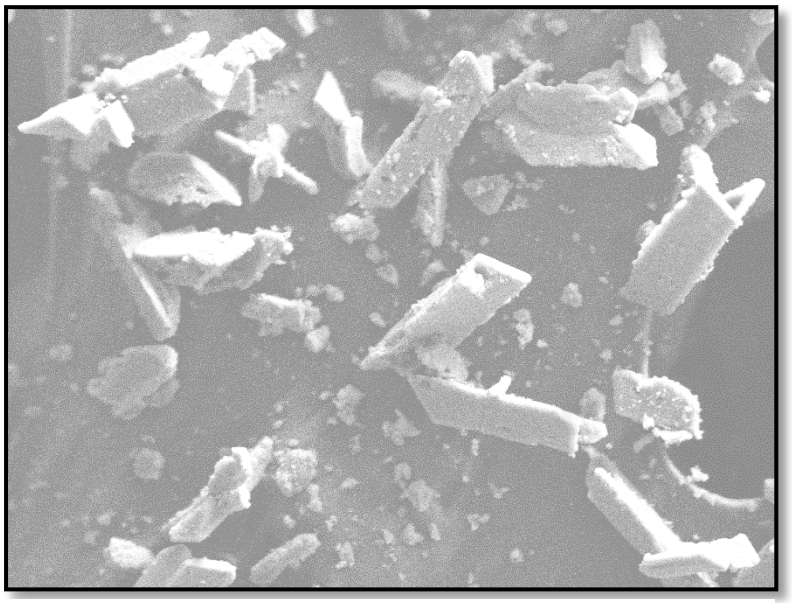

Figure 4-36: SEM image of solids that have not been filtered or washed.
From experiment S2 at pH 8.5

4.4.3.2 Impact of reject water type on particle size

There is a big difference in particle size between using synthetic and filtered real reject water as *Table 4-12* showed. Particle size with real reject water turned out to be much smaller than with synthetic reject water, although P recovery was about the same. *Appendix 8* shows examples of volume and number distribution graphs for S5 and R5f at Mg:P molar ratio of 2.34, as well as for the filtered reject water alone. The real reject water contains many small particles up to 4μm. It was calculated that the contribution of fine particles originating from the real reject water does not change volume based median particle size to a big extent, although there are many of them in the solution. Thus, it is not responsible for the low particle size measurements with real reject water. It is possible that other reject water constituents are blocking crystal sites and inhibiting growth. Ping, Li [49] showed that increasing TSS concentration gave lower P removal and smaller struvite crystals. However, since R5u and R5f gave close to the same P recovery as S5 (see *Chapter 4.1.2*.), and XRD showed that solids produced were close to pure struvite, this effect is not easily recognized. *Le Corre* [30] found that the presence of Ca in the solution inhibits growth of struvite crystals. At Mg:P=1.0 there is about 68% more Ca in the reaction solution with real reject water compared to synthetic reject water. This rate decreases to ∼23% at Mg:P=3.0 (Calculated from concentrations given in *Appendix 2*) since the amount of seawater increases. This could explain that the particle sizes are slightly approaching each other at increasing Mg:P molar ratios. *Capdevielle* [62] found that the presence of particulate organic matter and colloids slowed down kinetics and at the same time gave larger struvite crystals. The same study also showed that colloids prevented agglomeration. When comparing SEM images from S5 and R5 it it possible to detect more agglomerated particles in the case of synthetic reject water. This may contribute to false estimates of crystal size when we do particle size measurements.

4.5 Growth kinetics with synthetic reject

4.5.1 Effect of N:P and Mg:P molar ratios and pH

The results of crystal growth experiments show that N:P and Mg:P molar ratios as well as pH play important roles in the growth of struvite crystals. The main findings indicate that crystal growth rate increase with increasing N:P, Mg:P and pH, as *Figures 4-37* to *4-39* indicate. *Appendix 5* provide additional results for how PO_4-P, Mg^{2+} and Ca^{2+} concentrations change over time. Ca^{2+} was included in order to detect any co-precipitation of Ca-P. Results show that

Ca^{2+} concentrations are stable, indicating no Ca-P is forming.

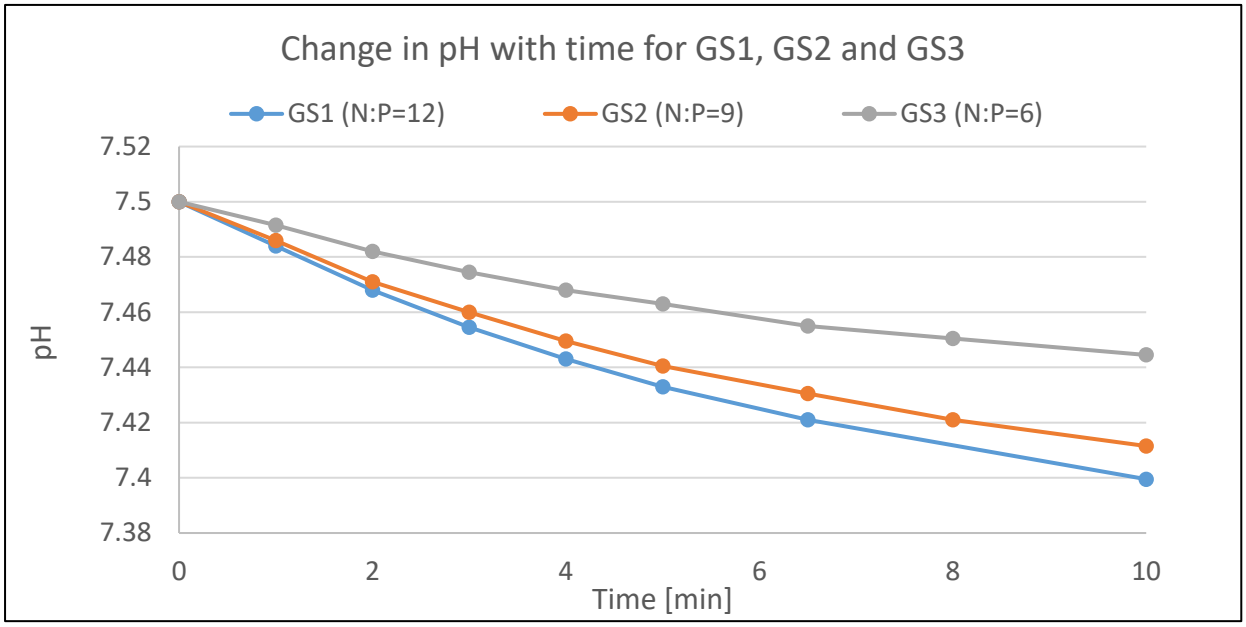

Figure 4-37: pH change with time at different N:P molar ratios.

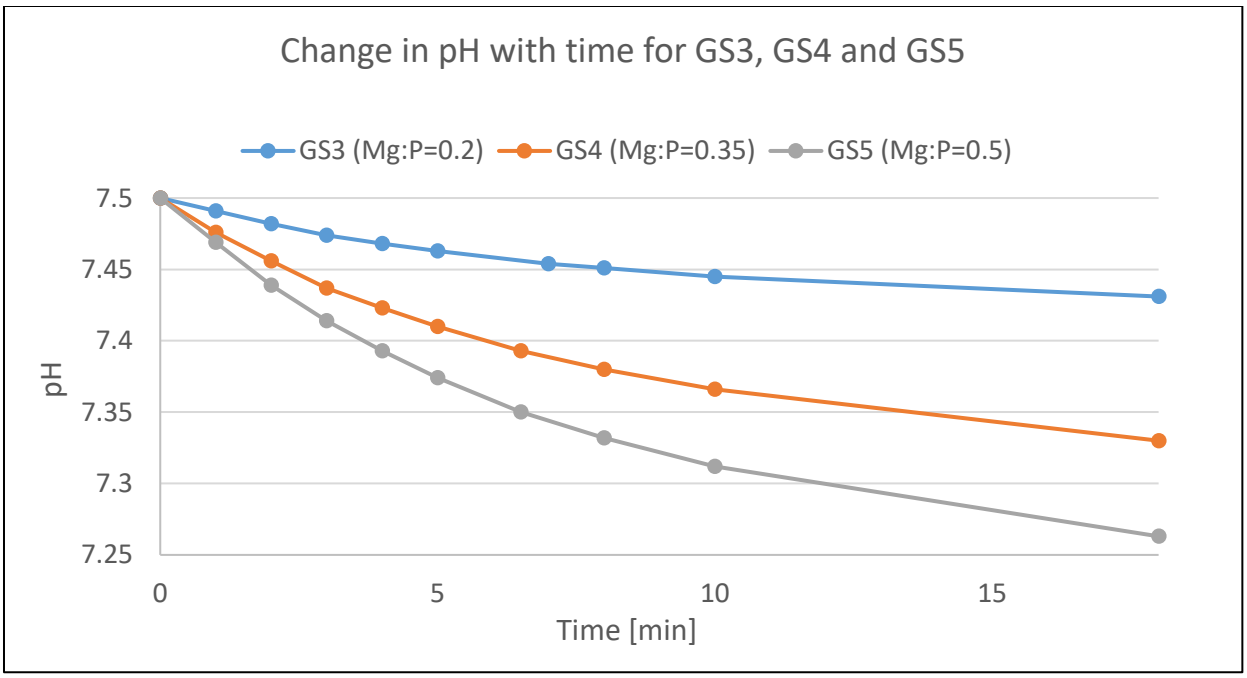

Figure 4-38: pH change with time at different Mg:P molar ratios.

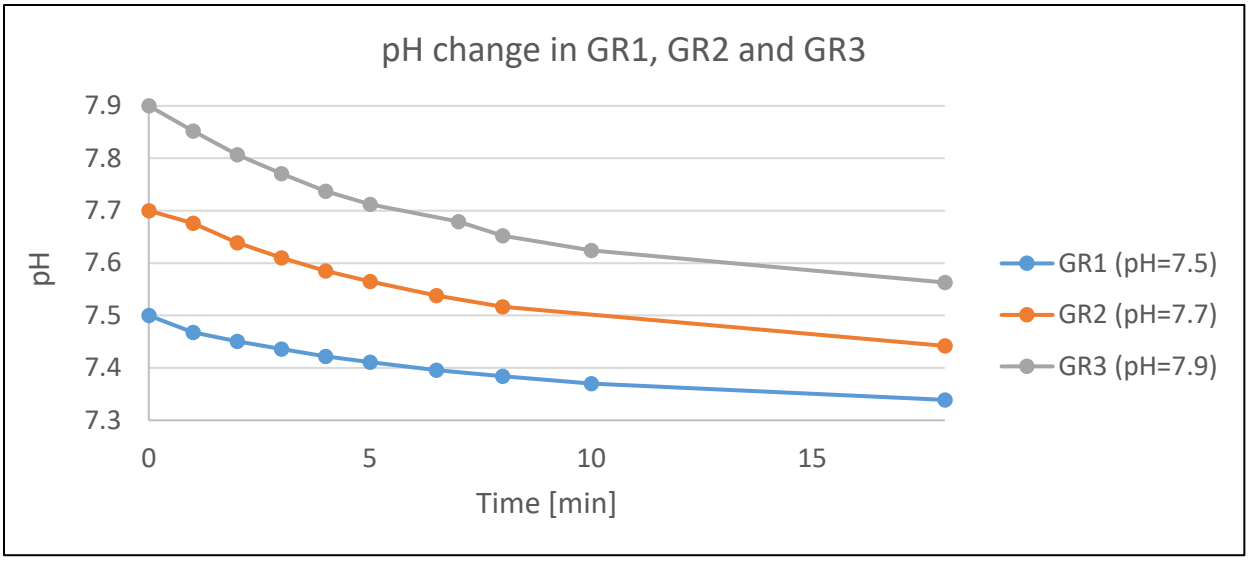

Figure 4-39: pH change with time at different initial pH values.

4.5.2 Future work on growth kinetics

Crystal growth kinetics is an important factor for operation of struvite reactors. It determines how we design reactors and operational conditions, and will eventually decide the end product characteristics. The crystal growth experiments conducted in this thesis is a preliminary study of possible factors affecting the crystal growth rate. By investigating the impact of N:P molar ratio we increase our understanding of how WWTPs with the ability to adjust N and P streams can change the crystallization process in a struvite reactor. This is the case if an additional step promoting P release from PAOs is added before an anaerobic digestion step. This can be a measure to control both P and N streams as well as prevent uncontrolled struvite precipitation, especially in plants with high Mg concentrations. It can also give insight into how struvite crystallization will be affected by changing wastewater composition or between plants treating different types of wastewater.

From experiments testing Mg:P molar ratio, we studied the impact of Mg addition, which is an obvious parameter to consider in all struvite precipitation reactors regardless of Mg source. Just as important is the operational pH, which we have seen has a great impact on supersaturation and recovery.

It is beyond the scope of this study to investigate the growth rate obtained in these experiments, but this would be a natural follow-up of the work that has been conducted. *Figure 4-40* shows a possible method for finding the change in concentration over time and eventually the relation

between the different parameters studied and crystal growth.

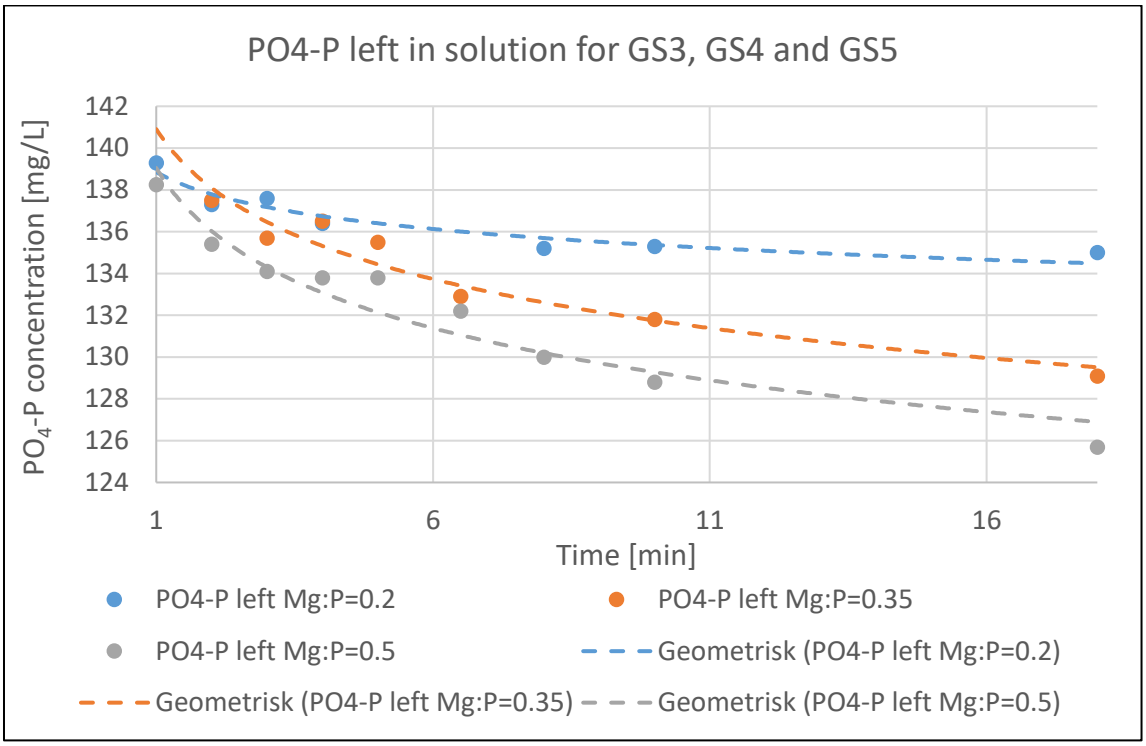

Figure 4-40: Change in PO_4-P concentration fitted with a power trendline (Geometrisk).

By calculating the change of concentration and the saturation along the time axis, we can find the growth coefficient K_G based on a diffusion-reaction model [63];

$$K_G = \frac{dm}{dt} \cdot \frac{1}{A \cdot (c - c*)^g}$$

Where m = mass of solids deposited in time t, A = surface area of the crystal, c = concentration in the solution, $c*$ = equilibrium saturation concentration, g = order of the crystal growth process. From this equation, the crystal growth rate R_G can be calculated by,

$$R_G = K_G(c - c*)^g$$

This can in turn be used for comparing the impact of reaction conditions and for reactor design purposes.

5. Cost estimation

The main reason for using seawater as magnesium source for struvite precipitation is the cost benefit. WWTPs located near the coast has unlimited access to a practically free magnesium source. Previous estimations of production costs of struvite vary greatly, from around 1.1 to 29.9 $ per kg phosphate removed [64]. The overall costs will depend on type of chemicals used, if the reactor is fluidized or mixed, energy consumption, reject composition, geographical location etc. In this chapter, a comparison of costs of using $MgCl_2$ and seawater is presented based on calculations made with a free computerized tool.

5.1 The simulation software

The computer program *The Struvite Process Design and Operational Tool* was first described in *Birnhack* [64]. The simulation tool can calculate the performance and cost of struvite precipitation in a fluidized bed reactor. It does so by utilizing the thermodynamic equilibrium-based computations in *PHREEQC*, which solves for and calculates equilibrium of mixtures, CO_2 stripping, pH, base dosage and effluent composition iteratively while exchanging information with a Python based environment where consumption of energy and chemicals and their associated costs are calculated. The database that provides *PHREEQC* with reaction kinetics for different chemical reactions is the same as *Visual MINTEQ* utilizes. Eventually, it calculates the purity of struvite, P removal and costs. The costs are given as "Opex", meaning operating costs per m^3 wastewater influent to the reactor and cost per kg of phosphorus removed.

5.2 The setup of software

The program allows the user to choose between three types of magnesium sources; $MgCl_2 \cdot 6H_2O$, $MgSO_4 \cdot 7H_2O$ and brine. The composition of brine can be modified to get the same composition as untreated seawater. The user also choose either NaOH or $Mg(OH)_2$ for pH adjustment, but pH elevation by CO_2 stripping is also possible to incorporate. Other important inputs are the composition of the stream going into the reactor, retention time, reactor pH, energy price, chemical price and Mg:P molar ratio. Allowing the solution to equilibriate with amorphous calcium phosphate (ACP) after struvite precipitation is optional, and will affect the purity of the end product and P recovery. When ACP is considered, HRT is an important parameter, as seawater rises the Ca:P molar ratio and ACP tend to have slower kinetics than struvite. As shown in *Lahav* [52], an HRT of less than 30 minutes gave very limited

precipitation of calcium phosphates when using NF brine as magnesium source.

For the purpose of comparing cost of using $MgCl_2$ and seawater, the cost of $MgCl_2$ is most important, as this decide how much can be saved. Some parameters, like energy cost, reactor depth and temperature will probably not affect the outcome with one magnesium source more than the other.

5.3 Comparison of costs of using $MgCl_2$ and seawater

5.3.1 Input values

The input values of our simulation can be seen in *Table 5-1* to *5-4*. Simulations with both $MgCl_2$ and seawater as magnesium sources were conducted. Since P recovery is slightly higher with $MgCl_2$ than with seawater if we include dilution, we use an Mg:P of 1.2 for $MgCl_2$ and 1.67 for seawater. This is estimated from our experiments to give approximately the same P recovery. It also gives a more realistic cost estimate, as we have to consider the need for more Mg when we use seawater due to lower supersaturation. Since the cost of using seawater is assumed to be negligible compared to chemical costs, the amount of seawater will only affect base costs in our simulation. The price of $MgCl_2$ used is taken from *Lahav* [52], although more accurate estimates would be possible if prices were retrieved from manufacturers. The result of the simulation must be seen in light of this. The HRT in the reactor and temperature of the influent were set to match our experiments. Precipitation at pH 7.5 and 8.0 were used. The reject water composition corresponds to the real filtered reject water used in experiments, not considering the contribution of Cl^- and Na^+ from salts used for P and N adjustment. The Mg^{2+} is also excluded so that Mg:P molar ratio is only a result of Mg addition. Simulations are run with the possibility of ACP precipitation. NaOH is used for pH adjustment. Since seawater is assumed to be free, the cost estimations are merely a comparison of chemical costs.

Table 5-1: Estimation of price for chemicals and energy to be used in cost estimation

	Basis for input	In Norwegian currency and 2018 price	Input to program***
Price of $MgCl_2$	140 $/ton [52]	950 NOK/ton*	120 $/ton
Price of NaOH	370 $/ton [64]	2520 NOK/ton*	330 $/ton
Energy price	Estimated spot price**	0.30 NOK/KWh	0.04 $/KWh

* Estimated from prices in 2013 by historical currencies and consumer price index

** Retrieved from https://www.ssb.no/elkraftpris

*** Calculated with the currency calculator of *DNB* (Den Norske Bank)

Table 5-2: Operational conditions of the struvite reactor

Operational conditions – Input values		
Parameter	**$MgCl_2$**	**Seawater**
Mg:P	1.2	1.67
Retention time	60 min	
pH in reactor	7.5 and 8.0	
Reactor depth	5 m	
Air-to-water ratio	0.001 (default)	
CO_2 mass transfer	0.02 (default)	

Table 5-3: Influent properties (Reject water composition) to be used in cost estimation.

Influent properties	
Parameter	**Input**
pH	6.5
P-tot [M]	0.004425
N-tot [M]	0.05385
Cl^- [M]	0.01608
Na^+ [M]	0.0139
Ca^{2+} [M]	0.000998
SO_4-S [M]	0.00084
K^+ [M]	0.00102
Alkalinity [eq/L]	0.0376 [64]
Temp. °C	20

Table 5-4: Brine properties (Seawater composition) to be used in cost estimation.

Brine properties [M]	
Cl^-	0.5354
SO_4^{2-}	0.0855
Na^+	0.4598
Mg^{2+}	0.0525
Ca^{2+}	0.01115
K	0.01005
Temp. °C	10.6 *
pH	8.1*
Alkalinity	0.00267**

***Average of reported min. and max. values of seawater from Trondheim Fjord**

**** Calculated from carbonic acid equillibrium based on bicarbonate content in typical seawater**

5.3.2 Results

The result of the simulation can be seen in *Table 5-5*. Opex is reduced by about 20% and 23% at pH 7.5 and 8.0 respectively when we use seawater instead of $MgCl_2$. We see also that seawater gives higher P recovery than $MgCl_2$ due to more ACP precipitation, especially at pH 7.5. This is because ACP has a lower potential to precipitate at pH 7.5 than 8.0. The need for base is less with seawater, which may be related to the seawater having a higher pH than the reject stream. In these simulations, no investment costs are considered. It should be noted that utilizing seawater will require a pumping and transport system to get seawater to the struvite reactor.

Table 5-5: Result of cost estimation with $MgCl_2$ and sweater as magnesium sources.

	$MgCl_2$		**Seawater**	
	pH 7.5	**pH 8.0**	**pH 7.5**	**pH 8.0**
Effluent P [M]	0.00061	0.00017	0.00027	0.00006
Effluent N [M]	0.05075	0.05026	0.04477	0.04424
Struvite [mol/L reject water]	0.004	0.004	0.004	0.004
Struvite purity (Molar ratio)	0.967	0.977	0.926	0.972
P removal (%)	86.7	96.5	92.0	98.2
Mg salt dose (M)	0.005	0.005	-	-
Mg salt cost ($/m3 reject)	0.129	0.129	-	-
Seawater mixing ratio [L/L]	-	-	0.141	0.141
Base dose (mol/L reject water)	0.057	0.071	0.053	0.065
Base cost ($/m^3 reject water)	0.754	0.934	0.696	0.859
Opex ($/m^3 reject water)	**0.88**	**1.06**	**0.7**	**0.86**
Cost per P removed ($/kg phosphorus)	**6.445**	**7.756**	**5.075**	**6.268**

5.4 Factors affecting cost

The cost of chemicals is a big part of overall operating expenses. Both 38% [64] and 75% [38] have been mentioned as the amount of total costs being spent on magnesium salt. The cost of adding chemicals for pH adjustment is also a significant parameter for overall costs. In our laboratory experiments, we added 1 M NaOH to keep pH constant, and *Figure 5-1* shows the amount that had to be added at different pH levels in experiment S4. We see that there is an exponential growth of NaOH needed as pH increase, which makes operation of a struvite reactor much more expensive at high pH. To keep costs low it is therefore beneficial to keep pH as low as possible. Another option is to use CO_2 stripping, although this will also generate costs.

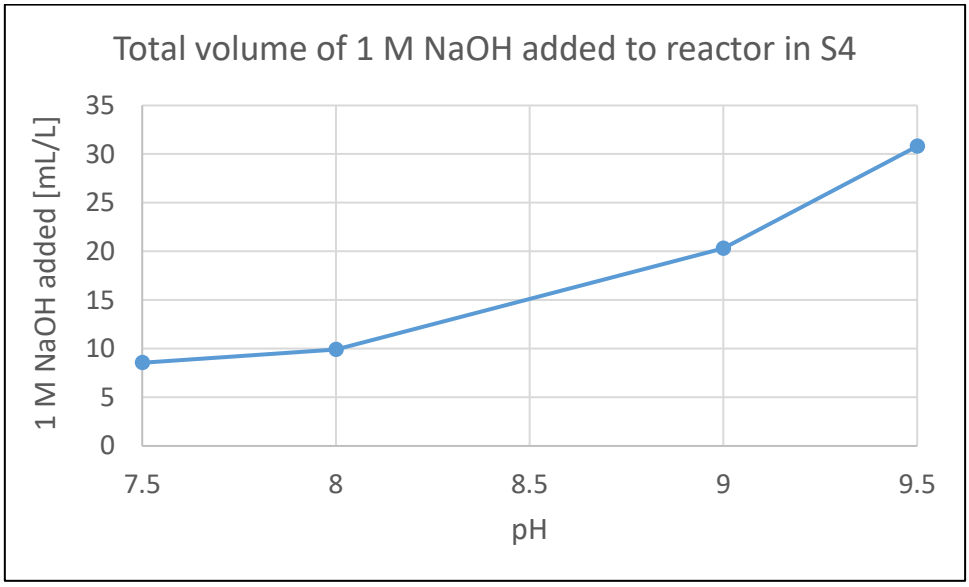

Figure 5-1: Addition of 1 M NaOH for pH adjustment in experiment S4

The base cost in the simulation in 5.3 ended up at 0.7 \$/m^3 at pH 7.5 when using seawater. If we simulate how base cost will change with increasing pH, we see that producing struvite gets more expensive as pH increases, and operating at pH 9 generates twice the base cost compared to pH 8.0 (Figure 5-2). This is an important factor to consider when designing struvite reactors and choosing which pH adjustment method to use.

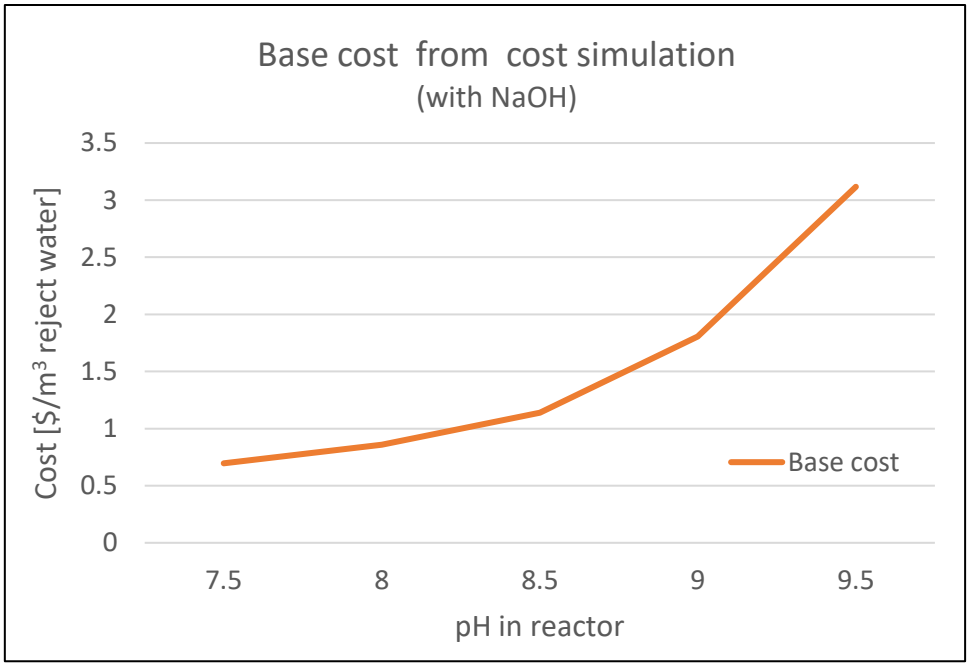

Figure 5-2: Base cost at different operating pH values.

6. Conclusion

This study has investigated some possible side-effects of using seawater as magnesium source in order to assess its applicability and performance. Results from laboratory experiments were supported by thermodynamic equilibrium calculations, and the results of calculations corresponded well with the results achieved in experiments.

Effect of seawater constituents

It was found that seawater constituents form more complexes and lowers P recovery compared to $MgCl_2$. This was most likely because of complexes formed due to the presence of Ca^{2+} and Na^{+}. The effect on P recovery was larger at low pH values (7.5-8.0), where supersaturation of struvite is already low. At the same time, calculations based on *Visual MINTEQ* showed that saturation of struvite deviates more at higher pH between solutions with seawater and $MgCl_2$. The particle size and crystal morphology of the products obtained with seawater did not deviate significantly from the products obtained with $MgCl_2$, although the crystal morphology obtained at pH 8.5 showed that supersaturation was slightly lower with seawater. Median particle size also seemed to change less with pH when seawater was used. Results indicate that increasing pH has less impact on supersaturation when seawater is used compared to $MgCl_2$.

Dilution effect of seawater

Dilution of reject water from seawater addition lowers the supersaturation of struvite. A P recovery of >90% was achieved in experiments with seawater for Mg:P molar ratios ≥1.67 at pH 8.0, whereas P recovery with $MgCl_2$ is expected to be >95%. It means that dilution affects recovery, but seawater still gives acceptable results. Increasing Mg:P molar ratio higher than 2.34 did not increase P recovery significantly. Yield of struvite per litre of reject water was found to increase with increasing Mg:P molar ratio up to 2.34, meaning it is possible to increase the struvite production without increasing pH even with seawater. However, increasing pH is more efficient. Thermodynamic equilibrium calculations with *Visual MINTEQ* showed that the maximum saturation occurred around an Mg:P molar ratio of 2.0-2.34 for a PO_4-P concentration of 137.1 mg/L in the reject water. The saturation peak occurred at a lower Mg:P molar ratio when PO_4-P concentration increased, but the amount of seawater was around 15% in both cases. It indicates that an optimum seawater amount in struvite reactors might exist, regardless of initial concentration of PO_4-P. Median particle size of produced solids did not change with more than 2μm between Mg:P molar ratios 1.0 and 3.0 when dilution effect was studied. Typical

coffin-shaped crystals indicating low supersaturation were found at all Mg:P molar ratios at pH 7.5, in both synthetic and real reject water.

Purity of precipitate

The purity of solids precipitated with seawater addition was analysed by X-ray diffraction and scanning electron microscope. Only struvite was identified in the precipitates regardless of reject water type. The combined effect of thermodynamics and kinetics favour struvite precipitation over other products even when we use seawater that contains ions that may compete with Mg^{2+} for phosphate. Traces of other types of solids were found, but the amounts were not large enough to be clearly identified with XRD.

Impact of N:P and Mg:P molar ratios and pH on crystal growth

Experiments showed that increasing the amount of NH_4-N relative to PO_4-P gives higher crystal growth rates. This means that WWTPs have a potential to increase the rate of struvite production by manipulating the feed streams into the reactor. Increasing Mg:P molar ratio and pH was also found to have a significant impact on crystal growth, which emphasize the importance of considering these parameters when deciding operating conditions for struvite reactors, also when seawater is used as Mg source.

Cost estimations

Potential cost savings of using seawater was estimated to be around 20-23% depending on operating pH in the reactor. This estimate was based only on chemical costs. It was also shown that base cost will increase significantly with increased operational pH in struvite reactors. It is therefore important that seawater, like pure magnesium sources, has the ability to increase struvite production per unit of reject water only by increasing Mg:P molar ratio.

Result of assessment

The assessment of seawater as an alternative Mg source performed in this study supports what has been found in previous studies. Seawater gave acceptable P recovery and had no substantial impact on the quality and purity of the end product. Costs of producing struvite with seawater are likely to be lower than when pure Mg sources are used. It is therefore recommended to consider using seawater for struvite production for wastewater treatment plants that have access to it.

7. Recommendations for future assessments

In order to fully understand the use of seawater as magnesium source for struvite precipitation, studies of the impact of salts being introduced to the main treatment train of WWTPs should be conducted. This is because the liquid phase of struvite reactors must be returned to the inlet for the plant. Thorough cost estimations including investment costs and operational costs of pumping and transporting seawater to the struvite reactor should also be performed. Since this study only considered one specific type of wastewater stream, results can not without further assessments be transferred to other cases. Pilot and full scale reactor operation with continuous feed of reject water and seawater will give more accurate estimations of how recovery and crystallization is affected by seawater.

8. References

1. Jasinski, S.M., et al., *Fertilizers - Sustaining Global Food Supplies*. 1999, U.S. Geological survey: https://minerals.usgs.gov/minerals/pubs/commodity/phosphate_rock/. p. 4.
2. Selman, M. and S. Greenhalgh, *Eutrophication: Sources and Drivers of Nutrient Pollution*, in *Water Quality: Eutrophication and Hypoxia*. 2009, World Resources Institute: http://www.wri.org/our-work/project/world-resources-report/publications. p. 8.
3. Cordell, D., J.-O. Drangert, and S. White, *The story of phosphorus: Global food security and food for thought.* Global Environmental Change, 2009. **19**(2): p. 292-305.
4. FAO, *THE STATE OF FOOD AND AGRICULTURE 2002*, in *FAO Agriculture Series*, E. Group and F.I. Division, Editors. 2002, Food and Agriculture Organization: Rome. p. 246.
5. Cordell, D. and S. White, *Peak Phosphorus: Clarifying the Key Issues of a Vigorous Debate about Long-Term Phosphorus Security.* Sustainability, 2011. **3**(10): p. 2027.
6. Grønlund, A., E. Brod, and O.S. Hanserud, *Potensial for gjenvinning og resirkulering av fosfor*, in *Vann*. 2015, Vannforeningen. p. 4.
7. European Commission, S.-G., *COMMUNICATION FROM THE COMMISSION TO THE EUROPEAN PARLIAMENT, THE COUNCIL, THE EUROPEAN ECONOMIC AND SOCIAL COMMITTEE AND THE COMMITTEE OF THE REGIONS Closing the loop - An EU action plan for the Circular Economy*. 2015, EUR-LEX: Brussels. p. 21.
8. European Commission. *Circular Economy - Implementation of the Circular Economy Action Plan*. 2018 07.03.2018 [cited 2018 08.04]; Available from: http://ec.europa.eu/environment/circular-economy/index_en.htm.
9. Shu, L., et al., *An economic evaluation of phosphorus recovery as struvite from digester supernatant.* Bioresource Technology, 2006. **97**(17): p. 2211-2216.
10. IVAR, *IVAR Årsrapport 2016*. 2016: https://issuu.com/admoment/docs/ivar-a__rsrapport_2016. p. 42.
11. Le Corre, K.S., et al., *Phosphorus Recovery from Wastewater by Struvite Crystallization: A Review.* Critical Reviews in Environmental Science and Technology, 2009. **39**(6): p. 433-477.
12. Prywer, J., A. Torzewska, and T. Płociński, *Unique surface and internal structure of struvite crystals formed by Proteus mirabilis.* Urological Research, 2012. **40**(6): p. 699-707.
13. Stratful, I., M.D. Scrimshaw, and J.N. Lester, *Conditions influencing the precipitation of magnesium ammonium phosphate.* Water Research, 2001. **35**(17): p. 4191-4199.
14. Doyle, J.D. and S.A. Parsons, *Struvite formation, control and recovery.* Water Research, 2002. **36**(16): p. 3925-3940.
15. Römer, W., *Vergleichende Untersuchung der Phosphatverfügbarkeit von Produkten des P-Recyclings und bekannter Phosphatdünger.* KA Korrespondens Abwasser, Abfall, 2006. **53**(5): p. 14.
16. Wang, J., et al., *Engineered Struvite Precipitation: Impacts of Component-Ion Molar Ratios and pH.* Journal of Environmental Engineering, 2005. **131**(10): p. 1433-1440.
17. Kataki, S., et al., *Phosphorus recovery as struvite from farm, municipal and industrial waste: Feedstock suitability, methods and pre-treatments.* Waste Management, 2016. **49**: p. 437-454.
18. Liu, Y., et al., *Magnesium ammonium phosphate formation, recovery and its application as valuable resources: A review.* Journal of Chemical Technology and Biotechnology, 2013. **88**(2): p. 181-189.
19. Acelas, N.Y., E. Flórez, and D. López, *Phosphorus recovery through struvite precipitation from wastewater: effect of the competitive ions.* Desalination and Water Treatment, 2015. **54**(9): p. 2468-2479.
20. Barbosa, S.G., et al., *A design of experiments to assess phosphorous removal and crystal properties in struvite precipitation of source separated urine using different Mg sources.*

Chemical Engineering Journal, 2016. **298**: p. 146-153.
21. Kataki, S., et al., *Phosphorus recovery as struvite: Recent concerns for use of seed, alternative Mg source, nitrogen conservation and fertilizer potential.* Resources, Conservation and Recycling, 2016. **107**: p. 142-156.
22. Ariyanto, E., H.M. Ang, and T.K. Sen, *Impact of various physico-chemical parameters on spontaneous nucleation of struvite (MgNH4PO4.6H2O) formation in a wastewater treatment plant: kinetic and nucleation mechanism.* Desalination and Water Treatment, 2014. **52**(34-36): p. 6620-6631.
23. Ohlinger, K.N., T.M. Young, and E.D. Schroeder, *Kinetics Effects on Preferential Struvite Accumulation in Wastewater.* Journal of Environmental Engineering, 1999. **125**(8): p. 730-737.
24. Bouropoulos, N.C. and P.G. Koutsoukos, *Spontaneous precipitation of struvite from aqueous solutions.* Journal of Crystal Growth, 2000. **213**(3): p. 381-388.
25. Ohlinger, K.N., T.M. Young, and E.D. Schroeder, *Predicting struvite formation in digestion.* Water Research, 1998. **32**(12): p. 3607-3614.
26. Merino-Jimenez, I., et al., *Enhanced MFC power production and struvite recovery by the addition of sea salts to urine.* Water Research, 2017. **109**(Supplement C): p. 46-53.
27. Mavinic, D.S., A. Adnan, and F.A. Koch, *Pilot-scale study of phosphorus recovery through struvite crystallization – examining the process feasibility.* Journal of Environmental Engineering & Science, 2003. **2**(5): p. 315-324.
28. Liu, X., et al., *Phosphorus recovery from urine with different magnesium resources in an air-agitated reactor.* Environmental Technology, 2014. **35**(22): p. 2781-2787.
29. Cerrillo, M., et al., *Struvite precipitation as a technology to be integrated in a manure anaerobic digestion treatment plant – removal efficiency, crystal characterization and agricultural assessment.* Journal of Chemical Technology & Biotechnology, 2015. **90**(6): p. 1135-1143.
30. Le Corre, K.S., et al., *Impact of calcium on struvite crystal size, shape and purity.* Journal of Crystal Growth, 2005. **283**(3): p. 514-522.
31. Bhuiyan, M.I.H., D.S. Mavinic, and R.D. Beckie, *Nucleation and growth kinetics of struvite in a fluidized bed reactor.* Journal of Crystal Growth, 2008. **310**(6): p. 1187-1194.
32. Abbona, F., H.E. Lundager Madsen, and R. Boistelle, *Crystallization of two magnesium phosphates, struvite and newberyite: Effect of pH and concentration.* Journal of Crystal Growth, 1982. **57**(1): p. 6-14.
33. Schneider, P.A., J.W. Wallace, and J.C. Tickle, *Modelling and dynamic simulation of struvite precipitation from source-separated urine.* Water Science and Technology, 2013. **67**(12): p. 2724-2732.
34. Rahman, M.M., et al., *Production of slow release crystal fertilizer from wastewaters through struvite crystallization – A review.* Arabian Journal of Chemistry, 2014. **7**(1): p. 139-155.
35. Mullin, J.W., *3 - Solutions and solubility*, in *Crystallization (Fourth Edition)*. 2001, Butterworth-Heinemann: Oxford. p. 86-134.
36. Bhuiyan, M.I.H., D.S. Mavinic, and R.D. Beckie, *A SOLUBILITY AND THERMODYNAMIC STUDY OF STRUVITE.* Environmental Technology, 2007. **28**(9): p. 1015-1026.
37. Lee, S.-h., R. Kumar, and B.-H. Jeon, *Struvite precipitation under changing ionic conditions in synthetic wastewater: Experiment and modeling.* Journal of Colloid and Interface Science, 2016. **474**(Supplement C): p. 93-102.
38. Crutchik, D. and J.M. Garrido, *Struvite crystallization versus amorphous magnesium and calcium phosphate precipitation during the treatment of a saline industrial wastewater.* Water Science and Technology, 2011. **64**(12): p. 2460-2467.
39. Lu, X., et al., *Accuracy and application of quantitative X-ray diffraction on the precipitation of struvite product.* Water Research, 2016. **90**: p. 9-14.
40. Nelson, N.O., R.L. Mikkelsen, and D.L. Hesterberg, *Struvite precipitation in anaerobic swine lagoon liquid: effect of pH and Mg:P ratio and determination of rate constant.* Bioresource

Technology, 2003. **89**(3): p. 229-236.
41. Jordaan, E.M., J. Ackerman, and N. Cicek, *Phosphorus removal from anaerobically digested swine wastewater through struvite precipitation.* Water Science and Technology, 2010. **61**(12): p. 3228-3234.
42. Hao, X.D., et al., *Struvite formation, analytical methods and effects of pH and Ca 2+*, in *Water Science and Technology*. 2008. p. 1687-1692.
43. Münch, E.V. and K. Barr, *Controlled struvite crystallisation for removing phosphorus from anaerobic digester sidestreams.* Water Research, 2001. **35**(1): p. 151-159.
44. Desmidt, E., et al., *Global Phosphorus Scarcity and Full-Scale P-Recovery Techniques: A Review.* Critical Reviews in Environmental Science and Technology, 2015. **45**(4): p. 336-384.
45. Wu, Q. and P.L. Bishop, *Enhancing struvite crystallization from anaerobic supernatant.* Journal of Environmental Engineering and Science, 2004. **3**(1): p. 21-29.
46. Matsumiya, Y., T. Yamasita, and Y. Nawamura, *Phosphorus Removal from Sidestreams by Crystallisation of Magnesium-Ammonium-Phosphate Using Seawater.* Water and Environment Journal, 2000. **14**(4): p. 291-296.
47. Jaffer, Y., et al., *Potential phosphorus recovery by struvite formation.* Water Research, 2002. **36**(7): p. 1834-1842.
48. Latifian, M., J. Liu, and B. Mattiasson, *Struvite-based fertilizer and its physical and chemical properties.* Environmental Technology, 2012. **33**(24): p. 2691-2697.
49. Ping, Q., et al., *Characterization of morphology and component of struvite pellets crystallized from sludge dewatering liquor: Effects of total suspended solid and phosphate concentrations.* Journal of Hazardous Materials, 2016. **310**: p. 261-269.
50. Dockhorn, T., *About the economy of phosphorus recovery*. International Conference on Nutrient Recovery from Wastewater Streams, ed. K. Ashley, D. Mavinic, and F. Koch. 2009, Vancouver, Canada: IWA Publishing.
51. Liu, B., et al., *Characterization of induced struvite formation from source-separated urine using seawater and brine as magnesium sources.* Chemosphere, 2013. **93**(11): p. 2738-2747.
52. Lahav, O., et al., *Struvite recovery from municipal-wastewater sludge centrifuge supernatant using seawater NF concentrate as a cheap Mg(II) source.* Separation and Purification Technology, 2013. **108**: p. 103-110.
53. Quist-Jensen, C., M. Koustrup Jørgensen, and M. Christensen, *Treated Seawater as a Magnesium Source for Phosphorous Recovery from Wastewater—A Feasibility and Cost Analysis.* Membranes, 2016. **6**(4): p. 54.
54. Lenntech, BV. *Conductivity convertor*. [cited 2018 05.06]; Available from: https://www.lenntech.com/calculators/conductivity/tds_engels.htm.
55. Richardsen, K.L., *Enhanced Biological Phosphorus Removal in Typical Norwegian Wastewater*, in *Department of Civil and Environmental Engineering*. 2017, Norwegian University of Science and Technology (NTNU). p. 134.
56. Lenntech, BV. *TDS and Electrical Conductivity*. [cited 2018 05.06]; Available from: https://www.lenntech.com/calculators/tds/tds-ec_engels.htm.
57. Cotruvo, J.A., *Water Desalination Processes and Associated Health and Environmental Issues*, in *Water Conditioning and Purification*. 2005, WC&P.
58. Yilmazel, Y.D. and G.N. Demirer, *Removal and recovery of nutrients as struvite from anaerobic digestion residues of poultry manure.* Environmental Technology, 2011. **32**(7): p. 783-794.
59. Drouet, C., *Apatite Formation: Why It May Not Work as Planned, and How to Conclusively Identify Apatite Compounds*. Vol. 2013. 2013. 490946.
60. Mekmene, O., et al., *Effects of pH and Ca/P molar ratio on the quantity and crystalline structure of calcium phosphates obtained from aqueous solutions.* Dairy Science & Technology, 2009. **89**(3): p. 301-316.
61. Scott A. Speakman, Ph.D., *Introduction to X-Ray Powder Diffraction Data Analysis*. Massachusetts Institute of Technology:

http://prism.mit.edu/xray/education/downloads.html. p. 20.
62. Capdevielle, A., et al., *Effects of organic matter on crystallization of struvite in biologically treated swine wastewater.* Environmental Technology, 2016. **37**(7): p. 880-892.
63. Mullin, J.W., *6 - Crystal growth*, in *Crystallization (Fourth Edition)*. 2001, Butterworth-Heinemann: Oxford. p. 216-288.
64. Birnhack, L., et al., *A new algorithm for design, operation and cost assessment of struvite (MgNH4PO4) precipitation processes.* Environ Technol, 2015. **36**(13-16): p. 1892-901.

Appendix 1

Real reject water composition was first estimated based on spectrophotometry measurements of NH_4-N, PO_4-P and Mg^{2+}. The results showing high Mg^{2+} concentration indicate that there might be seawater intrusion into the wastewater treatment plant where the reject water was retrieved from. When performing ion chromatography measurements of cations on the samples from experiment GR1 and GR3, it was possible to calculate K^+, Ca^{2+} and Na^+ concentrations. These turned out to be higher than what the seawater amount, salt addition for P and N adjustment and pH adjustment with NaOH would indicate. The calculated concentrations of these ions can be seen in Table A1.1 together with measured Mg^{2+} concentration and conductivity. By comparing these concentrations with the concentrations in seawater, it was possible to estimate a ratio of seawater to reject water concentrations, based on an assumption that the seawater going into *SNJ* has the same composition as the seawater used in this study.

Table A1.1: Calculated reject water concentrations based on IC and seawater composition

	Reject water	Seawater	Ratio of reject to seawater concentration
Na^+ [mg/L]	320	10570	0.03
Ca^{2+} [mg/L]	40	447	0.09
K^+ [mg/L]	40	393	0.10
Mg^{2+} [mg/L]	41.6	1276	0.03
Conductivity [µS/cm]	1744	31600	0.06

Since these cations also can originate from soils surrounding the places where intrusion takes place, the lowest estimate of a 0.03 ratio of seawater to reject water, or 3% is chosen for calculating concentration of Cl^- in the reject water. This gave a slightly higher conductivity (+0.2 mS/cm) than the measured one when all known and estimated seawater ions were put into the conductivity calculator found at:
https://www.lenntech.com/calculators/tds/tds-ec_engels.htm
and the conductivity converter found at:
https://www.lenntech.com/calculators/conductivity/tds_engels.htm.

Based on a 3% seawater amount, the Cl^- concentration in the reject water is 570 mg/L. The maximum value of 2360 mg/L given in Table 3-3 includes 1790 mg/L from NH_4Cl salt

contribution. As conductivity measurement of real reject water after N and P adjustment was not possible, it was calculated based on the conductivity in the original reject water, the addition of salts for P and N adjustment, and the deviation of +0.2 mS/cm. This gave a conductivity of 6600 µS/cm.

Appendix 2

Input values to *Visual MINTEQ* for S1, S2 S3, S4, S5 and R5f/R6a/R6b.

S1:

The pH was fixed at 7.5, 8.0, 8.5, 9.0 and 9.5. Na^+ is changing due to different NaOH concentrations. *Table A2.1* and *A2.2* show the ion composition of the mix of reject water and $MgCl_2$. Temperature was set to 20 ℃. Cl^- is added from both $MgCl_2$ and NH_4Cl-salt, whereas Na^+ is added from NaH_2PO_4-salt and pH adjustment with NaOH.

Table A2.1: Concentrations at all pH values in S1 [mg/L]

Ion	***Mg/L***
Mg^{2+}	107.55
$N\ (NH_4^+)$	754.28
$P\ (PO_4)$	137.06
Cl^-	2222.715

Table A2.2: Concentrations that changes with pH in S1 [mg/L]

	7.5	***8.0***	***8.5***	***9.0***	***9.5***
Na^+	294.824	345.494	451.87	600.0	912.82
H^+	0.451	-1.753	-6.38	-12.809	-26.43

S2:

The pH was fixed at 7.5, 8.0, 8.5, 9.0 and 9.5 in the five runs. The temperature was set to 20°C in all runs. *Table A2.3* shows the ion concentrations calculated from seawater characteristics and composition of the synthetic reject water. *Table A2.4* shows concentrations that depend on pH. Carbonate (CO_3^{2-}) is calculated from theoretical values of bicarbonate in typical seawater, using equilibrium equations for carbonate species. The CO_3^{2-} concentration change because bicarbonate and carbonic acid are pH dependant, and these are in equilibrium with carbonate. Sodium (Na^+) change with pH because we are adding different amounts of NaOH depending on which pH we are aiming at. The concentrations we put into *Visual MINTEQ* therefore matches the concentrations we ended up with in our experiments, calculated from the volume of 1 M NaOH that was added.

Table A2.3: Concentrations at all pH values in S2 [mg/L]

Ion	***mg/L***
P (PO_4)	137.06
N ($NH4^+$)	754.30
Mg^{2+}	107.55
Cl^-	3508.74
Ca^{2+}	37.67
S (SO_4)	77.09
K^+	33.13
N (NO_3^-)	3.05
Br^-	6.74

Table A2.4: Concentrations that change with pH in S2 [mg/L]

	7.5	***8.0***	***8.5***	***9.0***	***9.5***
H^+	1.14	-0.05	-1.25	-11.65	-21.35
CO_3^{2-}	0.30	0.92	2.53	5.59	9.04
Na^+	1169.89	1197.25	1224.84	1463.93	1686.94

S3:

The pH was fixed at 7.5, 8.0, 8.5, 9.0 and 9.5. Na^+ is changing due to different NaOH concentrations. *Table A2.5* and *A2.6* show the ion composition of the mix of synthetic reject water and $MgCl_2$. Temperature was set to 20℃. Cl^- is added from both $MgCl_2$ and NH_4Cl-salt, whereas Na^+ is added from NaH_2PO_4-salt and pH adjustment with NaOH.

Table A2.5: Concentrations at all pH values in S3 [mg/L]

Ion	***Mg/L***
Mg^{2+}	179.61
N (NH_4^+)	754.28
P (PO_4)	137.06
Cl^-	2432.92

Table A2.6: Concentrations that changes with pH in S3 [mg/L]

	7.5	*8.0*	*8.5*	*9.0*	*9.5*
Na^+	294.824	345.494	451.87	600.0	912.82

S4:

The pH was fixed at 7.5, 8.0, 8.5, 9.0 and 9.5 in the five runs. The temperature was set to 20°C in all runs. *Table A2.7* shows the ion concentrations calculated from seawater characteristics and composition of the synthetic reject water. *Table A2.8* shows concentrations that depend on pH. Carbonate (CO_3^{2-}) is calculated from theoretical values of bicarbonate in typical seawater, using equilibrium equations for carbonate species. The CO_3^{2-} concentration change because bicarbonate and carbonic acid are pH dependant, and these are in equilibrium with carbonate. Sodium (Na^+) change with pH because we are adding different amounts of NaOH depending on which pH we are aiming at. The concentrations we put into *Visual MINTEQ* therefore matches the concentrations we ended up with in our experiments, calculated from the volume of 1 M NaOH that was added.

Table A2.7: Concentrations at all pH values in S4 [mg/L]

Ion	***mg/L***
P (PO_4)	137.06
N ($NH4^+$)	754.3
Mg^{2+}	179.597
Cl^-	4580.419
Ca^{2+}	62.915
S (SO_4)	128.724
K^+	55.315
N (NO_3^-)	5.085
Br^-	11.26

Table A2.8: Concentrations that change with pH in S4 [mg/L]

	7.5	***8.0***	***8.5***	***9.0***	***9.5***
CO_3^{2-}	0.502	1.539	4.228	9.341	15.010
Na^+	1786.024	1817.06	1865.339	2141.219	2371.119

S5:

The pH was fixed at 7.5 and temperature was set to 20°C for all runs. The concentrations in *Table A2.9* were calculated for each Mg:P based on measured and reported seawater and synthetic reject water compositions. CO_3^{2-} is calculated from theoretical values of bicarbonate in typical seawater, using equilibrium equations for carbonic acid.

Table A2.9: Concentrations of ions in experiment S5, given in mg/L

Mg:P molar ratio	***1.0***	***1.67***	***2.34***	***3.0***
P (PO_4)	126.406	120.15	114.481	109.398
N ($NH4^+$)	695.665	661.23	630.037	602.063
Mg^{2+}	99.189	157.45	210.207	257.53
Cl^-	3236.045	4102.6	4721.294	5354.405
Na^+	1063.993	1546.6	1984.204	2372.441
Ca^{2+}	34.747	55.16	73.638	90.216
S (SO_4)	71.093	112.85	150.663	184.581
K^+	30.55	48.5	64.742	79.318
N (NO_3^-)	2.808	4.46	5.952	7.292
Br^-	6.22	9.87	13.179	16.146
CO_3^{2-}	0.277	0.44	0.511	0.72

R5f/R6a/R6b:

For thermodynamic calculations of R5f, R6a and R6b, the estimated composition of real filtered reject water is used (table 3-3), together with the measured ions of seawater. Temperature was set to 20°C. CO_3^{2-} is calculated from theoretical values of bicarbonate in typical seawater, using equilibrium equations for carbonic acid. pH was set to 7.5 in R5, and increased to 8.0 and 8.5 for R6a and R6b. The only difference between the R5 and R6 series is the concentration of H^+ and Na^+ due to pH adjustment with NaOH. These concentrations are given in *Table A2.11* and *A2.12* for pH 8.0 and 8.5 respectively.

Table A2.10: Concentrations [mg/L] of ions in experiment R5f, R6a and R6b (except Na^+ and H^+).

Mg:P molar ratio	***1.0***	***1.67***	***2.34***	***3.0***
P (PO_4)	128.54	120.66	117.36	111.18
N ($NH4^+$)	725.34	685.88	658.68	630.33
Mg^{2+}	93.61	141.65	198.6	240.92
Cl^-	3082.607	3869.396	4581.677	5220.328
**Na^+*	1028.950	1514.237	1950.120	2340.029
Ca^{2+}	58.214	77.440	94.875	110.511
S (SO_4)	68.526	110.368	148.305	182.331
K^+	55.638	72.3204	87.4495	101.017
N (NO_3^-)	1.723	3.425	4.967	6.351
Br^-	3.816	7.584	11	14.064
CO_3^{2-}	0.2	0.34	0.5	0.72
**H^+*	-0.124	-0.694	-1.04	-1.305

***Only for R5f**

Table A2.11: Concentrations at pH 8.0 in R6a and R6b

	R6a (Mg:P=1.67)	*R6b (Mg:P=2.34)*
Na^+	1545.273	1973.110
H^+	-2.044	-2.039

Table A2.12: Concentrations at pH 8.5 in R6a and R6b

	R6a (Mg:P=1.67)	*R6b (Mg:P=2.34)*
Na^+	1621.140	2005.296
H^+	-5.344	-3.439

Appendix 3

Table A3.1: SI of oversaturated compounds when using $MgCl_2$ at Mg:P=1.0 (S1)

	Saturation indexes at different pH in S3				
Compound	**7.5**	**8.0**	**8.5**	**9.0**	**9.5**
Mg3(PO4)2(s)	-	-	0.968	1.959	2.909
Struvite	1.127	1.656	2.135	2.554	2.850

Table A3.2: SI of oversaturated compounds when using seawater at Mg:P=1.0 (S2)

Saturation indexes at different pH for oversaturated compounds in S2					
Mineral	**7.5**	**8.0**	**8.5**	**9.0**	**9.5**
Ca3(PO4)2 (am1)	-	-	0.512	1.208	1.603
Ca3(PO4)2 (am2)	1.334	2.371	3.283	3.979	4.374
Ca3(PO4)2 (beta)	2.425	3.463	4.374	5.070	5.465
Ca4H(PO4)3:3H2O(s)	1.938	3.002	3.887	4.474	4.656
CaHPO4(s)	0.331	0.357	0.331	0.222	0.009
CaHPO4:2H2O(s)	0.023	0.050	0.023	-	-
Hydroxyapatite	10.056	12.104	13.954	15.454	16.458
Mg3(PO4)2(s)	-	-	0.649	1.607	2.538
Struvite	0.974	1.501	1.983	2.387	2.678
Dolomite (ordered) $CaMg(CO_3)_2$	-	-	-	-	0.116

Table A3.3: SI of oversaturated compounds when using $MgCl_2$ at Mg:P=1.67 (S3)

	Saturation indexes at different pH in S3				
Compound	**7.5**	**8.0**	**8.5**	**9.0**	**9.5**
Mg3(PO4)2(s)	-	0.505	1.514	2.504	3.454
$MgHPO_4:3H_2O$(s) (Newberyite)	0.081	0.116	0.122	0.117	0.093
Struvite	1.288	1.814	2.293	2.712	3.008

Table A3.4: SI of oversaturated compounds when using seawater at Mg:P=1.67 (S4)

Saturation indexes at different pH for oversaturated compounds in S4					
Mineral	**7.5**	**8.0**	**8.5**	**9.0**	**9.5**
Ca3(PO4)2 (am1)	-	0.020	0.942	1.676	2.142
Ca3(PO4)2 (am2)	1.755	2.791	3.713	4.447	4.913
Ca3(PO4)2 (beta)	2.846	3.882	4.805	5.538	6.004
Ca4H(PO4)3:3H2O(s)	2.471	3.532	4.429	5.064	5.336
CaHPO4(s)	0.445	0.469	0.444	0.346	0.151
CaHPO4:2H2O(s)	0.137	0.161	0.136	0.037	-
Hydroxyapatite	10.783	12.831	14.701	16.266	17.392
Mg3(PO4)2(s)	-	0.052	1.056	2.000	2.905
Struvite	1.077	1.600	2.077	2.476	2.757
Dolomite (disordered) $CaMg(CO_3)_2$	-	-	-	-	0.344
Dolomite (ordered) $CaMg(CO_3)_2$	-	-	-	-	0.915

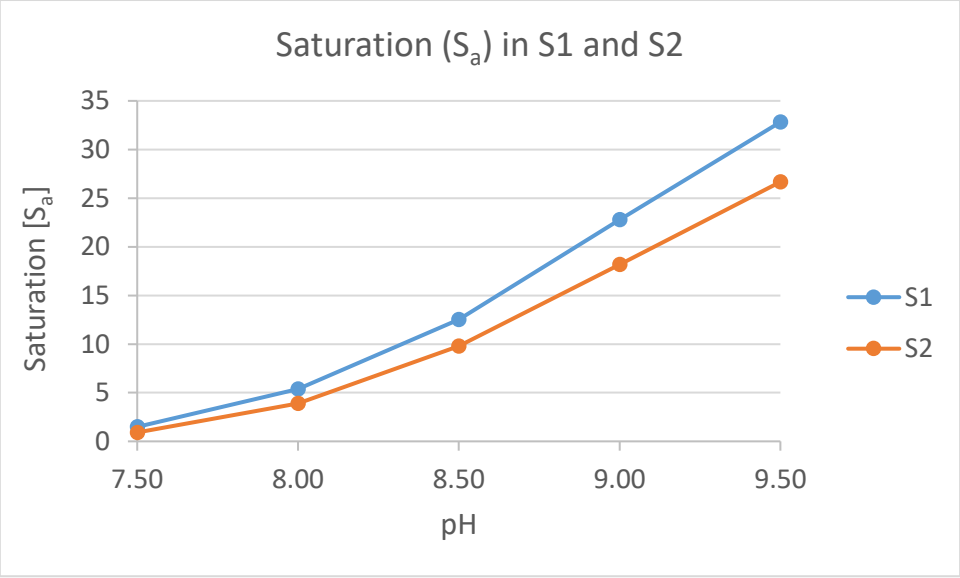

Figure A3.1: Saturation of struvite in S1 and S2.
Calculated from SI in tables A3.1 and A3.2, equation 3 and 4.

Appendix 4

Result of P and Mg recovery in experiment series S2, with measured minimum, maximum and average values based on 2 replicates.

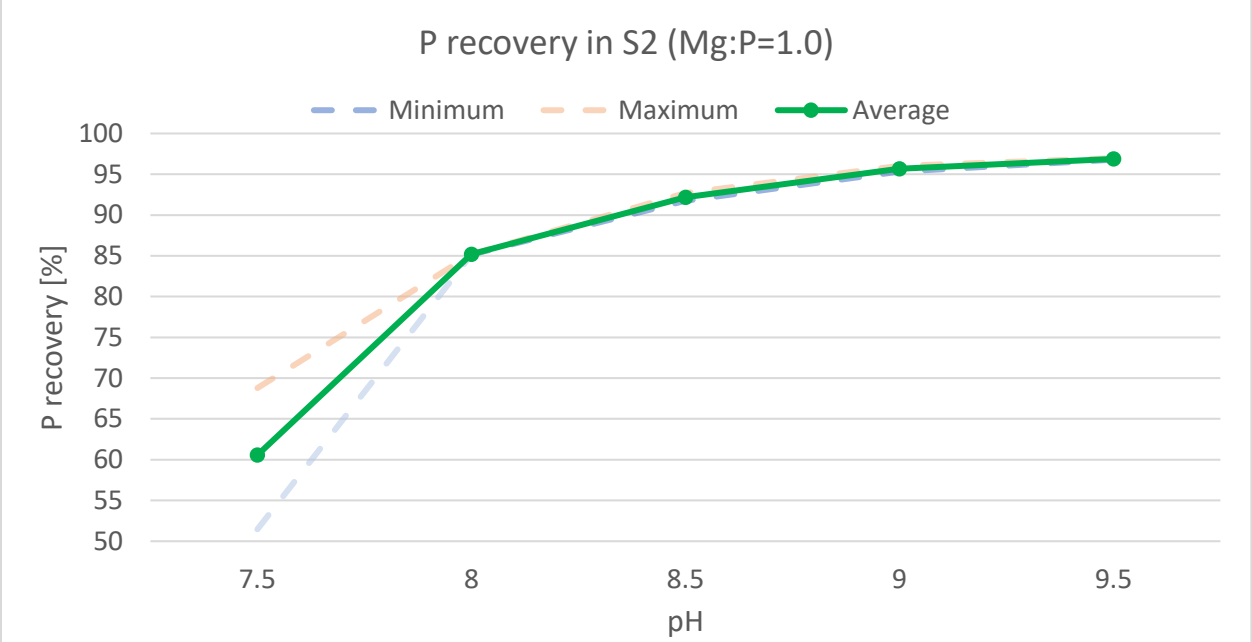

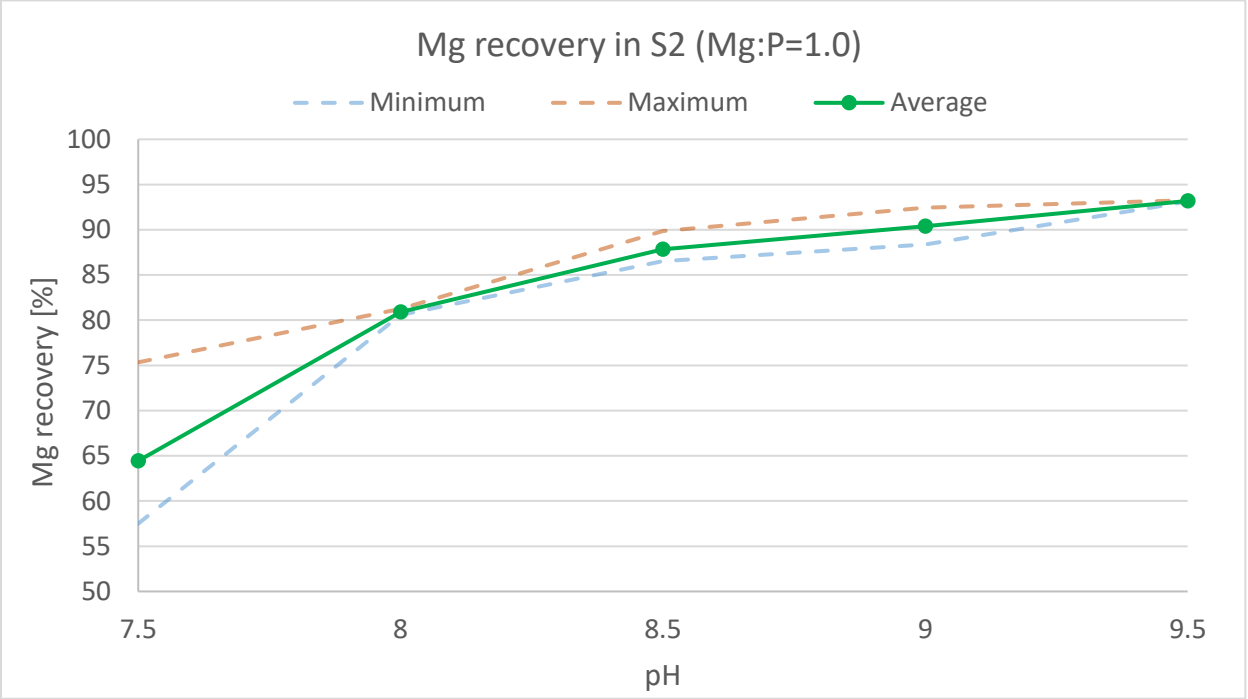

Appendix 5

Additional results from crystal growth experiments

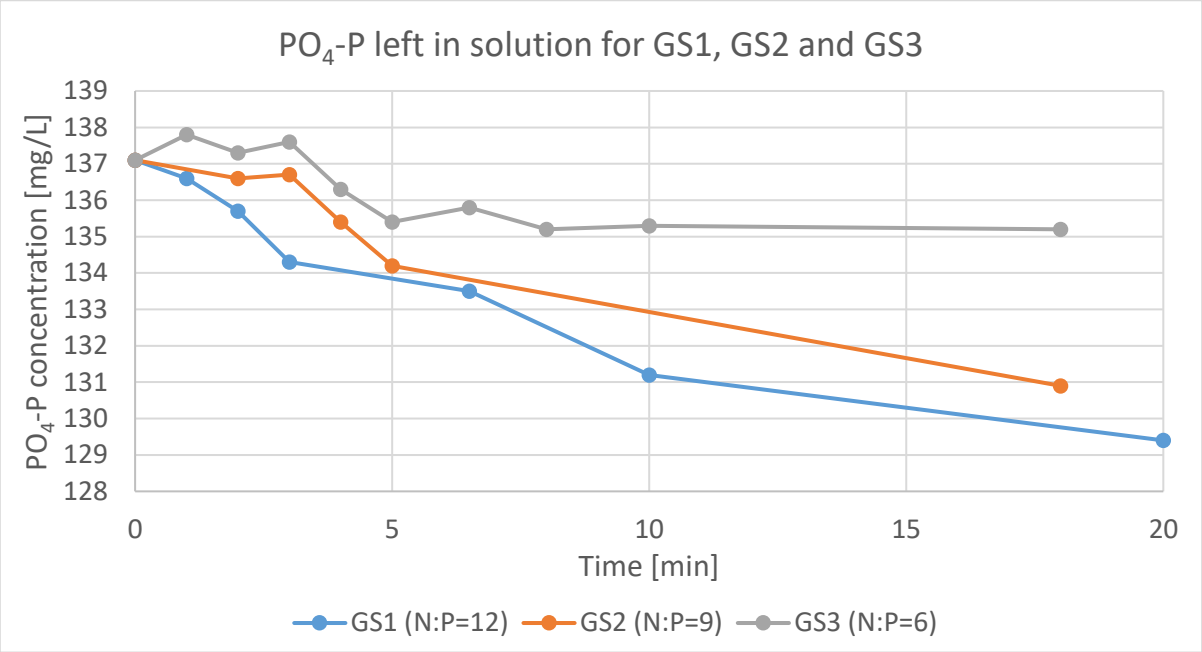

Figure A5.1: PO_4-P concentration in solution at 1 to 18-20 minutes after seed crystals were added.

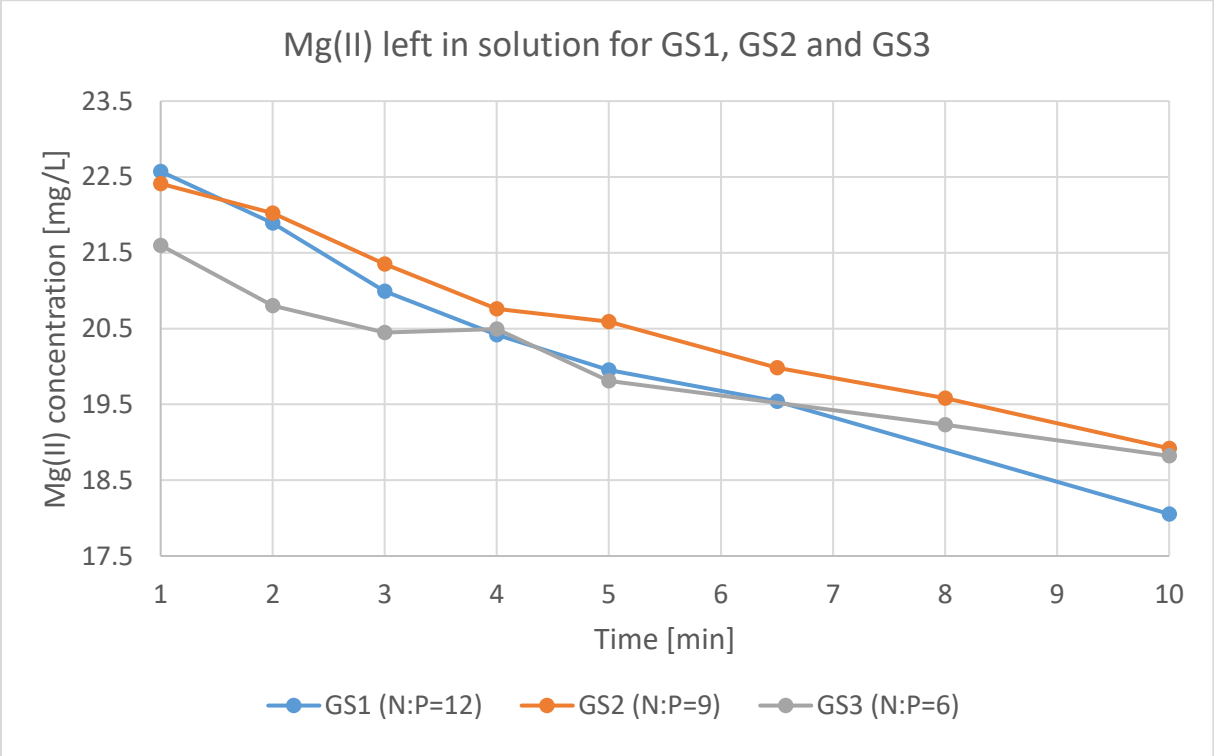

Figure A5.2: Mg(II) concentration in solution at 1 to 10 minutes after seed crystal addition.

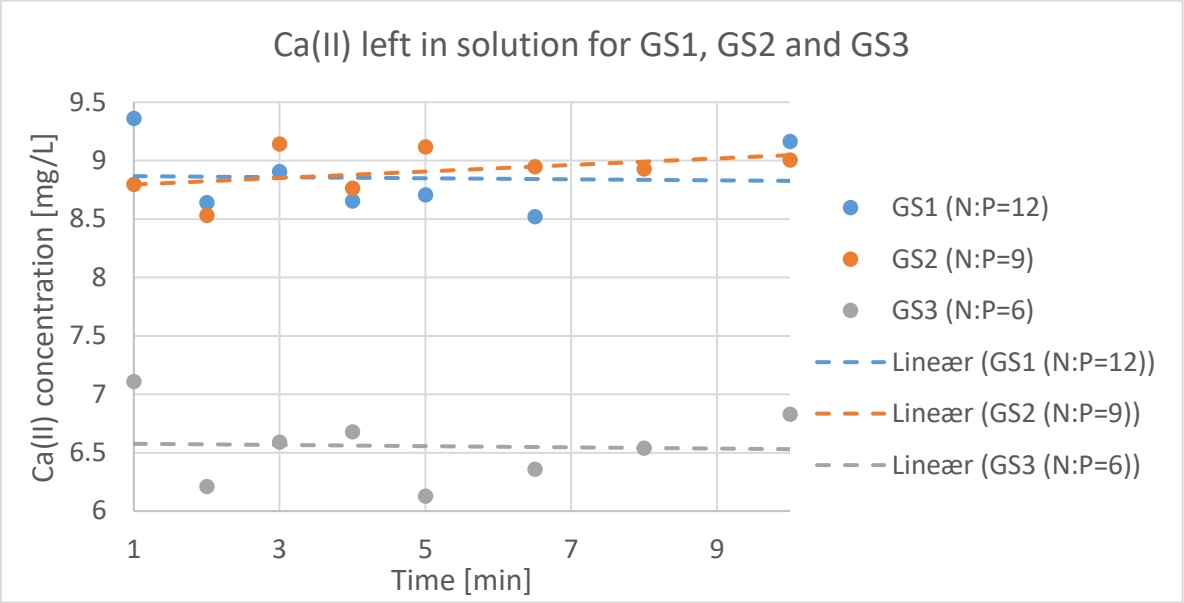

Figure A5.3: Ca(II) concentration in solution at 1 to 10 minutes after addition of seed crystals. The lower concentrations in GS3 are due to errors in ion chromatography results, which was not seen as crucial for the purpose of this figure.

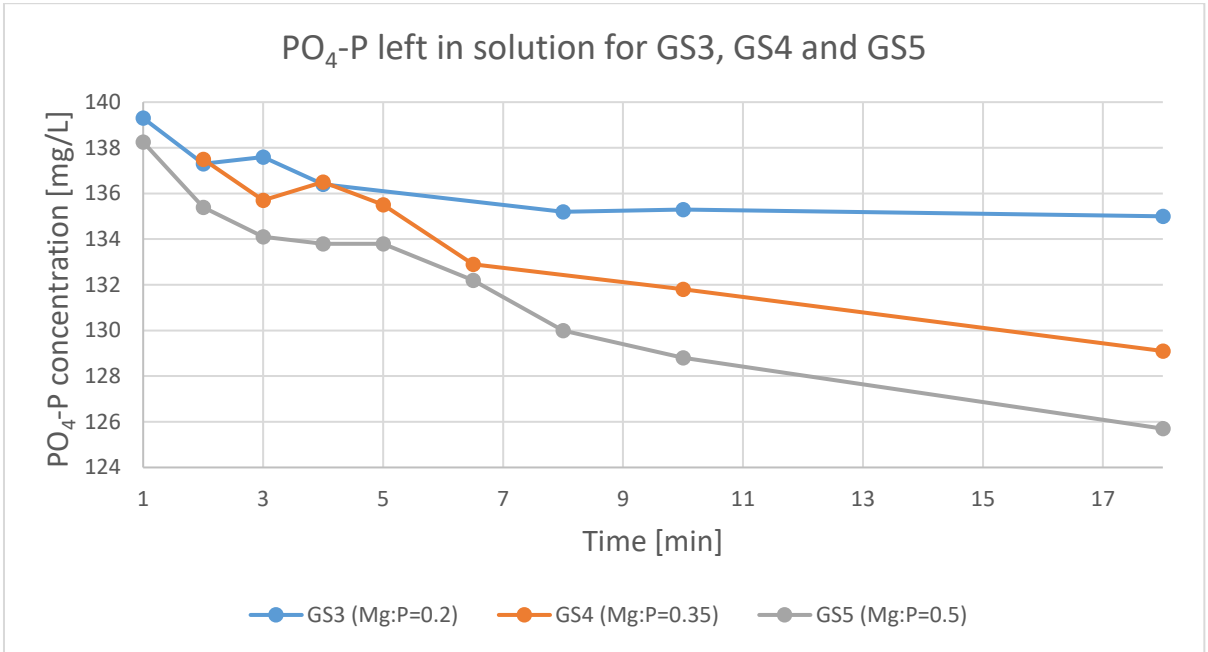

Figure A5.4: PO_4-P concentration in solution at 1 to 18 minutes after seed crystals were added.

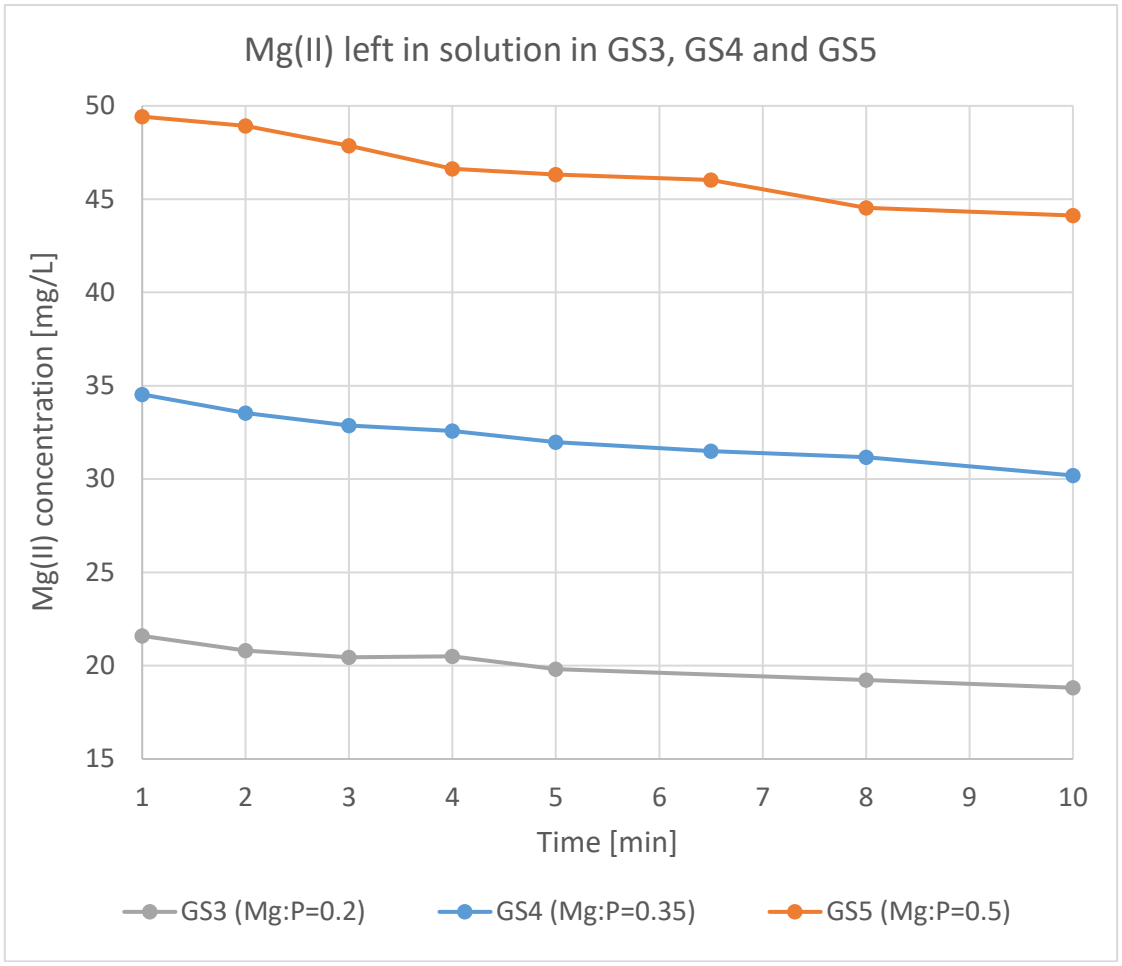

Figure A5.5: Mg(II) concentration in solution at 1 to 10 minutes after seed crystal addition

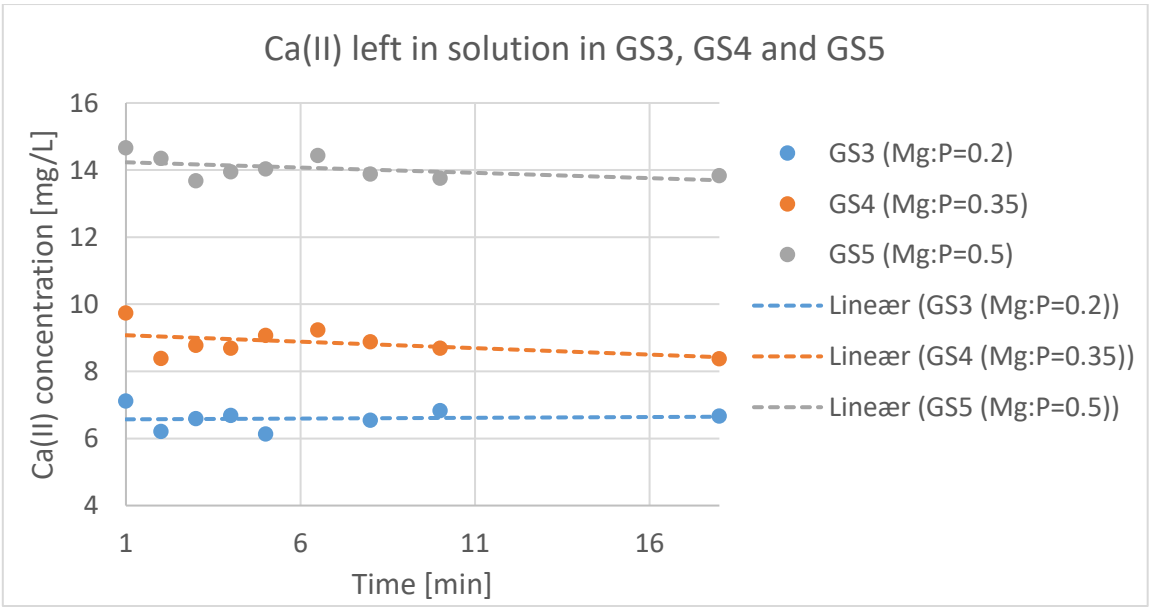

Figure A5.6: Ca(II) concentration in solution at 1 to 10 minutes after addition of seed crystals.

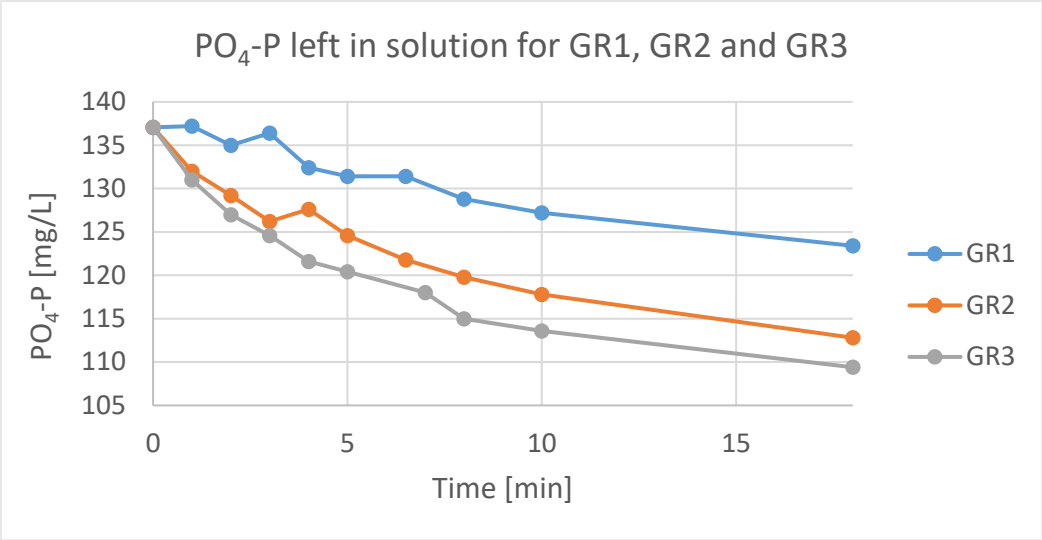

Figure A5.7: PO_4-P concentration in solution at 1 to 18 minutes after seed crystals were added.

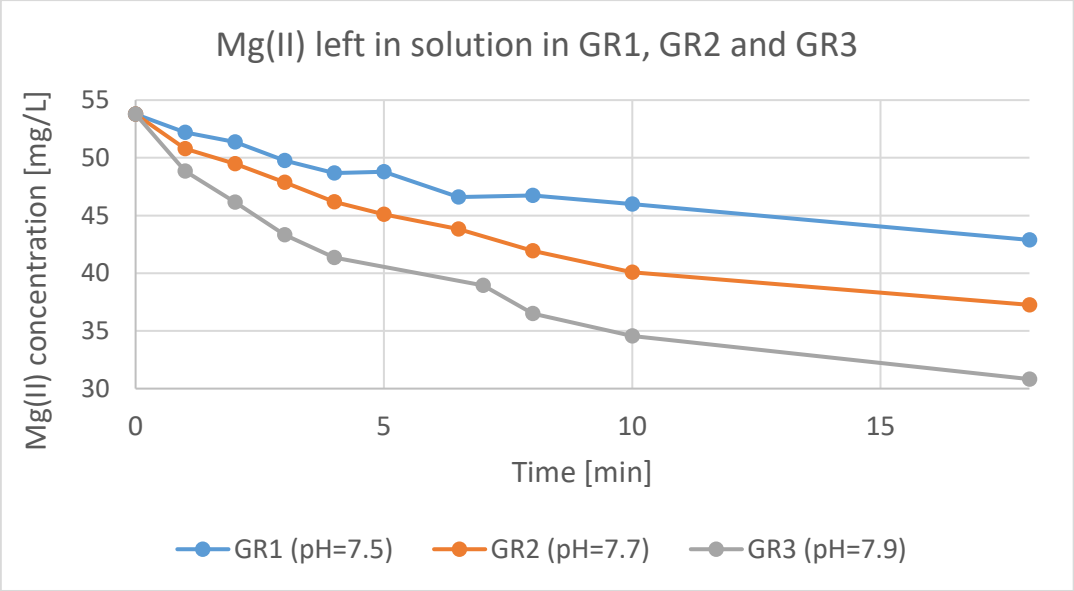

Figure A5.8: Mg(II) concentration in solution at 1 to 10 minutes after seed crystal addition

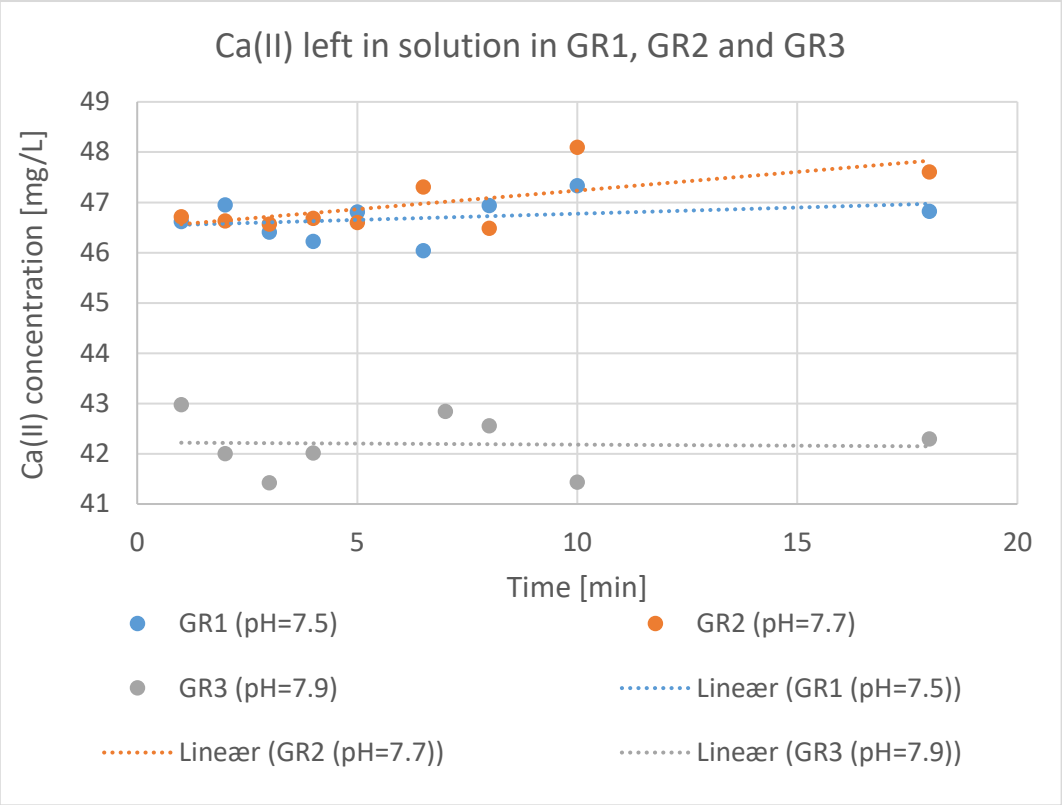

Figure A5.9: Ca(II) concentration in solution at 1 to 18 minutes after seed crystal addition.

Appendix 6

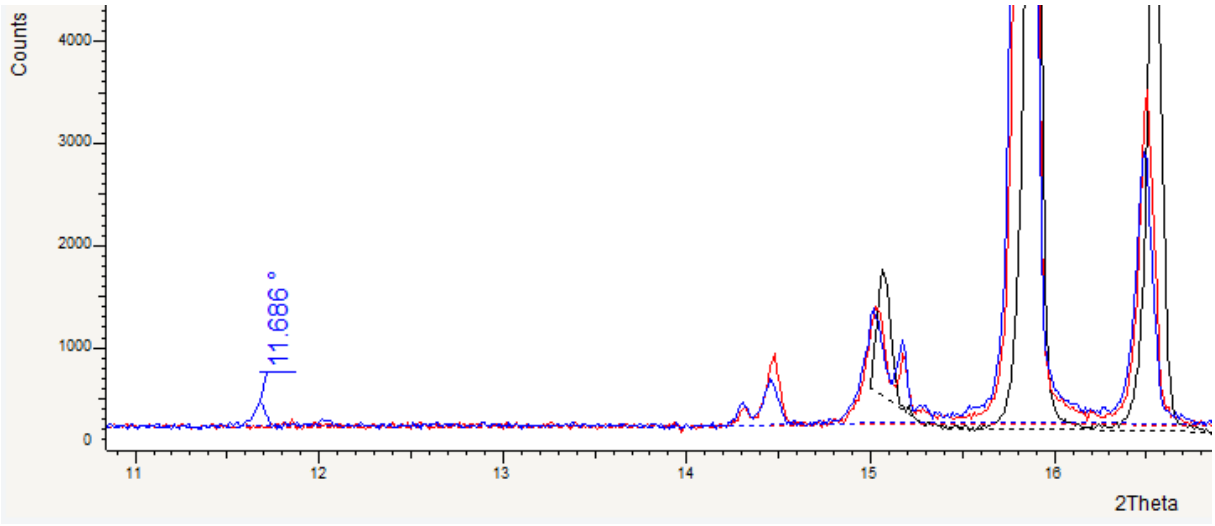

Figure A6.1: XRD pattern showing possible co-precipitation when using seawater. The blue pattern is of solids from experiment series S2 at pH 8.5, that have not been washed or filtered. The peak matches the 2Theta placement for one of the main peaks of brushite. The red pattern is from the same series at pH 7.5, also not washed or filtered.

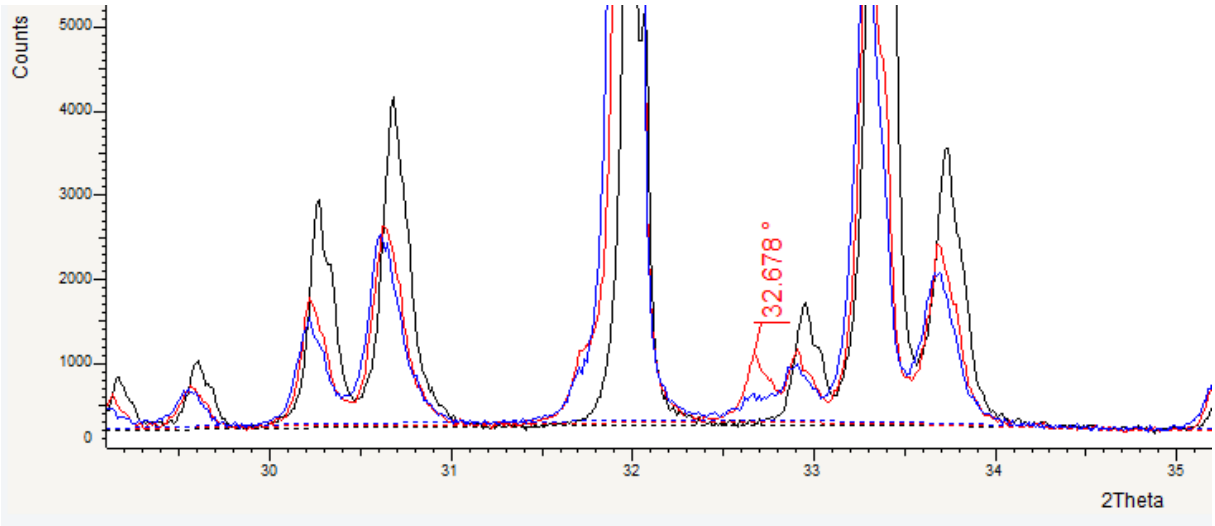

Figure A6.2: XRD pattern showing possible co-precipitant when using seawater. The red pattern is of solids from experiment series S2 at pH 7.5, that have not been washed or filtered. The blue pattern is from the same series at pH 8.5, also not washed or filtered.

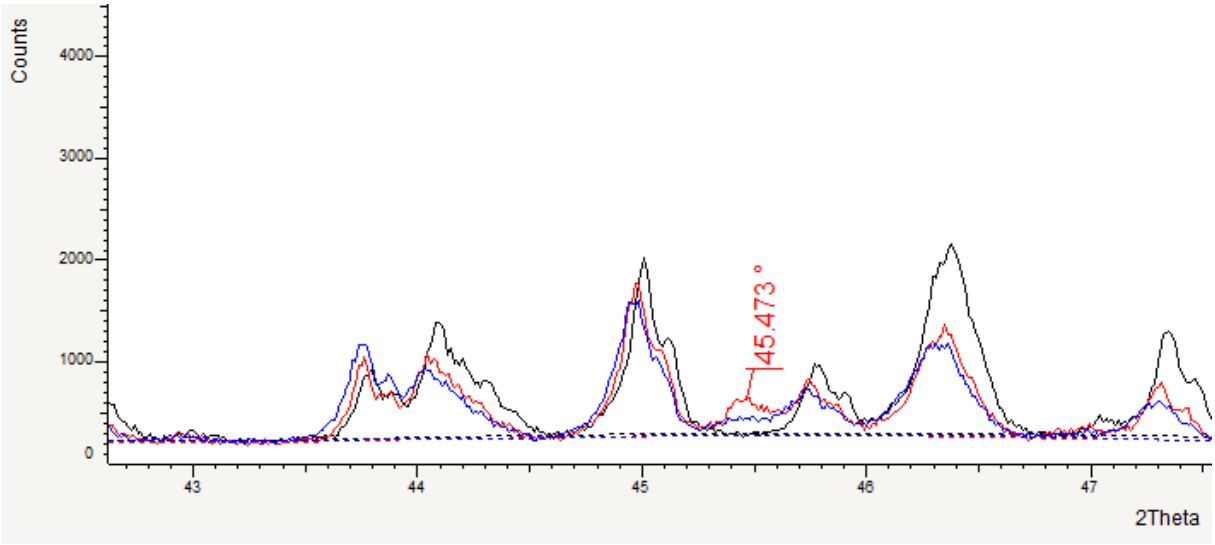

Figure A6.3: XRD pattern showing possible co-precipitant when using seawater.
The red pattern is of solids from experiment series S2 at pH 7.5, that have not been washed or filtered.
The blue pattern is from the same series at pH 8.5, also not washed or filtered.

Appendix 7

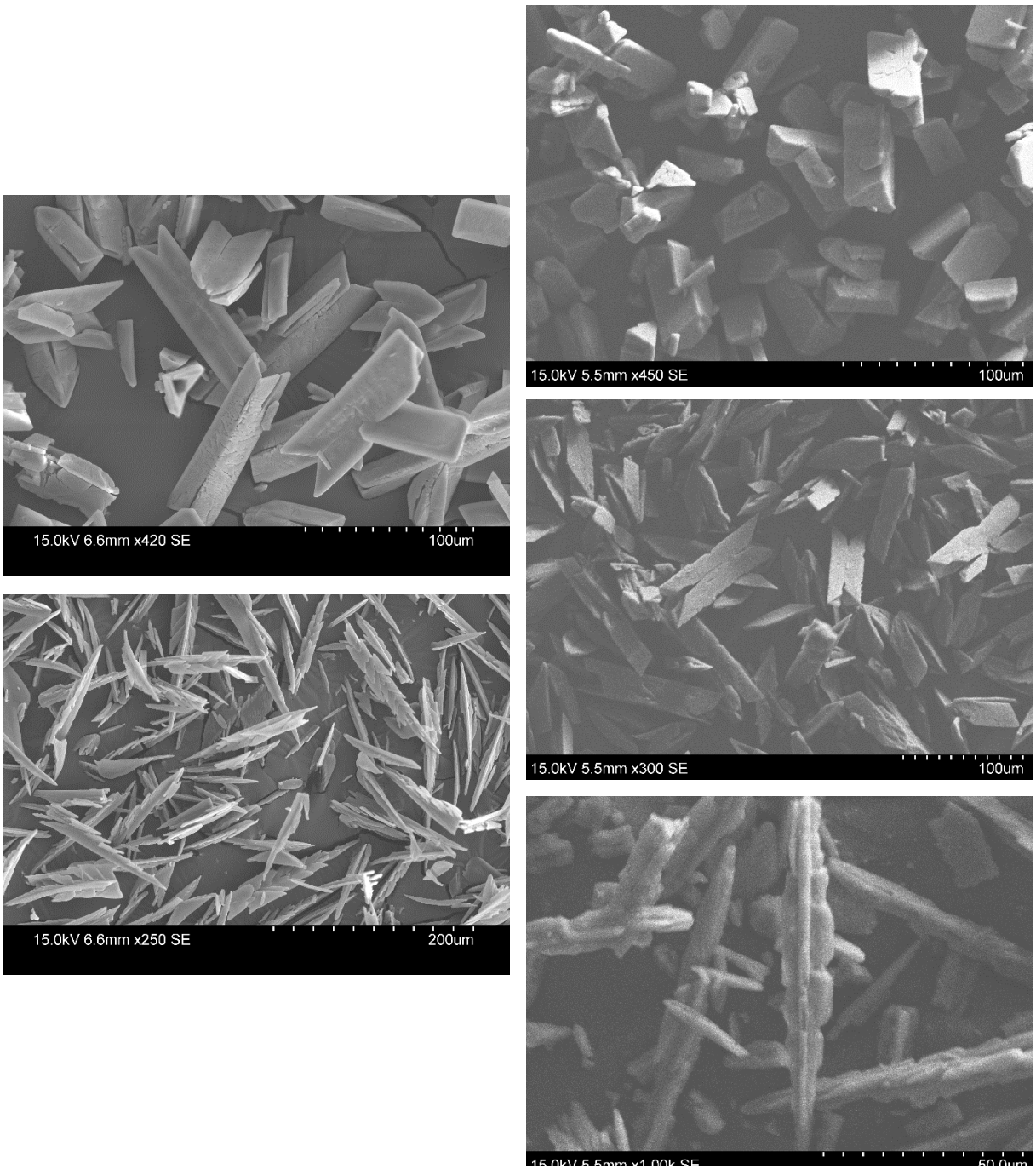

Figure A7.1: SEM images of struvite.

Left: $MgCl_2$ and synthetic reject water at pH 8.0 (top) and 9.0 (bottom) at Mg:P molar ratio of 1.67 (S3).

Right: Seawater and synthetic reject water at pH 7.5 (top), 8.5 (middle) and 9.5 (bottom) at Mg:P molar ratio of 1.67 (S4).

Appendix 8

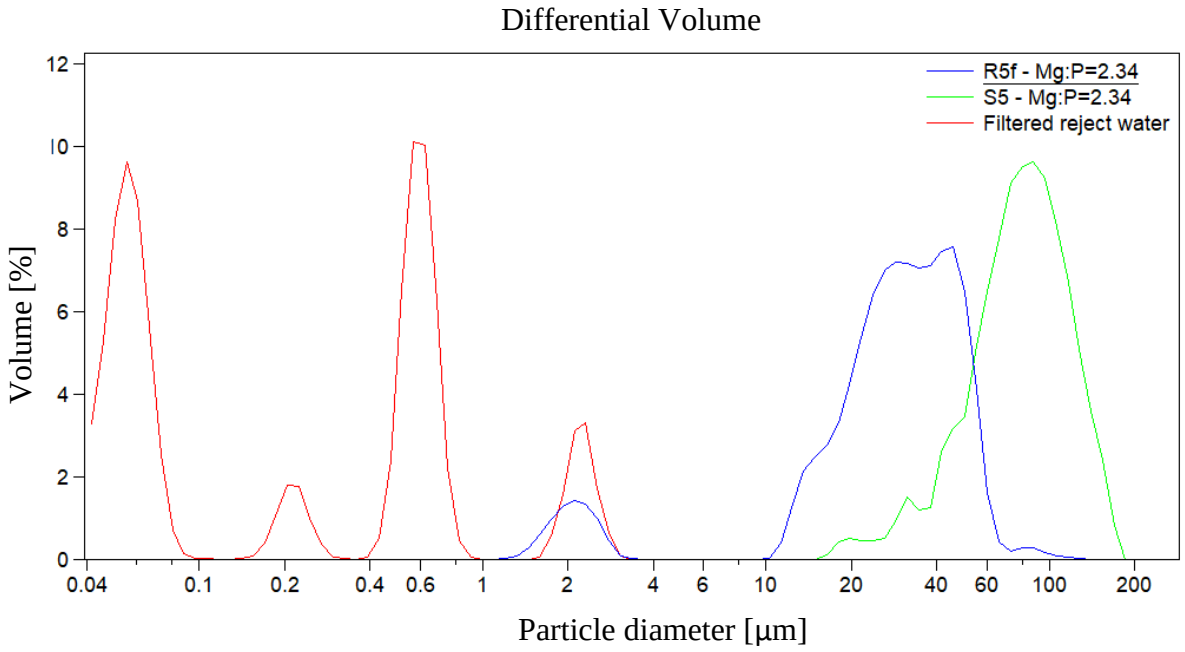

Figure A8.1: Particle size volume distribution in S2 and R5f at Mg:P molar ratio of 2.34. Blue line: R5f. Green line: S5. Red line: Filtered reject water.

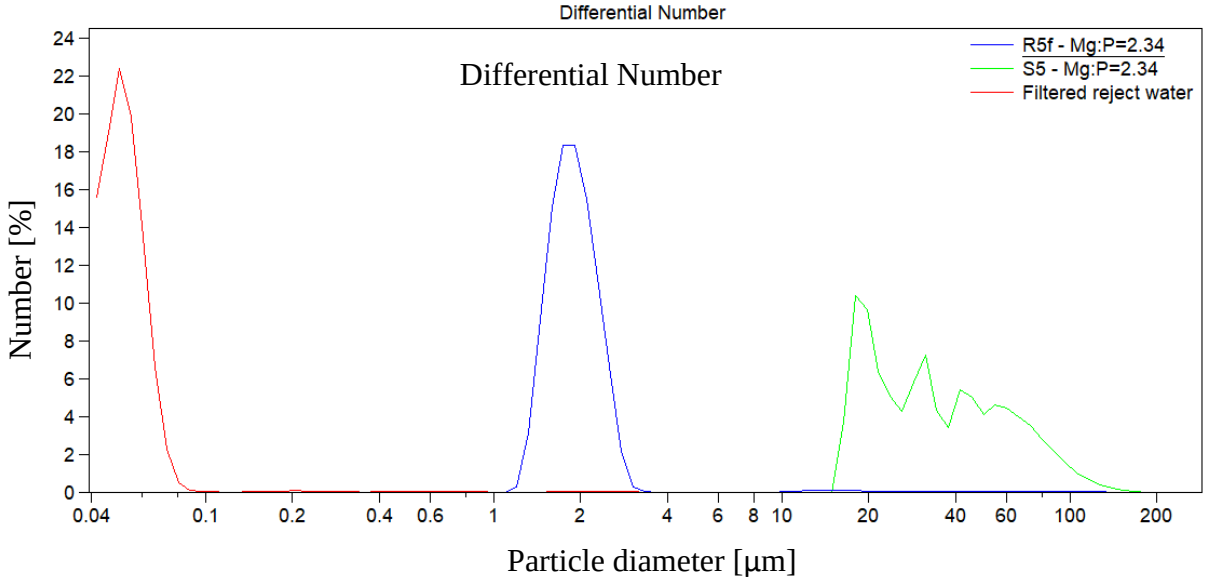

Figure A8.2: Particle size number distribution in S5 and R5f at Mg:P molar ratio of 2.34. Blue line: R5f. Green line: S5. Red line: Filtered reject water